Universidade de São Paulo

Instituto de Astronomia, Geofísica e Ciências Atmosféricas

Departamento de Ciências Atmosféricas

Beatriz Sayuri Oyama

Contribution of the vehicular emission to the organic aerosol composition in the city of Sao Paulo

Contribuição da emissão veicular para a composição do aerossol orgânico na cidade de São Paulo

Tese de doutorado

São Paulo

2015

BEATRIZ SAYURI OYAMA

Contribution of the vehicular emission to the organic aerosol composition in the city of Sao Paulo

Contribuição da emissão veicular para a composição do aerossol orgânico na cidade de São Paulo

(Final version, original copy available in the libraray)

Thesis submitted in partial fulfillment of the requirements for the degree of Doctor of Sciences in the Institute of Astronomy, Geophysics and Atmospheric Sciences

Major Field: Meteorology

Supervisor: Prof. Dr. Maria de Fátima Andrade

Sao Paulo

2015

Aos meus pais, Tadao e Sonia

Acknowledgements

Ao Laboratório de Física Atmosférica (IF USP), em especial a Ana e Fernando, pela ajuda na preparação das amostras e calibração de equipamento.

À CETESB por todo suporte durante as campanhas realizadas nesse trabalho, principalmente ao Carlos e ao Diácomo.

Aos funcionários do IAG, às equipes do Suporte Técnico, do Departamento de Ciências Atmosféricas e da Seção de Pós Graduação.

My thanks also go to my friends in Utrecht: Elena, Samuel, Narcisa, Guillaume, Madaglena, Marion, Siddharth, Abhijit and Abdel. It was very nice to spend so good time in your company during my stay in Utrecht. My thanks also go to Joseph not only for helping me during my measurements, but also for the friendship. I also thank Sudanshu for his funny way to make hard situations look easier. And Celia and Supun, for supporting me on my arrival, for nice dinners, trip, and talks… for being such nice friends. Also Dorota, the time we spend together is always so pleasant, specially that afternoon in Amsterdam. And a special thanks to Markella. You made our house, our home and adopt me in your family (to which I also thank). I did not know that when I was moving to Utrecht, I was going to meet other part of my family, my Cypriot sister.

I would like to express special thanks to Patrick (Pätty) for the last years. Thank you for all nice recommendations about my research; but mainly I thank you for representing so much in my life.

Aos meus amigos da USP, que compartilharam as dificuldades desse trabalho, risos e cafés: Emília, Bruna, Camila, Gláuber, Vinícius, Marcelo, Pâmela, Luana, Leonardo, Samara, Vivian e Benedito. E um 'obrigada' especial a Viviana e João, pela amizade sincera que resiste à distância e ao tempo.

Às amigas que trouxeram um toque especial nos meus dias: Ayumi, Mariana, Milene e Milena. À Madalena, que me ensina muito mais que outra língua, que me ajuda a ver o mundo com um olhar crítico, mas não severo. E claro, à Divina, por todo seu amor e carinho desde quando era pequena. Também ao Ricardo e Norberto, que acompanharam toda essa caminhada

E por último, mas não menos importante; agradeço à minha família, por todo amor e compreensão especialmente nos dias mais difíceis. Principalmente agradeço aos meus pais, Tadao e Sonia, que sempre me acompanharam em cada passo e nunca duvidaram que eu conseguisse. Sem vocês nada disso seria possível e por isso eu serei eternamente grata. À minha irmã Priscila, pela amizade verdadeira e cumplicidade, por sempre me incluir na sua rotina tão corrida. Ao meu irmão Leonardo, por estar presente apesar de toda a distância física que estivemos nos últimos anos. Agradeço ainda às suas famílias, que ao aumentarem, trouxeram mais luz aos meus dias.

You see things; and say,' Why?'

But I dream things that never were; and I say, 'Why not?'

George Bernard Shaw

RESUMO

Este trabalho teve como tema o estudo da composição do material particulado fino (MP$_{2.5}$) oriundo das emissões veiculares, em especial a caracterização de sua componente orgânica. Uma vez que os veículos são a principal fonte de MP$_{2.5}$ na cidade de São Paulo, amostras de MP$_{2.5}$ foram coletadas em três campanhas na cidade: duas em túneis (Túnel Jânio Quadros- TJQ- caracterizado por ter principalmente tráfego de veículos leves - VL- e Túnel Rodoanel - TRA- com relevante participação da frota de veículos pesados- VP), e uma ambiental durante o inverno de 2012 (no campus da Universidade de São Paulo em São Paulo). O MP$_{2.5}$ foi caracterizado na sua composição orgânica e inorgânica. As análises por gravimetria, Fluorescência de Raio-X e reflectância foram utilizadas para a determinação das concentrações de MP$_{2.5}$, elementos traço e Black Carbon (BC), respectivamente.

Medidas inéditas da caracterização da fração orgânica do MP$_{2.5}$ foram realizadas nas amostras de São Paulo: *Thermal-Desorption Proton-Transfer-Reaction Time-of-Flight Mass Spectrometer* (TD-PTR-ToF-MS) para quantificar e identificar compostos orgânicos e também *Isotope-Ratio Mass Spectrometry* (IRMS) e *Accelerator Mass Spectrometry* (AMS) para identificar os isótopos de carbono ^{13}C e ^{14}C respectivamente. As medidas realizadas pelo TD-PTR-ToF-MS e IRMS foram realizadas no Instituto de Pesquisa Marinha e Atmosférica, na Universidade de Utrech, e as medidas de IRMS, no centro de Pesquisa de Isópotos, na Universidade de Groningen, ambos na Holanda. Ainda as concentrações de carbono orgânico e elementar (EC, OC respectivamente) foram determinadas pelo método *Thermal Optical Transmittance* (TOT) no Departamento de Química e Bioquímica, na Universidade do Estado de Arizona, nos Estados Unidos.

Foram calculados os fatores de emissão dos compostos orgânicos considerando-se os dados obtidos pelos métodos TOT e TD-PTR-ToF-MS. Para ambos os métodos, as maiores emissões de aerossol orgânico (AO) e carbono orgânico (OC) foram oriundas dos VP à diesel e, ainda, as emissões de OC representaram 36 e 43% do MP$_{2.5}$ originado de VL e VP, respectivamente. A quantidade de oxigênio medida no AO foi maior que a presente nos combustíveis, e ainda os compostos contendo oxigênio representaram cerca de 70% do AO. Já os compostos nitrogenados corresponderam a aproximadamente 20% do AO, possivelmente devido a processos químicos envolvendo o NO$_x$ durante a combustão. A diferença entre as emissões de VL e VP não foi observada apenas na volatilidade dos compostos (VP emitiram AO mais volátil que VL), mas também nas médias dos espectros de massa (obtidos pelo TD-ToF-PTR-MS), que também sugeriram alguns possíveis compostos traçadores de gasolina, biodiesel e combustão de motores veiculares.

As análises de ^{13}C mostraram a presença de aerossóis mais voláteis e também mais empobrecidos em ^{13}C nos túneis que na campanha de inverno, enquanto que entre as amostras coletadas nos túneis não foi observada diferença significativa. Com relação a campanha de inverno, amostras coletadas durante dia de semana foram mais voláteis e mais empobrecidas em ^{13}C que as amostras coletadas nos finais de semana, possivelmente associado ao menor tráfego de veículos na cidade. Para confirmação de tal hipótese foi realizada a divisão de fontes de OC e EC para as três campanhas utilizando-se os dados obtidos das análises de TOT, IRMS e AMS.

A divisão de fontes para as campanhas dos túneis indicou que as emissões veiculares de OC e EC são especificamente dominadas pela queima de combustível fóssil (gasool e diesel- com 5% de biodiesel). O estudo de determinação de fontes nas amostras ambientais indicou que as emissões veiculares de OC foram maiores durante dia de semana que no final de semana, e que essas emissões foram estimadas como as principais fontes de OC (também OC secundário) e EC, respondendo por mais que 50% e 80% de suas concentrações totais, respectivamente. Também, as análises das amostras ambientais indicaram que a queima de biomassa é a fonte predominante (65%) de OC primário. As contribuições de plantas C3 e C4 foram consideradas praticamente constantes, principalmente de plantas C3, devido ao ponto de amostragem estar cercado por parques. Embora ainda falte um estudo de sensibilidade (considerando diferentes valores na literatura) para estimativa das incertezas das fontes, os resultados aqui apresentados são uma importante estimativa inédita na caracterização de fontes de OC e EC na atmosfera urbana de São Paulo.

Palavras- chave: Aerossol orgânico, emissões veiculares, fatores de emissão, divisão de fontes, TD-PTR-MS, IRMS, AMS

ABSTRACT

The main goal of this work was the study of fine particulate matter ($PM_{2.5}$) originated from vehicular emissions, focusing on the characterization of organic compounds. Since vehicles are the main source of $PM_{2.5}$ in the city of Sao Paulo, three campaigns were performed in the city: two in tunnels (Janio Quadros tunnel (TJQ) with a dominance of light duty vehicles (LDV); and Rodoanel tunnel (TRA) with a high number of heavy duty vehicles (HDV)), and an ambient campaign. The ambient air campaign was performed during the Southern Hemisphere winter 2012, inside the campus of University of Sao Paulo, and the tunnel campaigns in 2011. $PM_{2.5}$ was characterized by its organic and inorganic composition. Gravimetric, X-Ray Fluorescence and reflectance analyses were performed to determine the $PM_{2.5}$, trace elements, and black carbon (BC) concentrations, respectively.

For the first time the organic fraction of particle filter samples collected in the city of Sao Paulo were analyzed by: (i) a *Thermal-Desorption Proton-Transfer-Reaction Time-of-Flight Mass Spectrometer* (TD-PTR-ToF-MS) to identify and quantify organic compounds, (ii) an *Isotope-Ratio Mass Spectrometry* (IRMS) and (iii) an *Accelerator Mass Spectrometer* (AMS), the two latter used to identify the carbon isotopes ^{13}C and ^{14}C, respectively. TD-PTR-ToF-MS and IRMS measurements were performed at the Institute for Marine and Atmospheric Research, University of Utrecht, and AMS measurements at the Center for Isotope Research, University of Groningen, both in the Netherlands. Additionally, the organic carbon (OC) and elemental carbon (EC) concentrations were determined by the *Thermal Optical Transmittance* (TOT) method by the Department of Chemistry & Biochemistry, Arizona State University, in United States.

Emission factors were calculated from the data obtained from TOT and TD-PTR-ToF-MS methods. For both methods, HDV using diesel emitted more OA and OC than LDV using mainly gasohol. OC emissions represented 36 and 43% of $PM_{2.5}$ emissions from LDV and HDV, respectively. Additionally, a high amount of compounds containing oxygen (70%) for both type of fleet was observed, suggesting that the oxygenation occurs during fuel combustion and that the oxygen content of the fuel itself contributes to the oxygen in the OA. Nitrogen-containing compounds contributed around 20% to the EF values for both types of vehicles, possibly associated to chemical processes involving nitrogen oxides (NO_x) during the combustion. More differences between both fleets were seen by means of volatility (HDV emitted more volatile OA than LDV), but also of the mass spectra obtained by the TD-PTR-MS, which suggested possible tracers for gasoline, biodiesel and vehicle engine combustions.

The ^{13}C analysis showed that aerosols sampled in the tunnels were more volatile and more depleted in ^{13}C values than samples from the ambient campaign. For the ambient campaign, samples collected on weekdays were more depleted in ^{13}C and more volatile than weekend samples, possibly associated to the lower number of vehicles on the weekend. In order to confirm this hypothesis, a source apportionment was performed to OC and EC concentrations for the three campaigns by using the TOT, IRMS and AMS analyses.

The source apportionment for the tunnel campaigns indicated that the vehicular emissions of OC and EC are specifically dominated by the fossil fuel burning (gasohol and diesel-containing 5% of biodiesel).The source apportionment study in the ambient samples indicated that the OC originated from vehicular emissions was higher during the weekday than weekend; besides, they were identified as the main source of primary and secondary OC and EC, corresponding to more than 50% and 80% of total OC and EC, respectively. Furthermore, biomass mass burning was found to be the dominant source (65%) of OC_{prim} concentrations in the ambient samples. The estimative contributions from C3 and C4 plants were approximately constant in the city of Sao Paulo, where the main contribution came from C3 plants due to the fact that the sampling point is surrounded by parks. Although a sensitivity study (considering different values in the literature) to estimate the uncertainties is missing, the results presented here give an important and unique estimation for the source apportionment of OC and EC in the atmosphere of Sao Paulo.

CONTENTS

LIST OF FIGURES

LIST OF TABLES

LIST OF ABBREVIATIONS

Abbreviation	Meaning
AMS	Accelerator Mass Spectrometry
BC	Black Carbon
BVOC	Biogenic Volatile Organic Compound
EC	Elemental Carbon
EF	Emission Factors
$F^{14}C$	Fraction of Modern Carbon
HC	Hydrocarbon
HDV	Heavy Duty Vehicles
HOA	Hydrocarbon-Like Organic Aerosol
PAH	Polycyclic Aromatic Hydrocarbon
IRMS	Isotope Ratio Mass Spectrometry
OA	Organic Aerosol
LV-OOA	Low Volatile Oxidized Organic Aerosol
PNPB	National Program of Production and Usage of Biodiesel
LDV	Light Duty Vehicles
MASP	Metropolitan Area of Sao Paulo
PM	Particulate Matter
PM_1	Particulate Matter with diameters smaller than 1 μm
$PM_{2.5}$	Fine Particulate Matter
PM_{10}	Coarse Particulate Matter
POA	Primary Organic Aerosol
Proalcool	National Pro Alcohol Program
PROCONVE	Program for Controlling Vehicular Emission
PTR-ToF-MS	Proton-Transfer-Reaction Time of Flight Mass-Spectrometer
SOA	Secondary Organic Aerosol
SV-OOA	Semi-Volatile Oxidized Organic Aerosol
TC	Total Carbon
TD-PTR-MS	Thermal Desorption Proton-Transfer-Reaction Mass Spectrometry
THEODORE	two-step heating system for EC/OC determination of radiocarbon in the environment
TJQ	Janio Quadros tunnel
TOT	Thermal-Optical Transmittance
TRA	Rodoanel Mario Covas tunnel
VOC	Volatile Organic Compound

1. Introduction

Atmospheric aerosols consist of solid or liquid particles in the atmosphere usually referred to as particulate matter (PM) (SEINFELD; PANDIS, 2006). Its composition and size depends on its sources and chemico-physical processes in the atmosphere (WHITBY, 1978). Aerosols can be emitted directly by e.g. sea spray and dust, thus called primary aerosols, or formed in the atmosphere by gas-to-particle conversion, thus called secondary aerosols, involving gaseous compounds from biogenic emissions and human activities (RAES et al., 2000; SEINFELD; PANDIS, 2006).

The size of particles is expressed based on its diameter, which ranges from few nanometers to micrometers. Ultra fine particles (smaller than 0.01 μm), Aitken nuclei (0.01 to 0.8 μm) and accumulation mode (~0.8 to 2 μm) are constituents of the so called fine particulate matter (particles with a diameter smaller than 2.5 μm, $PM_{2.5}$). Coarse particles include all particles with diameter ranging from 2 to 10 μm (FINLAYSON-PITTS; PITTS, 2000) and are usually formed by mechanical processes, such as windblown dust, grinding operations, volcanic activities, and vegetation emissions (spores, pollen, and plants debris). Its residence time in the atmosphere is shorter due to sedimentation. On the other hand, $PM_{2.5}$ can be formed by nucleation, condensation and coagulation processes and its main removal processes in the atmosphere are rainout and washout. Therefore, its residence time can vary from days to weeks (SEINFELD; PANDIS, 2006).

Aerosols are composed mainly by the inorganics sulfate (SO_4^{2-}), ammonium (NH_4^+), nitrate (NO_3^-), sodium, chloride, trace elements, and crustal elements, beside water and carbonaceous material (FINLAYSON-PITTS; PITTS, 2000; SEINFELD; PANDIS, 2006). Furthermore, the carbonaceous fraction of particulate matter consists of elemental carbon (EC)or black carbon (BC), the nomenclature depends on the method used, which represent the main absorbing fraction of aerosols, and organic carbon (OC) (SEINFELD; PANDIS, 2006). Its contribution to the $PM_{2.5}$ mass estimated in models is in the range of 20-90% (KANAKIDOU et al., 2005). BC or EC are related to two different methods to measure the non-organic aerosol, as discussed in section 2. OC includes both secondary organic aerosols (SOA) and primary organic aerosols (POA). POA are emitted directly in the atmosphere by biogenic (e. g. plant debris) and human activities (e. g. combustion processes). SOA is formed from gas-phase oxidation products, which either form new particles or, more likely, condense onto existing atmospheric aerosols.

Overall, aerosols can have a cooling or heating effect on climate by e.g. scattering or absorbing sunlight, which is called the direct effect (CHARLSON et al., 1992; RAMANATHAN et al., 2007). The indirect effect refers to the impact on the cloud formation, where particles act as cloud condensation nuclei, influencing the cloud properties (NAKAJIMA et al., 2001). The chemical composition determines the scattering and light-absorbing properties, e.g. BC present in PM has a heating effect on the atmosphere by absorbing the light and reducing the albedo of the surface. On the other hand, the presence of sulfate has a highly reflective effect, resulting to cool down the atmosphere (SCHWARTZ, 1993).

The effects of aerosols are not only important for the climate, but have also adverse health effects, such as cardiovascular and respiratory diseases, and cancers (ANDERSON; THUNDIYIL; STOLBACH, 2012; BRITO et al., 2010; POPE et al., 2002). Especially smaller particles such as the $PM_{2.5}$ fraction can easily reach the deepest recesses of the lungs and have therefore the highest impacts on health. The composition of aerosols was explored by e.g. Peng et al. (2009), who related high EC and OC concentrations to higher cardiovascular and respiratory admissions in the hospital, respectively.

1.1.   Organic aerosols

Volatile organic compounds (VOC's) are the main precursors of OA. They have different volatilities, potentials to ozone formation, polarities and also different effects on the environment (HOSHI et al., 2008; KROLL; SEINFELD, 2008). They can comprise hundreds of thousands of gaseous organic molecules and non-methane VOC's excluding carbon monoxide (CO), carbon dioxide (CO_2) and methane (CH_4) (KROLL; SEINFELD, 2008; SEINFELD; PANDIS, 2006). Hydrocarbons represent the largest group of VOC's (HOSHI et al., 2008; KROLL; SEINFELD, 2008). VOC's can be emitted to the atmosphere from anthropogenic activities (e.g. vehicular emission, fuel and biomass burning, industrial activities) and biogenic sources (mainly vegetation) (KOPPMANN, 2007). On a global scale, global VOC budget is estimated to be in the order of 1150 Tg of C/year (GUENTHER et al., 1995). Biogenic emissions contribute with 90% of VOC's (called BVOC's), including isoprene (50% of total BVOC's), monoterpenes (15%), and sesquiterpenes (3%) (GUENTHER et al., 2012). In turn, 10% of globally emitted VOC's are of anthropogenic origin, including e.g. alkanes, alkenes, benzene and toluene.

Figure 1.1 shows a sketch of different pathways that the VOC's can undergo within the atmosphere. Although wet and dry deposition are an important removal processes of VOC's from the atmosphere, chemical oxidation is the main sink for organic trace gases by reaction

with OH radical and Ozone (O_3) at daytime, and NO_3 radicals, which are the most important oxidant during night due to the absence of OH radicals. VOC's can interact with sunlight and photolysis to smaller fragments. These products have usually a lower volatility than their precursors and thus can form new particles called nucleation, condensate on available particles in the atmosphere, in both cases forming SOA.
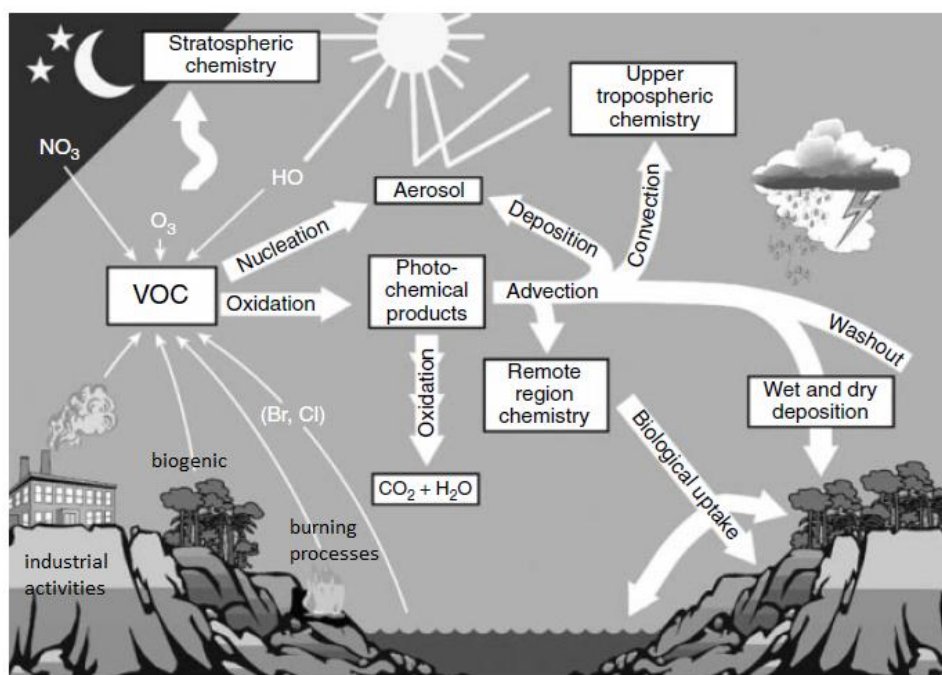
Figure 1.1: Sketch of different processes which determine the fate of VOC's in the atmosphere. Figure adapted from Koppmann (2007).

The contribution of each compound to the total aerosol mass depends on the aerosol sources. Jimenez et al. (2009) reported aerosol mass spectrometric measurements taken at different sites in the Northern Hemisphere, showing the average total mass and chemical composition of particulate matter with diameters smaller than 1 μm (PM_1). Sulfate, nitrate, ammonium, chloride and organics were the dominant compounds with highly variable abundances. By using factor analysis (PAATERO; TAPPERT, 1994; PAATERO, 1997; ULBRICH et al., 2008), Jimenez et al. (2009) classified the organics in hydrocarbon-like OA (HOA), semi volatile OOA (SV-OOA), and low volatile OOA (LV-OOA). Furthermore, compounds presenting high molecular O/C ratios indicated more oxidized aerosol, associated to aging processes, forming SOA, and often related to photochemical reactions. On the other hand, HOA presenting low O/C ratios and high H/C ratios, indicate fresh aerosols with high volatilities.

1.2. Carbon isotope measurements in aerosols

In nature, the following carbon isotopes occur: ^{12}C, ^{13}C (both stable) and ^{14}C (radioactive). ^{12}C is the most abundant isotope, ^{13}C corresponds to 1.1%, and ^{14}C occurs every 1 in a trillion carbon ^{12}C in living material. Usually the abundance of the heavier isotopes ^{13}C and ^{14}C is reported relative to ^{12}C. The ^{13}C isotope ratios are expressed in the delta notation, with respect to the Vienna Pee Dee Belemnite standard (VPDB):

$$\delta^{13}C = \left(\frac{\left(^{13}C/^{12}C\right)_{sample}}{\left(^{13}C/^{12}C\right)_{VPDB}} - 1 \right) x \ 1000‰ \qquad (1.5)$$

The relative abundance of ^{13}C (δ^{13}C) can give important information about the sources and chemical processes forming organic aerosols.

Source characterization studies assume that a particular source has an approximately constant carbon isotopic signature. For instance, the fact that δ^{13}C of aerosols from marine sources are different from that of terrestrial emissions has been used in different studies (CACHIER; BREMOND; BUAT-MÉNARD, 1989; CACHIER et al., 1985; CEBURNIS et al., 2011) According to how the carbon is fixed during the photosynthesis, the plants can be divided into CAM, C3 and C4 plants. Among the terrestrial sources of carbon aerosol, C3 plants dominate, whose metabolism strongly discriminates ^{13}CO$_2$ during CO$_2$ uptake. As a consequence, δ^{13}C values are depleted with values around -25 and -30‰ (SMITH; EPSTEIN, 1971). Sometimes a signature of a given source, e.g. C3 plants, shows interference with other sources, e.g. particles emitted from biofuels (gasohol and biodiesel vehicles, ca. -25‰) (LÓPEZ-VENERONI, 2009). Therefore, it is difficult to distinguish fossil and biogenic emissions by δ^{13}C measurements alone. However, since ^{13}C in C4 plants is less depleted, with δ^{13}C values around -13‰, the contribution to carbon aerosol from C4 plants (such as sugarcane or maize) can be distinguished from the contribution of C3 plants. For example, δ^{13}C values of ambient aerosol in a C4 dominated landscape in Brazil ranged from - 20.0 to -22.8‰ (MARTINELLI et al., 2002), which is much more enriched than typical continental aerosol. The burning processes of C3 and C4 plants were investigated by Turekian et al. (1998) under laboratory conditions. They found that particles that originated from combustion of C4 plants were approximately 3.5‰ lighter than the unburned plant material. On the other hand, particles produced during combustion of C3 plants were around 5‰ heavier than unburned plants.

More detailed source apportionment is possible if other aerosol parameters are measured in addition to δ^{13}C. Widory et al. (2004) distinguished road traffic and industrial

particle sources by using lead isotope ratios and differentiated diesel emissions and fuel oil from other sources by using carbon isotopes. Ceburnis et al. (2011) used $\delta^{13}C$ values associated to ^{14}C measurements to estimate the carbonaceous matter origin in marine aerosol. Wang et al. (2013) performed a source apportionment using $\delta^{13}C$ values combined with potassium (K^+) and ^{14}C measurements.

The relative abundance of ^{14}C is mainly used for aerosol source apportionment to distinguish fossil and contemporary sources. ^{14}C is naturally formed in the upper stratosphere from cosmic radiation, where it is rapidly oxidized to $^{14}CO_2$. Once it enters in the lower atmosphere, it participates in photosynthesis and respiration processes, entering in equilibrium with all living organisms. After a living organism dies, ^{14}C concentrations start to decrease exponentially with a half-life of 5730 years. Fossil fuel contains no ^{14}C by definition, since it is much older than the half-life of ^{14}C (CURRIE, 2004).

The abundance of radiocarbon is frequently expressed relative to the abundance of ^{12}C and the value of this ratio for a sample is expressed relative to an oxalic acid standard (primary modern radiocarbon standard). The activity of the oxalic acid standard is related to the atmospheric CO_2 activity under natural circumstances in the year 1950. The nomenclature used here is the same as adopted by Dusek et al. (2013a) and described in Reimer et al. (2004). The fraction of modern carbon ($F^{14}C$) is expressed by

$$F^{14}C = \frac{\frac{^{14}C}{^{12}C}(sample)}{\frac{^{14}C}{^{12}C}(1950)} \qquad (1.6)$$

Assuming equilibrium between all living material and the atmosphere, the fraction of modern carbon in the current atmosphere would be equal to one ($F^{14}C = 1$). However, two anthropogenic activities changed the atmospheric $F^{14}C$ relative to the year 1950: nuclear bomb tests and the combustion of fossil fuels. In the 1960's nuclear tests almost doubled ^{14}C levels in the Northern Hemisphere. Due to the ban of above-ground tests, the abundance of ^{14}C has been decreasing because it has been taken up by oceans and terrestrial biosphere. The other anthropogenic activity is the increase of fossil fuel burning, which implies in a dilution of atmospheric $^{14}CO_2$, since the fraction of modern carbon of fossil fuels is considered zero. Currently, the value of atmospheric CO_2 is approximately 1.04 (LEWIS; KLOUDA; ELLENSON, 2004), due its origin from living material. Therefore, ^{14}C measurements on aerosol carbon can be used to distinguish fossil sources from contemporary sources.

The total aerosol carbon can be subdivided into OC and EC, which have different sources. The EC sources are mainly related to burning processes, usually fossil fuel and

biomass burning (SZIDAT et al., 2007). On the other hand, OC can be directly emitted as particles from combustion processes, or can be formed from gaseous precursors (SOA formation). Many studies presented source apportionment of carbonaceous aerosols using ^{14}C values from Total Carbon (TC) measurements (GELENCSÉR et al., 2007; GENBERG et al., 2011; GLASIUS; LA COUR; LOHSE, 2011; YTTRI et al., 2011). In these studies the different sources for OC and EC were not directly determined. OC and EC measurements performed separately usually allow more detailed source apportionment (DUSEK et al., 2013a, 2014; GLASIUS; LA COUR; LOHSE, 2011; HEAL et al., 2011; SZIDAT et al., 2004, 2006, 2008)

1.3. Contribution from vehicular emission to the aerosol of the city of Sao Paulo

The Metropolitan Area of Sao Paulo (MASP) is composed of 39 municipalities, with a fleet of more than 7 million vehicles (CETESB, 2014), which nowadays run on three different types of fuel: diesel (with 5% of biodiesel, referred to as diesel afterwards), hydrated ethanol and gasohol (gasoline with 25% of ethanol). The number of vehicles has grown more rapidly than the population in the last 15 years. In 2000, the population was around 10 million and the number of vehicles was 0.9 million in the city of Sao Paulo. In 2013, these values increased to 11.4 million and around 4.5 million, respectively (Infocidade, 2015; Cetesb, 2014). Figure 1.2 presents the evolution of initial registrations of new vehicles in Sao Paulo, classified by fuel usage over the past 40 years (CETESB, 2014). In 2003, a new vehicle technology was introduced: *flex* fuel vehicles, which are able to operate on any proportion of ethanol and gasohol.

The implementation of the National Pro Alcohol Program (Proalcool) in Brazil during the 1980's had an important influence on the increase in vehicles running on hydrated ethanol. In the early 1970's, the ethanol production was not significantly higher than 1 million cubic meters in Brazil. However, due to the Proalcool program, this value increased to more than 10 million cubic meters in the mid-1980's (STATTMAN; HOSPES; MOL, 2013). This program stimulated the use of alcohol from sugarcane as fuel in order to decrease the dependence on imported fuel and also to stimulate industrial and agricultural growth (RICO; SAUER, 2015; STATTMAN; HOSPES; MOL, 2013). Besides that, the addition of 10% of ethanol to gasoline was legally mandated between 1973 and 1974. Also at that time, the hydrated alcohol price was significantly lower than the price for gasoline (64.5% less) due to governmental incentives (STATTMAN; HOSPES; MOL, 2013). Following a governmental change in 1985, the subsidy for

alcohol decreased dramatically, thus the alcohol price increased, followed by a fall in sales of ethanol fueled vehicles (Figure 1.2).

In the early 1990's the number of vehicles increased substantially due to a political decision of increasing the sales of vehicles to stimulate the economy. Following international regulations for vehicular emissions, the Program for Controlling Vehicular Emission (PROCONVE) was implemented in the late 1980's. This program established emission standards for new vehicles with the aim of reducing these emissions (SZWARCFITER; MENDES; LA ROVERE, 2005). Despite an increase in the number of vehicles, the program resulted in an improved air quality with lower concentrations of carbon monoxide (CO), sulfur dioxide (SO_2) and coarse particulate matter (with diameters between 2.5 and 10 μm, PM_{10}), as shown by Carvalho et al. (2015). Pérez-Martínez et al. (2014) did not observe a decreasing trend of $PM_{2.5}$ and ozone (O_3). On the other hand, Salvo and Geiger (2014) demonstrated that the ozone levels have increased during high ethanol consumption events, in accordance to a HC-limited regime.
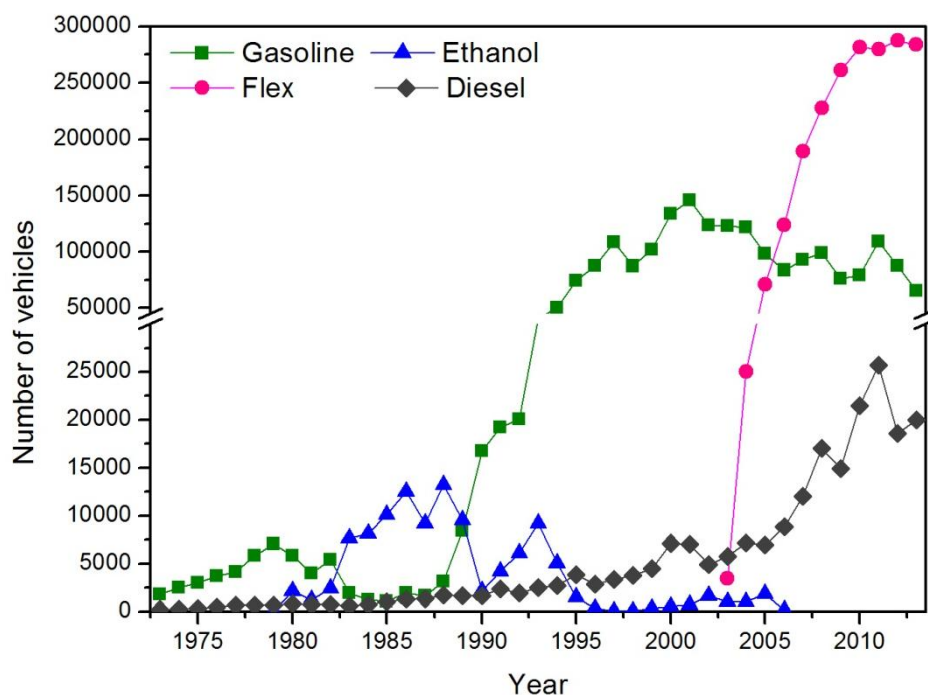
Figure 1.2: Annually registrations of new vehicles in the city of Sao Paulo.

In 2004, the National Program of Production and Usage of Biodiesel (PNPB) was created in order to stimulate the use of biofuels as well as the associated agricultural activities for its production. The main motivation was to decrease the dependence on imported diesel (STATTMAN; HOSPES; MOL, 2013), similar to Proalcool. In the same year, the addition of 2% of biodiesel to conventional diesel fuel was authorized, but only since 2008 this addition has

become mandatory. Until 2010, the percentage has gradually increased to the current 5% (MME, 2015). Rico and Sauer (2015) and Stattman et al. (2013) discussed in detail the impact of the biodiesel production on agricultural and economical activities. Nowadays, 74.7% of the biodiesel produced in Brazil is made from soybean oil, 20.4% from animal fat (mainly bovine), and 4.9% from other sources (ANP, 2015).

The burning of biofuels and fossil fuels causes substantial emissions of VOC's, important precursors of tropospheric ozone and organic fine particles, and BC, mainly emitted from the burning of diesel. Andrade et al. (2012) reported the fraction of BC in $PM_{2.5}$ for six Brazilian cities with values ranging from 15% in coastal regions to 30% in urban areas. Furthermore, according to official inventories from the Brazilian Environmental Agency the vehicular fleet is responsible by more than 90% of CO and hydrocarbon (HC) emitted to atmosphere and 80% of NO_x (CETESB, 2013a).

Due to its density population, political and economic importance, the MASP has been in the focus of several studies that investigated the impact of vehicular emissions on the concentration and composition of particulate matter (ALBUQUERQUE; ANDRADE; YNOUE, 2012; ANDRADE et al., 2012; MIRANDA; ANDRADE, 2005; MIRANDA et al., 2002). The distinction between contributions from light duty vehicles (LDV) and heavy duty vehicles (HDV) is still a challenge. Different methods can be used in order to estimate the emissions from the vehicular fleet. Emission factors (EF) for gaseous and particulate compounds have been calculated based on tunnel measurements, and recent results were presented by Pérez-Martínez et al. (2014). The analysis of $PM_{2.5}$ in tunnels was described by Brito et al. (2013). They performed a chemical characterization of $PM_{2.5}$ by separating the total mass into organic carbon, elemental carbon, and contributions from other trace elements. They concluded that the organic aerosol fraction estimated from OC measurements represented around 40% of $PM_{2.5}$ emitted by LDV and HDV.

In spite of all the development and studies concerning the composition and sources of aerosols in the area, very few studies have analyzed the organic composition of particulate matter in Sao Paulo. Previous studies estimated the contribution of OC present within the particulate matter in the city of Sao Paulo, as described in Castanho and Artaxo (2001), and Miranda and Andrade (2005). In a more recent study, Albuquerque et al. (2012) attributed a part of the non-explained mass obtained from the mass balance model to OA. In a study performed in 2008, Souza et al. (2014) estimated from OC measurements that around 26% of the $PM_{2.5}$ was composed of particulate organic matter. Recently, Almeida et al. (2014)and Brito et al. (2013) discussed the aerosol composition including the OC and in more details, Polycyclic Aromatic Hydrocarbon (PAH).

1.4. Objectives

The main goal of this study is to identify and quantify the organic compound fraction of the fine particulate matter in the city of Sao Paulo, focusing on the vehicular contribution. Secondary objectives are:

- The analysis of $PM_{2.5}$ inorganic compounds, considering trace elements (measured by Energy Dispersive X-Ray) and BC (Reflectance), as well as their source apportionment using receptor models (Principal Components Analysis).

- The determination and analysis of the emission factors of organic particles from LDV and HDV and the composition of OA in ambient air. The samples are comprised from aerosol filter samples ($PM_{2.5}$) collected in traffic tunnels and ambient air. For the first time, Thermal Desorption Proton-Transfer-Reaction Mass Spectrometry (TD-PTR-MS) was applied to filter samples from Sao Paulo, where hundreds of organic compounds were classified and their contribution to OA were estimated.

- The OC and EC source apportionment by carbon isotope measurements, considering vehicular emissions, contributions from biomass burning and plant emissions as well. For the first time, measurements of ^{13}C (by Isotope Ratio Mass Spectrometry) and ^{14}C (by Accelerator Mass Spectrometry, AMS) were performed for Sao Paulo City.

This thesis is organized in the following way: the methodology is described in Chapter 2, presenting the campaigns and analysis of the organic and inorganic material; Chapter 3 contains results and discussions for the inorganic analysis, emission factors from vehicular emissions, and OC and EC source apportionment; chapter 5 presents discussions and conclusions.

2. Experimental Section

2.1. Campaings

The field campaigns were performed at two different tunnels: the first campaign took place in the Janio Quadros tunnel (TJQ) from 4th to 13rd May 2011 and a second campaign was performed in the Rodoanel Mario Covas tunnel (TRA) from 6th to 17th July 2011. In a third campaign, daily ambient particle samples were collected during the Southern Hemisphere Winter from 6th July to 9th September 2012 on the roof of a building on the University of Sao Paulo campus. Figure 2.1 presents the location of the sampling sites of the three campaigns.
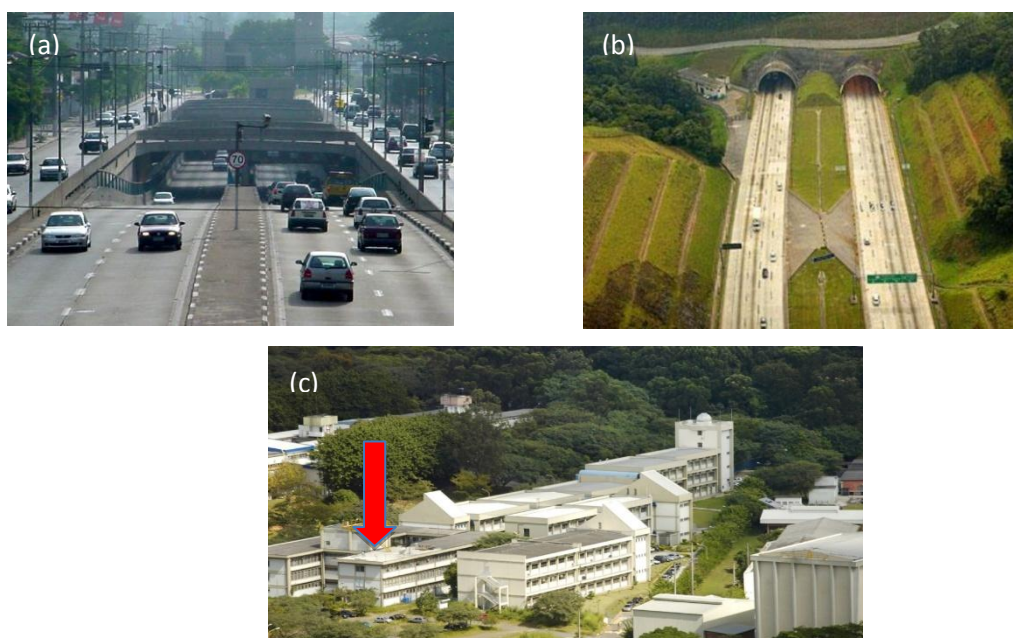
Figure 2.1: Location of the sampling sites where the samples were collected (a) Janio Quadros Tunnel (TJQ), (b) Rodoanel Tunnel (TRA), and (c) Institute of Astronomy, Geophysics and Atmospheric Sciences (Source: Google, 2015)

TJQ is a two-lane tunnel located in the center of Sao Paulo and characterized mainly by LDV traffic. The direction of the car traffic in this tunnel alternated twice a day at 6 AM and 9 AM. TJQ has a length of 1.9 km, speed limit of 60 km/h, and a natural wind flow velocity ranging from 1.0 to 4.9 m/s during congested and normal traffic conditions, respectively, as described by (PÉREZ-MARTÍNEZ et al., 2014). TRA is located on the outskirts of the city on a highway ring. This tunnel is an important alternative route for HDV due to traffic restrictions in the center of Sao Paulo. With a length of 1.7 km and a speed limit of 70 km/h for the HDV and

90 km/h for the LDV, the traffic flow is always on four lanes in one direction. Pérez-Martínez et al. (2014) described that the natural flow velocity ranged from 1.0 to 6.1 m/s during congested and normal traffic conditions, respectively.

In TJQ, the traffic of vehicles was monitored by cameras and the number of vehicles was obtained by counting from recorded videos. The fleet was classified into four different groups: HDV, LDV, motorcycles and taxis. For this study, the motorcycles and the taxis were considered as LDV, since they use hydrated ethanol or gasohol. The TRA campaign had an automated counting system by weighing vehicles, which sorts the fleet into the two categories LDV and HDV. The other two kinds of vehicles were excluded mainly due to the fact that motorcycles hardly circulate on highways with high speed limit and circulation of taxis is very limited far from the city center. A detailed discussion about the traffic of the vehicles during these campaigns is shown by Brito et al. (2013) and Pérez-Martínez et al. (2014).

Filter samples were collected at the midpoint of both tunnels. Two samplers were deployed in parallel: a low-volume sampler (Partisol Dichotomous Ambient Particle Sampler, with the sampling rate of 16.6 L/min) collected simultaneously $PM_{2.5}$ and $PM_{2.5-10}$ on two different filters (fine and coarse particles, comprising PM_{10}) and a mini-volume sampler (Airmetrics, with a sampling rate of 5 L/min) sampled only the $PM_{2.5}$ fraction. On the Mini-volume sampler, the samples were collected on pre-heated quartz fiber filters ($800^{o}C$, for 12 hours), subsequently wrapped in aluminum foil (pre-cleaned at $550^{o}C$, for 8 hours) and stored inside polyethylene bags in a freezer at $-18^{o}C$ until analysis. Table 2.1 summarizes the samplers and the methodology used during the tunnels campaigns.

Table 2.1: Compounds measured in the Janio Quadros (TJQ) and Rodoanel (TRA) tunnels, methodology and instrumentation for the analysis.

	Sampler	Methodology
$PM_{2.5}$ $PM_{2.5-10}$	Partisol 2000-D polycarbonate filters	Gravimetry
		X-ray Fluorescence
		Reflectance
$PM_{2.5}$ $PM_{2.5-10}$	Partisol 2000-D quartz filters	Proton-Transfer Mass Spectrometry
		Isotopic Ratio Mass Spectrometry (^{13}C)
		Accelerator Mass Spectrometry (^{14}C)
$PM_{2.5}$	Minivolume quartz filters	Thermal–optical transmittance
CO		Non-dispersive infrared photometry
CO_2		Infrared analysis

Measurements of carbon monoxide (CO) and carbon dioxide (CO_2) were performed inside and outside the tunnels during the whole campaigns. CO measurements were done with a non-dispersive infrared photometry equipment (Thermo Electron 48B). CO_2 was measured using a LICOR-6262 instrument inside and a Picarro-G1301 instrument outside the tunnels, as described in detail elsewhere (PÉREZ-MARTÍNEZ et al., 2014). Trace gas concentrations were averaged to the filter sampling times. These values as well as the information regarding the samples are summarized in Table 2.2. The gaseous concentrations were obtained on an hourly base and the average value was calculated for the same period of the particulate samples

Table 2.2: Averages and standard deviations of the numbers of LDV and HV, and averages and standard deviations of CO_2 and CO concentrations of the filters collected inside and outside the tunnels.

	Sampler	# vehicles		Inside		Outside	
		LDV	HDV	CO_2	CO	CO_2	CO
TJQ	Dichotomous	17345 (7169)	90 (109)	490.8 (34.1)	4.73 (1.68)	404.1 (14.9)	1.15 (0.31)
	Mini Vol	23259 (10079)	115 (112)	484.5 (33.5)	4.35 (1.46)	404.4 (15.3)	1.14 (0.3)
TRA	Dichotomous	11087 (1991)	4984 (494)	692.6 (27.2)	4.45 (0.86)	416.1 (3.2)	1.20 (0.51)
	Mini Vol	11859 (2281)	5349 (875)	688.1 (38.3)	4.39 (0.98)	416.3 (2.5)	1.20 (0.54)

The sample identification of the quartz filters, the volume sampled and the sampling time, together with the corresponding amount of vehicles that circulate during the sampling and the average concentrations of CO_2 and CO are presented in Table A.1-Table A.4, in the Appendix, for the measurements performed in the two tunnels and in ambient air. Table 2.2 presents the average per campaign and sampler of the number of vehicles, CO_2 and CO inside and outside the tunnels

The ambient atmospheric air measurement campaign was performed during the Southern Hemisphere wintertime in 2012 on the roof of the building of the Astronomy, Geophysics and Atmospheric Sciences Institute, located on the campus of the University of Sao Paulo. The measured compounds, sampling and analysis methods and instrumentation used in the tunnel campaigns are summarized in Table 2.3.

Three samplers for PM collection were deployed in parallel: low volume and mini-volume samplers (the same used on the tunnel campaigns), as well as high volume samplers (with the sampling rate of 1.13 m³/min). The PARTISOL sampler was used to collect samples on polycarbonate filters for 12 hours between 6th July and 9th September and were changed twice per day (at 7 am and at 7 pm). The high-volume samplers collected daily $PM_{2.5}$ samples on quartz filters between 8th August and 9th September 2012. These filters were changed every

day at 9 am. Additionally, mini-volume samplers collected daily PM$_{2.5}$ samples for 24 h, which were changed every day at 10 am between 7th August and 7th September. The analytical methods and data treatment used for these measurements were the same as for the tunnel samples. Table A.5 and Table A.6, in the Appendix, present the sample identification collected on quartz filters, the volume sampled and the sampling time for samples collected by mini volume and high volume sampler.

Table 2.3: Particulate matter measured during the ambient 2012 campaign, sampling and analysis methodology and instrumentation.

Compound	Analyzer	Methodology
PM$_{2.5}$ PM$_{2.5-10}$	Partisol 2000-D	Gravimetry
	polycarbonate filters	X-ray Fluorescence
		Reflectance
PM$_{2.5}$ PM$_{2.5-10}$	Highvolume quartz filters	Proton-Tranfer Mass Spectrometry
		Isotopic Ratio Mass Spectrometry (^{13}C)
		Accelerator Mass Spectrometry (^{14}C)
PM$_{2.5}$	Minivolume quartz filters	Thermal–optical transmittance

2.1.1. Description of meteorological conditions during the ambient campaign

Meteorological conditions have a strong influence on atmospheric concentrations of chemical compounds (CETESB, 2013b). High pollution episodes are often observed during the winter season in the city of Sao Paulo, characterized by the predominance of anticyclones associated to air mass subsidence, which inhibits cloud formation (SÁNCHEZ-CCOYLLO; ANDRADE, 2002). On a micro scale, these episodes are also characterized by temperature inversions, which happen when the radiative cooling dominates over the heating processes in the urban canopy. Furthermore, the urban heat island had interferences on the local rainfall (COLLIER, 2006).

Infrared images satellites (Figure 2.2) were used to analyze the weather conditions during the ambient campaign (CPTEC, 2014), where five cold fronts were identified to influence the weather conditions during the campaign. Cold fronts are associated to low pressure systems and cloud cover, often associated to precipitation. After the cold fronts had passed, MASP was dominated by high pressure systems as well as low temperatures and low relative humidities. Average daily values of ambient air temperature and pressure as well as

accumulated precipitation are shown in Figure 2.3. The data was obtained at Agua Funda Meteorological Station located around 20 km away from the ambient sampling point.
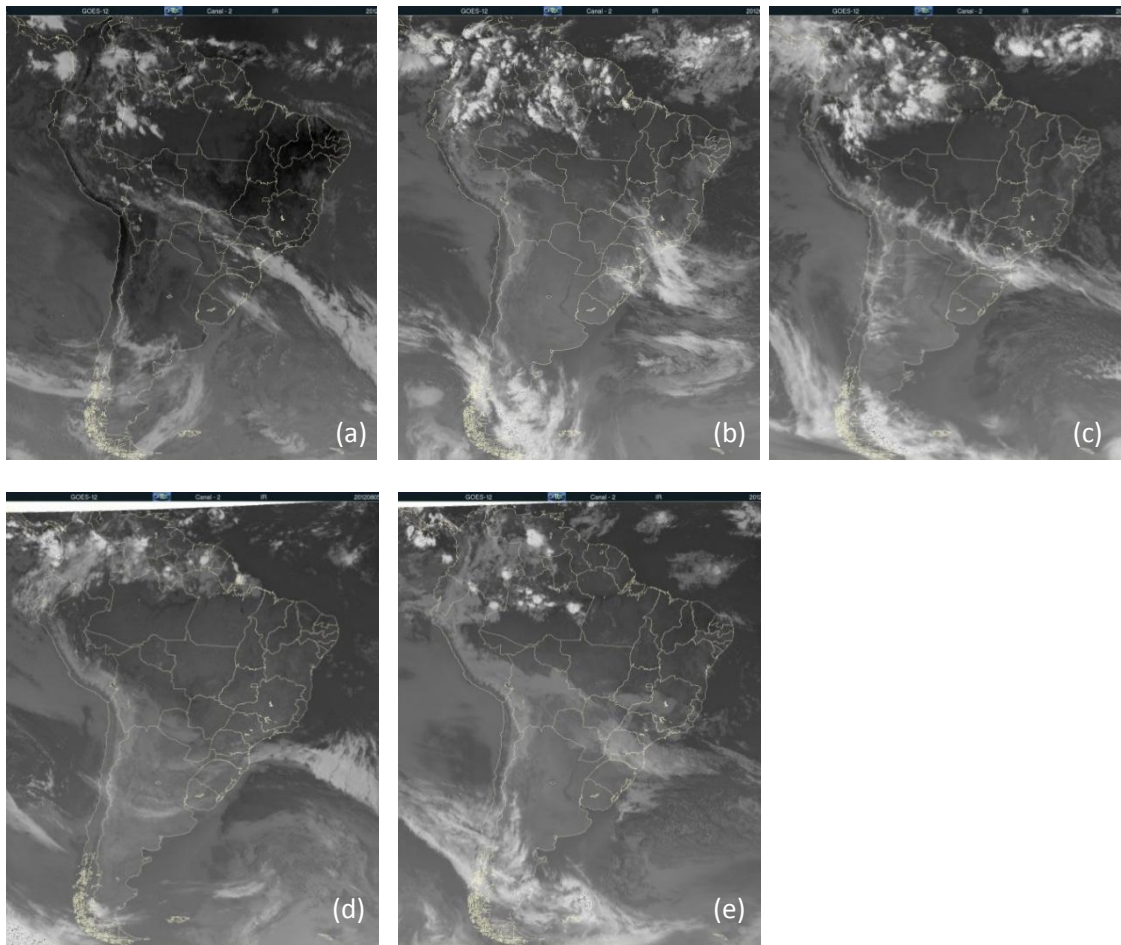
Figure 2.2: Infrared satellite images (GOES-12) for the five cold fronts identified during the ambient campaign: (a) 7th July, (b) 17th July, (c) 30th July, (d) 5th August (e) 28th August (CPTEC, 2014).

During July, the temperatures ranged from 11 to 20°C. The precipitation during this period was associated to cold front entrances, mainly on 17th July, when the maximum accumulated precipitation was observed (41.2 mm) and low pressure was associated to it. Additionally, the higher relative humidity values were also related to the entrance of cold fronts. During August, the temperatures were similar to those in July, with the minimum average daily value of 15°C. No significant precipitation was observed (Figure 2.3d). But due to the distance between the sampling point and the meteorological station, it could not be certainly affirmed that rain may have affected the sampling site.
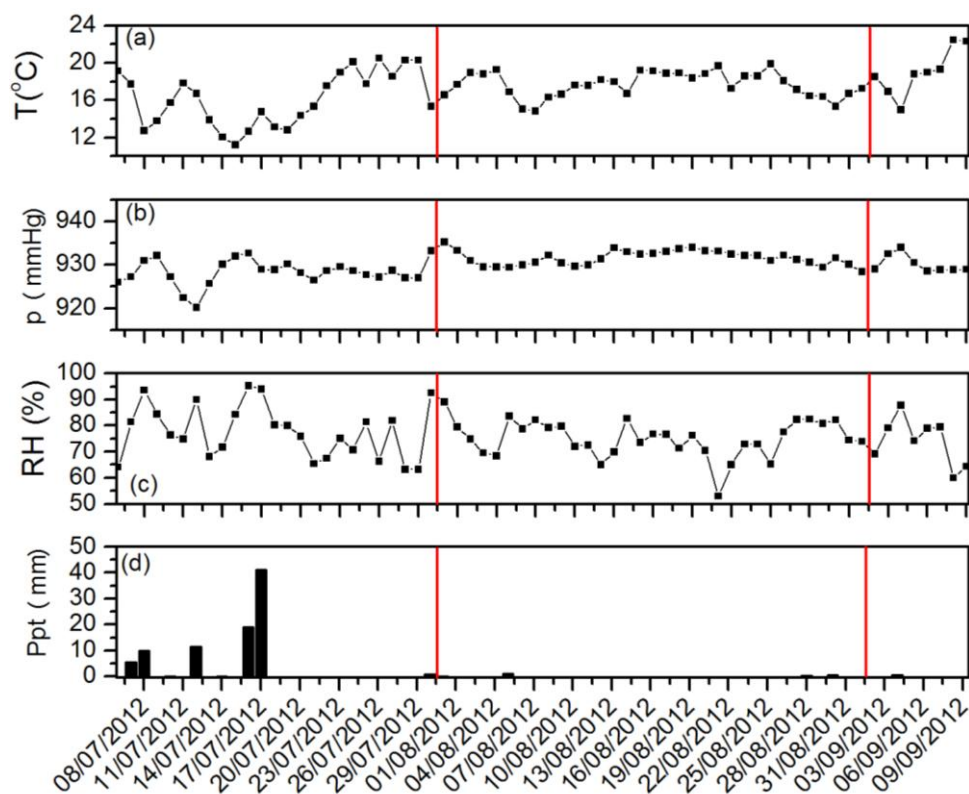
Figure 2.3: Average daily values of (a) temperature (in ^{o}C), (b) pressure (in mmHg) (c) relative humidity (RH, in %) and (d) accumulated precipitation for each day (in mm), at Agua Funda Meteorological Station during the ambient campaign. The red lines represent the beginning of August and September, respectively.

2.2. Inorganic analyses

PM$_{2.5}$ samples were collected on different membrane filters according to the compounds to be analyzed. Quartz filters were used for analyses of OC/EC and organic compounds speciation in the fine particulate matter. Polycarbonate filters were used for the following analyses of the inorganic fractions: mass concentration of PM$_{2.5}$, black carbon equivalent (BCe) determination, trace element composition, and concentrations of water-soluble ions. This section describes the methodology used to determine these compounds.

For the determination of mass concentration, the polycarbonate filters were analyzed by gravimetry, meaning by weighing the filters before and after sampling. A balance (Mettler Toledo, model MX5), with a nominal precision of 1 µg was used and operated in a controlled room at 22°C and relative humidity of 45%. The filters were weighted after their electrostatic charge was removed. This method is described in detail by Andrade et al. (2012), Brito et al. (2013) and Pérez-Martínez et al. (2014).

The black carbon equivalent concentrations were determined by optical reflectance using a smoke stain reflectometer (model 43D; Diffusion Systems Ltd, London, UK). The calibration curve used to convert reflected light into BC concentrations was determined and described by Hetem (2014).

The trace element concentrations were determined by a X-ray Fluorescence (PANalytical, model Epsilon 5) and the following species were identified: Na, Mg, Al, Si, P, S, Cl, K, Ca, Ti, V, Cr, Mn, Fe, Ni, Cu, Zn, Se, Br, Rb, Sb, and Pb. The methodology used in this work was the same as discussed by Brito et al. (2013). A more complete discussion of this method can be found in Spolnik et al. (2005).

2.3. Organic analyses

2.3.1. Proton-Transfer-Reaction Time-of-Flight Mass Spectrometer

A Proton-Transfer-Reaction Time-of-Flight Mass Spectrometer (PTR-ToF-MS, model PTR-TOF8000, Ionicon Analytik GmbH, Austria, referred to as PTR-MS hereafter) which is often used to perform the analysis of VOC's was adapted in this work to analyze organic compounds on the filters samples (collected by the low volume sampler, Partisol). The setup used is installed at the Institute for Marine and Atmospheric Research, University of Utrecht, Holanda. Briefly, the PTR-MS uses a soft chemical ionization technique, reducing the fragmentation compared to electron impact ionization. Reactions between protonated water (H_3O^+) and organic species in the sample lead to mostly non-dissociative proton transfers, with the advantage that most organic compounds can be detected quantitatively. A detailed discussion of this instrument, using a quadrupole detector, can be found in Hansel et al. (1995) and Lindinger et al. (1998), while Graus et al. (2010) and Jordan et al. (2009) describe the PTR-MS using the time-of-flight mass spectrometer.

The PTR-ToF-MS used in this study operated with the following settings: drift tube temperature at 120^oC; inlet tube temperature at 180^oC; and an E/N value of 130 Td.

A thermal desorption system was used for the filter sample analysis, as described by Timkovsky et al. (2015). In short, the setup consisted of a cylindrical quartz glass tube surrounded by two ovens: the first oven, where the sample was inserted using a filter holder, can be controlled over a temperature range of 50 to 350^oC. The second oven worked at a constant temperature of 180^oC. An aliquot of 0.20 cm^2 area from each filter was introduced to the first oven at 50^oC and heated in temperature steps of 50^oC from 100 to 350^oC, allowing 3

minutes for the measurement at each temperature. The N_2 flow rate (ultrapure nitrogen, 5.7 purity, Airproducts) was usually adjusted by a thermal mass-flow controller (MKS Instruments, Germany) at 100 ml/min, except for a few tunnel samples, which were measured at a flow rate of 50 ml/min. Pure N_2 was used as carrier gas and transported organic molecules desorbed from the sample to the PTR-MS. Each filter was measured three times and unless otherwise stated the respective average of the three replicas is presented and discussed hereafter.

2.3.1.1. TD-PTR-MS data treatment

The TD-PTR-MS data evaluation was performed with custom routines described in Holzinger et al. (2010) by implementing the widget-tool, using Interactive Data Language (IDL, version 7.0, ITT Visual Information Solutions), described in Holzinger (2015). In total, 762 ions were detected in the mass spectra. In order to avoid primary ions and inorganic ions, all ions with m/z<40 Da were excluded, except m/z 31.077 (CH_2OH^+) and 33.033 (CH_4OH^+). Additionally, ions associated with the inorganic ion NO_2^+ and higher water clusters (($H_2O)_2H_3O^+$) were removed. After this screening, the final mass list contained 712 ions that were attributed to organic molecules.

The concentration data (in volume mixing ratios, VMR, nmol/mol) had a temporal resolution of 5 s. Similar to the procedure described by Timkovsky et al. (2015), the instrument background ($VMR_{i,instrbgd}$), identified in Figure 2.4 by the first horizontal gray line, was subtracted from the measured volume mixing ratio ($VMR_{i,measeured}$) for each ion 'i' at each temperature step:

$$VMR_i = VMR_{i,measured} - VMR_{i,instrbgd} \quad (2.1)$$

Where: VMR_i is the volume mixing ratio of ion 'i' corrected by the background. This calculation was done for all filter samples and all field blanks. Figure 2.4 presents an example of this procedure: the sum of the volume mixing ratios for all m/z>50 Da per time interval of 5 s (also called cycles). The different temperature plateaus are separated by the vertical gray lines. The background is calculated by averaging the first eight cycles before heating starts as indicated by the first short horizontal line (close to zero). All other short horizontal lines represent the average VMR's obtained at each temperature step.

All filter samples were measured three times. From these measurements, the average of the VMR per filter was calculated for each ion i at each temperature step ($\overline{VMR_i}$). Note that all VMR_i values have been normalized to a N_2 carrier gas flow of 100 ml/min.
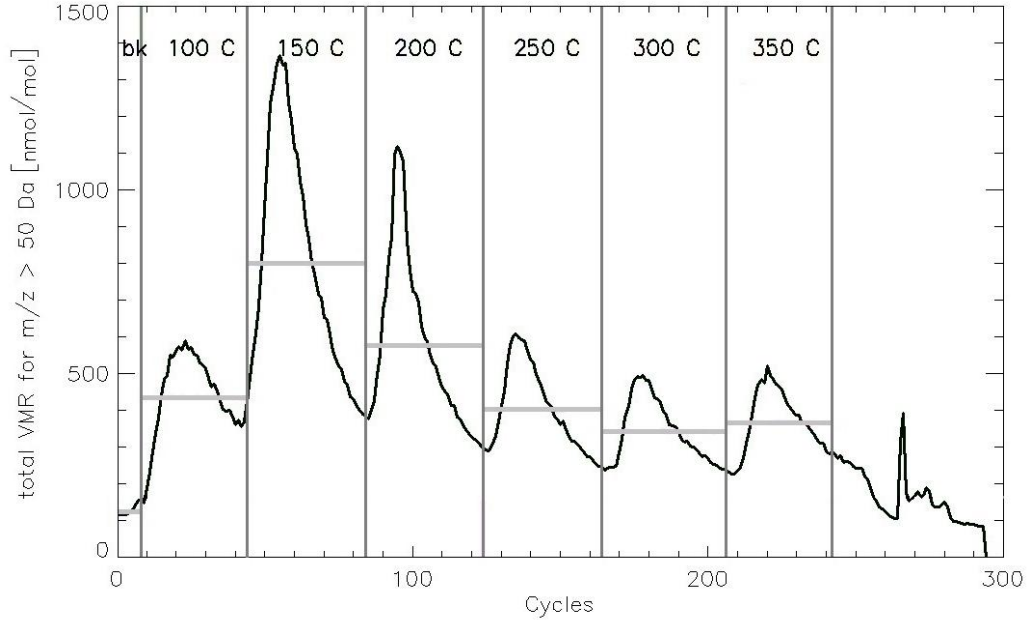
Figure 2.4: Example of a filter analysis (No. TRA 10, see below) by the TD-PTR-MS. The figure shows the total volume mixing ratios (VMR, in nmol/mol) of all ions above 50 Da with a temporal resolution of 5 s. The vertical lines represent the heating steps as indicated on the top of the figure. The horizontal gray lines between these vertical lines are the concentration averages at each temperature step, and the background level (the first short horizontal line) is subtracted from these values before further analysis.

A t-test was performed in order to confirm the statistical significance of the ion signals compared to the blank filters. After this test, 605 (TJQ), 627 (TRA) and 440 (ambient) ions were kept in the database as their signal was significantly above the signal of the blank filters.

For the remaining masses, the median VMR of the field blanks (*fb*) was subtracted from the average VMR of the sampled filters (($\overline{VMR_{i,sampled}}$)) for each ion '*i*' and each temperature step.

$$VMR_{i,final} = \left(\overline{VMR_{i,sampled}}\right) - \left(\overline{VMR_{i,fb}}\right)_{MED} \qquad (2.2)$$

The $VMR_{i,final}$ was used to calculate the concentration (in ng m^{-3}) for a specific ion '*i*', at a specific temperature step (C_i), according to Timkovsky et al. (2015):

$$C_i = \frac{VMR_{i,final} * M_i * V_{Nitrogen}}{V_{samp} * f} \qquad (2.3)$$

Where: M_i is the molecular weight of the ion '*i*' (minus one atomic mass unit (amu)., once TD-PTR-MS measures protonated ions), V$_{Nitrogen}$ is the amount of N$_2$ carrier gas (in mol),

V_{samp} is the volume of air during sampling (in m^3), and f is the area of the measured filter aliquot divided by the area of the whole filter (TIMKOVSKY et al., 2015).

The total concentrations (the sum of all temperature steps) estimated by the PTR-MS for tunnel and ambient campaigns are presented on Table A.1, Table A.3 and Table A.5, in the Appendix.

2.3.2. Thermal-Optical Transmittance

The filters collected by the mini-volume sampler were used for the quantification of Total Carbon (TC) separated in organic (OC) and elemental (EC) carbon using Thermal-Optical Transmittance (TOT) with a Sunset Laboratory Inc. instrument (Sunset labs, Tigard, USA) as described by Brito et al. (2013). The analysis was performed at the School of Molecular Sciences, Arizona State University. The evaluation of OC occurred at temperature steps of 310, 475, 615, and 870°C, with heating times ranging from 60 to 200 s. Furthermore, the EC measurements were performed at temperature steps of 550, 625, 700, 775, and 850°C for 45 s, and a final one at 870°C for 120 s. The concentrations over all temperature steps for the tunnel and ambient campaigns are presented in Table A.2, Table A.4 and Table A.6 in the Appendix.

Figure 2.5 presents a comparison of the concentrations obtained by the TOT, PTR-MS and reflectance methods. OC showed higher values than OA, which is due to fact that the TOT method converts all material to CO_2 and also reaches higher temperatures than the TD-PTR-MS. In addition, organic compounds can be combusted to CO_2 during thermal desorption, which is not measured by the PTR-MS. A good correlation between these two methods is observed for the ambient and the TJQ campaign (Figure 2.5a), but not for the TRA campaign. It may be related to the high concentrations of EC that might influence the determination of OC. A comparison between these two methods is discussed on the section 3.3. A comparison between EC and BC is presented on Figure 2.5b. BC presented higher concentrations than EC, related to the fact that the reflectance method gives the amount of aerosols that absorbs light. This does not only include EC, which explains also the correlation found for the ambient samples. A good correlation is observed during the TJQ campaign due to the fact that only one source, mainly vehicles, contributes to the emission of OC and EC.
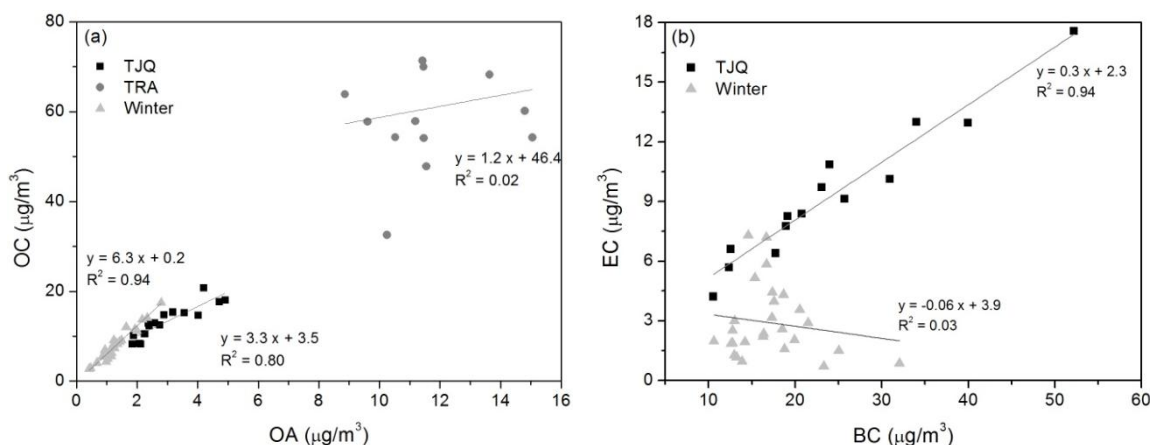
Figure 2.5: Comparison between (a) the OC (TOT method) and OA (PTR-MS method) concentrations (in $\mu g/m^3$) and (b) the EC (TOT method) and BC (reflectance method) concentrations (in $\mu g/m^3$).

2.3.3. Isotope-Ratio Mass Spectrometry measurements

Isotope-Ratio Mass Spectrometry (IRMS) is used to measure the relative abundance of stable isotopes, such as $^2H/^1H$, $^{13}C/^{12}C$, $^{15}N/^{14}N$ and $^{18}O/^{16}O$. In this study, the $\delta^{13}C$ values of particulate organic carbon collected on quartz filters are determined using a Delta IRMS.

A thermal desorption system was developed for the analysis of filter samples. The system used in this study was described and evaluated in detail by Dusek et al. (2013a). Briefly, the set up consisted of a cylindrical quartz glass tube surrounded by two ovens: In the first oven the sample was inserted using a filter holder and the temperature could be adjusted in a range between 50 to 400^oC. The second oven was filled with a platinum catalyst and was held at a constant temperature of 550^oC. This setup is installed at the Center for Isotope Research, University of Groningen, the Netherlands.

Before starting the measurements the system was flushed for 5 min with O_2 (at a flow of 50 ml/min), and then more 5 min with He (100 ml/min), with the filter in the first oven at room temperature. Under the same He flow, the sample was heated from 100 to 400^oC at temperature steps of 50^oC for 5 minutes each. At each temperature step organic compounds were desorbed from the filter. In the second oven these compounds were fully oxidized to CO_2. The CO_2 was concentrated and purified in two liquid nitrogen traps, followed by gas chromatography, in order to isolate CO_2 from any possible contamination such as NO_2 and N_2O. Water vapor was removed by a Nafion dryer before the flow entered the IRMS via an open split interface.

Filter pieces of 0.79 cm^2 were cut from filters collected in the tunnels. Pieces of 0.79 or 0.39 cm^2 were cut from filters of the ambient campaign, depending on the amount of material collected on the filter. Each sample was analyzed twice.

2.3.3.1.   IRMS data treatment

The Isodat NT 2.0 software was used to evaluate the thermograms. The δ^{13}C of each sample peak was first determined with respect to a pure CO$_2$ laboratory standard measured before each sample peak and subsequently converted to the VPDB scale using the known δ^{13}C value of the laboratory standard (-33.860‰). This software performs a standard correction for C^{17}OO isotopes, which have the same nominal mass like ^{13}CO$_2$.

The measured δ^{13}C values of an aerosol filter sample are corrected for contaminations due to filter handling and storage by δ^{13}C values measured on field blank filters:

$$\delta^{13}C_S = \left(\frac{\delta^{13}C_m \cdot A_m - \delta^{13}C_b \cdot A_b}{A_m - A_b} \right) \qquad (2.4)$$

Where: δ^{13}C$_s$ is the actual δ^{13}C value of the aerosol sample collected on the filter. The index '*m*' refers to the measured values of the filter samples, which includes aerosol and blank contribution and the index '*b*' refers to the blank filters. *A* is the peak area measured by the IRMS normalized by the size of the filter piece in the oven. This is proportional to the carbon amount desorbed at each temperature step per filter area.

A number of samples from the two tunnel campaigns and the ambient ambient campaign were selected for IRMS analyses. Filter ID's and their respective δ^{13}C values, already corrected for the blank values, are shown in Table 2.4 -Table 2.6. For the TJQ campaign, filters collected during the day (for 12 hours) were chosen as representative of the light-duty vehicular traffic (Table A.1, in the Appendix). The TRA campaign had fixed sampling times and no significant difference regarding the fleet profile and amount of vehicles running was noticed for the different sampling times inside the tunnel (Table A.1 and Table A.3). The ambient campaign samples were selected based on the air mass history by calculating 72 h back trajectories, using the model HYSPLIT (NOAA, 2014). The air mass history was often similar for a few days and therefore one of these samples was selected to represent this short period. Figure A.1 in the Appendix shows the 72 h back trajectories for the samples selected for IRMS analyses. The selected filter samples and their respective δ^{13}C values are shown in Table 2.6. In general, the air masses originated either from the continent (preferentially from the North East) or the ocean (usually South and South East). However, δ^{13}C values did not

show a consistent dependence on air mass back trajectories, which indicates that the regional influence of the metropolitan area was stronger than the long-range transport.

Table 2.4: δ^{13}C (‰) and IRMS peak area normalized by the area of the analyzed filter piece (in Vs/cm^2) per temperature step for the TJQ campaign.

T step (°C)	TJQ 14F		TJQ 15F		TJQ 16F		TJQ 17F		TJQ 18F		TJQ 19F	
	Peak area	δ^{13}C (‰)	Peak area	δ^{13}C (‰)	Peak area	δ^{13}C (‰)	Peak area	δ^{13}C (‰)	Peak area	δ^{13}C (‰)	Peak area	δ^{13}C (‰)
100	0.44	-27.00	0.36	-26.31	0.49	-26.48	0.75	-25.54	0.44	-25.90	0.27	-26.26
150	8.86	-27.26	6.08	-26.77	9.25	-27.21	8.28	-26.72	9.44	-27.11	6.23	-26.65
200	9.20	-27.08	5.76	-26.30	9.71	-27.15	8.15	-26.84	8.89	-26.99	5.86	-26.10
250	6.19	-26.05	2.06	-26.10	7.15	-26.15	6.61	-25.83	6.57	-26.03	2.35	-25.57
300	1.73	-25.96	1.04	-25.73	2.50	-25.03	3.71	-24.91	2.84	-24.89	1.27	-23.71
340	1.42	-25.40	0.84	-25.28	1.99	-24.90	2.96	-24.62	2.48	-24.60	1.12	-23.52
390	1.99	-25.69	1.13	-25.46	2.54	-25.19	3.71	-24.92	2.91	-24.63	1.43	-24.28

Table 2.5: δ^{13}C (‰) and IRMS peak area normalized by the area of the analyzed filter piece (in Vs/cm^2) per temperature step for the TRA campaign.

T step (°C)	TRA 08F		TRA 09F		TRA 10F		TRA 11F		TRA 12F		TRA 15F	
	Peak area	δ^{13}C (‰)	Peak area	δ^{13}C (‰)	Peak area	δ^{13}C (‰)	Peak area	δ^{13}C (‰)	Peak area	δ^{13}C (‰)	Peak area	δ^{13}C (‰)
100	1.01	-25.41	0.90	-25.32	0.95	-24.74	0.81	-25.08	0.76	-24.78	0.83	-25.12
150	8.12	-26.95	5.79	-27.29	7.68	-26.81	8.49	-26.95	7.70	-26.85	7.52	-26.79
200	6.95	-26.58	5.14	-26.43	5.93	-26.52	5.23	-26.42	4.91	-26.31	5.48	-26.71
250	4.64	-25.69	4.59	-25.58	3.76	-25.43	4.44	-25.42	4.28	-25.30	3.45	-26.22
300	2.65	-25.36	3.61	-25.27	2.99	-25.11	3.09	-24.96	3.74	-25.09	2.78	-25.66
340	1.68	-25.26	2.55	-24.71	2.34	-24.69	2.47	-24.40	2.02	-23.79	2.04	-25.74
390	1.91	-24.98	2.57	-24.75	2.34	-24.65	2.58	-24.14	1.94	-23.79	1.79	-25.22

Table 2.6: δ^{13}C (‰) and IRMS peak area normalized by the area of the analyzed filter piece (Vs/cm^2) per temperature step for the ambient campaign.

T step (°C)	HV 01		HV 02		HV 03		HV04		HV 05		HV-08	
	Peak area	δ^{13}C (‰)	Peak area	δ^{13}C (‰)	Peak area	δ^{13}C (‰)	Peak area	δ^{13}C (‰)	Peak area	δ^{13}C (‰)	Peak area	δ^{13}C (‰)
100	2.94	-25.36	4.17	-25.13	7.15	-24.87	4.38	-25.85	7.73	-25.27	1.60	-25.26
150	21.26	-25.87	57.90	-25.60	37.23	-25.20	25.54	-25.18	45.83	-25.01	13.93	-25.77
200	18.33	-25.67	41.32	-26.00	28.48	-24.98	21.18	-25.50	36.84	-25.38	11.03	-25.75
250	8.25	-24.37	22.36	-25.09	11.82	-23.32	13.74	-24.59	21.73	-24.37	6.83	-24.72
300	7.82	-24.04	20.42	-24.26	11.34	-23.32	12.50	-23.53	19.61	-23.31	6.09	-23.66
340	7.36	-24.05	19.19	-23.87	11.20	-23.25	12.82	-23.05	20.25	-22.88	5.57	-23.61
390	9.88	-24.47	24.51	-24.51	14.92	-23.83	15.68	-23.55	25.04	-23.27	7.69	-24.23

Table 2.6: continue

T step (°C)	HV 12		HV 14		HV 16		HV 19		HV 21		HV 24	
	Peak area	$\delta^{13}C$ (‰)	Peak area	$\delta^{13}C$ (‰)	Peak area	$\delta^{13}C$ (‰)	Peak area	$\delta^{13}C$ (‰)	Peak area	$\delta^{13}C$ (‰)	Peak area	$\delta^{13}C$ (‰)
100	2.52	-25.48	4.74	-26.03	2.57	-24.53	2.26	-24.96	1.51	-25.59	6.67	-25.05
150	13.63	-25.43	25.36	-25.69	18.85	-25.41	12.47	-25.40	11.24	-26.17	30.69	-25.56
200	12.60	-24.99	20.24	-25.50	18.04	-25.61	12.17	-24.54	7.32	-26.13	22.07	-25.89
250	5.42	-23.48	12.99	-24.51	7.94	-24.39	4.40	-22.40	4.96	-25.19	12.83	-24.84
300	4.93	-23.06	12.16	-23.77	7.48	-23.92	3.21	-22.66	4.35	-24.49	11.71	-24.00
340	5.02	-22.76	12.33	-23.67	7.03	-23.83	2.85	-22.22	3.88	-24.69	10.83	-23.74
390	7.38	-23.25	15.48	-24.02	11.26	-24.45	4.56	-22.94	4.67	-25.36	14.20	-24.75

Table 2.6: continue

T step (°C)	HV 25		HV 29		HV 30		HV 32	
	Peak area	$\delta^{13}C$ (‰)	Peak area	$\delta^{13}C$ (‰)	Peak area	$\delta^{13}C$ (‰)	Peak area	$\delta^{13}C$ (‰)
100	8.02	-25.75	4.09	-24.16	4.01	-24.58	5.78	-25.56
150	34.57	-25.80	36.74	-25.14	30.82	-25.21	43.38	-25.06
200	31.51	-25.54	34.16	-25.33	27.20	-25.15	43.08	-24.99
250	16.36	-24.67	17.89	-24.22	11.55	-23.27	28.53	-23.79
300	16.06	-23.82	17.52	-23.41	11.90	-23.49	28.17	-22.97
340	15.86	-23.32	17.17	-23.42	12.05	-23.38	28.62	-22.63
390	20.10	-23.92	22.18	-23.91	14.83	-23.98	34.16	-22.36

2.3.4. Accelerator Mass Spectrometry measurements

An Accelerator Mass Spectrometer (AMS) measured the abundance of ^{14}C in organic carbon and elemental carbon of the filter samples, separately converted to CO_2 by combustion in pure O_2 and separated from other interfering gases.

The methodology used in this work is similar to THEODORE (two-step heating system for EC/OC determination of radiocarbon in the environment) introduced by Szidat et al. (2004) and presented in detail by Dusek et al. (2014). In summary, the system consisted of two parts: (a) the extraction line, where the combustion and CO_2 formation took place and (b) the CO_2 purification line, where CO_2 was collected, purified, and stored. The first part of the system consisted of a quartz glass tube surrounded by three ovens. Oven 1 operated at 360°C and was used for OC combustion by keeping the filter sample for 10 min in this oven. Oven 2 was used for EC combustion: first the filter was water extracted to remove the water-soluble OC. Then the remaining water-insoluble OC was removed at 360°C for 10 min, followed by combustion for 3 min at 450°C to completely remove OC, along with a small fraction of EC. The remaining

EC was extracted at 650°C for 8 min. Oven 3 was filled with a platinum catalyst for a complete oxidation of all organic compounds to CO_2. Combustion took place in a pure O_2 flow at a flow rate of approximately 60 ml/min, regulated by a needle valve at the end of the combustion tube. Via the needle valve the flow entered the purification line. There, reaction products with sufficiently low vapor pressure were frozen in a cryogenic trap, while the O_2 gas was removed by pumps. Subsequently, CO_2 and other condensed gases were released from the trap and water vapor and nitrous oxides were removed.

The purified CO_2 was converted to graphite on a porous iron pellet in presence of hydrogen gas at a molecular ratio of H_2/CO_2 = 2.5. The water vapor formed during the process was cryogenically removed using Peltier cooling elements. After the graphitization, the pellet is pressed into 1.5 mm target holders and analyzed by Accelerator Mass Spectrometry at the Center for Isotope Research (CIO) at the University of Groningen.

The AMS system is a high-throughput mass spectrometer, dedicated to ^{14}C measurements (VAN DER PLICHT et al., 2000). It simultaneously measures $^{14}C/^{12}C$ and $^{13}C/^{12}C$ ratios. Samples are analyzed along with oxalic acid (HOxII) and ^{14}C-free reference materials (graphite and ^{14}C-free CO_2 gas). The $^{14}C/^{12}C$ ratio of each sample is reported as modern carbon fraction and normalized for fractionation to $\delta^{13}C$ = -25‰ using the $\delta^{13}C$-value measured by the AMS. Contamination during the extraction, graphitization, and AMS measurement causes an increase of $F^{14}C$ values of the ^{14}C-free reference materials, and a decrease in $F^{14}C$ of the HOxII with decreasing sample size. The deviation from the nominal $F^{14}C$ values of the standards can be used to calculate the contamination with modern and fossil carbon, respectively, which in turn can be used to correct the samples for these contaminations (DE ROOIJ; VAN DER PLICHT; MEIJER, 2010). With the set-up used in this study, the modern carbon contamination during the graphitization process and AMS measurement was around 0.4 μg C. The fossil carbon contamination was around 1.5 μg C. The fossil and modern carbon contamination of extraction and graphitization combined are around 5 and 2 μg, respectively, based on two combustion standards taken during this analysis. The value of 5 μg fossil contamination is an outlier and is usually significantly lower, roughly 2 μg, based on repeated measurements of the standards over several years. These combustion standards were used only as internal checks. The correction of the filter samples for contamination, not only during extraction and graphitization, but also during handling and storage, was done by using field blank filters. The blank correction was performed similarly as for $\delta^{13}C$ measurements:

$$F^{14}C_S = \frac{F^{14}C_m \cdot L_m - F^{14}C_b \cdot L_b}{L_m - L_b} \qquad (2.5)$$

Where: $F^{14}C_s$ is the $F^{14}C$ value of the aerosol sample collected on the filter. The indexes '*m*' and '*b*' are related to the measurements of sampled filters and blank fields, respectively and '*L*' is the carbon mass concentration on the filter in μg/cm^2.

Table 2.7: Amount of carbon (in μg C/cm^2) for the blank filters and sampled filters for tunnel and ambient campaigns, respectively

	Tunnels			Ambient		
	Blank	Sampled		Blank	Sampled	
		TJQ	TRA		Weekend	Weekday
OC	0.53	9.77	21.78	0.71	32.58	27.41
EC	0.21	4.05	74.18	0.12	11.20	12.46

The extraction was performed on all remaining pieces of filters from previous analyses (using PTR-MS and IRMS). Only for the TJQ campaign, the nighttime samples were excluded for not being representative of the vehicular fleet, due to the small number of vehicles in circulation. For the tunnel campaigns, all the filter pieces from one tunnel were collected in one large filter holder and combusted together. The ambient extractions were divided into weekend and weekday samples. The fact that the volume of vehicles running during the weekend is considerable lower than during the week, leads to a better comprehension of vehicular fleet influence on the aerosol composition. The ^{14}C values discussed in section 3.4 are therefore an average over many individual filter samples. The amount of carbon (in μg C/cm^2) extracted per campaign is shown on Table 2.7. These values do not correspond directly to the OC and EC concentrations; they are related to the amount of material extracted from the filters to perform the ^{14}C analysis.

2.4. Methodology for emission factor calculation

Emission factors (EF) in units of mg of pollutant per kg of burned fuel were calculated according to equation 2.6 (Martins et al., 2006; Kirchstetter et al., 1999; Miguel et al., 1998), assuming that under normal driving conditions the fuel is converted to CO and CO_2 while contributions from other carbon compounds are negligible:

$$EF_P = 10^3 \left(\frac{\Delta[P]}{\Delta[CO_2] + \Delta[CO]} \right) \omega_c \qquad (2.6)$$

Where: EF_P is the emission factor of pollutant P (in mg of P per kg of burned fuel); $\Delta[P]$ is the increase of [P] above the background levels (in ng/m^3); $\Delta[CO_2]$ and $\Delta[CO]$ are the

increases of the CO_2 and CO concentrations, respectively, above the background levels (in µg of carbon/m^3). The ω_c term is the fuel carbon weight fraction (in g of C/g of fuel) for a fuel c - ω_G = 0.757 for gasohol (26.5% ethanol, 73.5% gasoline) and ω_D = 0.818 for diesel (5% biodiesel, and 95% diesel).

The emission factors for LDV were directly calculated from the filters sampled in the TJQ tunnel due to the fact that LDV dominated the emissions in this tunnel. However, the HDV EF can just be estimated after subtracting LDV emissions from the samples collected in the TRA. Previous studies, also performed in tunnels, have shown that HDV and LDV emit comparable amounts of CO per travelled distance (KIRCHSTETTER et al., 1999; MIGUEL et al., 1998; PIERSON et al., 1996). The CO_2 emissions from the diesel burning could be estimated according to the following equation:

$$\frac{\Delta[CO_2]_D}{\Delta[CO_2]} = \frac{f_D\, U_D\, \rho_D\, \omega_D}{f_D\, U_D\, \rho_D\, \omega_D + ((1-f_D).\, U_G\, \rho_G\, \omega_G)} \tag{2.7}$$

Where $\Delta[CO_2]_D$ is the component of $\Delta[CO_2]$ related to the emissions from diesel vehicles (equal to HDV), f_D is the fraction of HDV, U is the average fuel consumption rate (75 g/km for gasohol and 251 g/km for diesel), ρ is the fuel density (765 g/l for gasohol, 854 g/l for diesel). The subscripts G and D denote gasohol and diesel, respectively.

The contribution of HDV to the concentration of a pollutant P can be estimated by the equation:

$$\Delta[P]_{HDV} = \Delta[P] - \Delta[CO](1-f_D)\left(\frac{\Delta[P]_{LDV}}{\Delta[CO]_{LDV}}\right)_{TJQ} \tag{2.8}$$

Where $\Delta[P]_{HDV}$ is the contribution of $\Delta[P]$, related to HDV emissions, $\Delta[CO](1-f_D)$ is the fraction of $\Delta[CO]$ attributed to the LDV emissions. The last term in equation 2.8 was calculated from the measurements in the TJQ campaign.

The presented EF's are the averages of several filters. The HDV emission factors are averages from all filters collected in the TRA tunnel, and the LDV emission factors are averages of all afternoon and 12 hours weekday samples from the TJQ tunnel, as these samples were less impacted by background ambient aerosol (see on section 3.3).

In order to calculate emission factors according to Kirchstetter et al. (1999) and Pérez-Martínez et al. (2014), ambient samples were used to determine background concentrations which were subtracted from the inside tunnel concentrations. The ventilation system in the tunnels brings the air from the outside to the interior by ventilation fans on the roof of the tunnel operating continuously to provide fresh air inside. The ambient samples were collected

on the roof of the Institute of Astronomy, Geophysics and Atmospheric Sciences building, located on the campus of the University of Sao Paulo. Previous studies were already performed at this site (MIRANDA et al., 2002; SÁNCHEZ-CCOYLLO; ANDRADE, 2002; YNOUE; ANDRADE, 2004). From 8th August to 9th September 2012 (winter time), daily PM$_{2.5}$ samples were taken at 9 am after sampling with a high volume sampler (1.13 m^3/min) for 24 hours. 31 filter samples were obtained in total. The analytical methods and data treatment used for these measurements were the same as for the tunnel samples. In order to minimize the effect of meteorological conditions, the concentrations were averaged over the sampled period and this average was used as the background concentration for both tunnel campaigns.

Many studies have been performed concerning the identification of the sources of atmospheric aerosols in Sao Paulo and they have shown that the dominant source of PM$_{2.5}$ is vehicular emission (ALBUQUERQUE; ANDRADE; YNOUE, 2012; ANDRADE et al., 2012). These studies, performed during the Southern Hemisphere wintertime, showed similar behavior in different years of analysis from 2010 to 2014 in terms of concentration and composition of the PM$_{2.5}$ fraction. The authors performed the identification of these sources using a multivariate analysis and found that the vehicular emissions explained 60% of the PM$_{2.5}$. Furthermore, PM$_{2.5}$ concentrations from different stations in the city of Sao Paulo showed similar yearly averages in 2011 and 2012 (CETESB, 2012, 2013c): 25 ± 19 µg/m^3. Therefore, the ambient data was considered as an adequate background concentration for the EF study in the tunnels.

2.5. Source apportionment methods

One important question considered in this study was the evaluation of the vehicular emission impact considering bio-fuels and fossil fuels. Since the samples collected inside the tunnels corresponded to primary vehicle emissions, it was possible to estimate the contribution of biofuels and fossil fuels to OC and EC in the tunnel (OC$_{tunnel}$ and EC$_{tunnel}$, respectively) by the following equations:

$$OC_{tunnel} = OC_b + OC_{f,tunnel} \qquad (2.9)$$

$$EC_{tunnel} = EC_b + EC_{f,tunnel} \qquad (2.10)$$

The indexes '*b*' and '*f*' correspond to biofuel and fossil fuel, respectively. Additionally, OC$_{tunnel}$ and EC$_{tunnel}$ average concentrations were determined by the TOT method. Since the fraction of modern carbon for fossil fuel is zero (F^{14}C$_f$ = 0), OC$_b$ and EC$_b$ can be obtained from equations 2.11 and 2.12

$$OC_b = \frac{F^{14}C_{OC\,tunnel} \cdot OC_{tunnel}}{F^{14}C_b} \qquad (2.11)$$

$$EC_b = \frac{F^{14}C_{EC\,tunnel} \cdot EC_{tunnel}}{F^{14}C_b} \qquad (2.12)$$

Where: $F^{14}C_{OCtunnel}$ and $F^{14}C_{ECtunnel}$ are the modern carbon fraction of OC and EC in the tunnels, respectively, obtained from AMS measurements. $F^{14}C_b$ is the fraction of modern carbon for biofuels, such as ethanol and biodiesel. Table 2.8 presents the parameters used for the source apportionment.

Table 2.8: Summary of parameters used for source apportionment of OC and EC concentrations

Parameter	Value	Reference
$F^{14}C_b$	1.04	Lewis et al. (2004)
$F^{14}C_{other,sec}$	1.07	Gelencsér et al. (2007)
$(OC/EC)_{bb}$	5	Szidat et al. (2007)
$\delta^{13}C_{C3}$	-28.00	Smith and Epstein (1971)
$\delta^{13}C_{C4}$	-16.00	Turekian et al. (1998)

A more complex source apportionment is necessary for the ambient campaign, since more and different sources contribute to OC and EC concentrations in the ambient air samples. The average concentrations of OC and EC were determined from the TOT measurements, by selecting the same filters analyzed by IRMS. The main sources for EC are biomass burning (EC_{bb}) and vehicular emission (EC_{veh}), both related to primary emissions. Considering that only these sources contribute to EC, it can be expressed as:

$$EC = EC_{bb} + EC_{veh} \qquad (2.13)$$

EC_{veh} can be estimated by isolating EC_{bb} (Eq 2.13) and replacing it in the following equation:

$$F^{14}C_{EC} \cdot EC = F^{14}C_{bb} \cdot EC_{bb} + F^{14}C_{EC\,veh} \cdot EC_{veh} \qquad (2.14)$$

Where: $F^{14}C_{EC}$ is the fraction of modern EC measured by the AMS, $F^{14}C_{bb}$ is the fraction of modern biomass burning (Table 2.8), and $F^{14}C_{EC\,veh}$ is obtained from the tunnel campaigns. In this study, $F^{14}C_{EC}$ from the TRA tunnel was used for $F^{14}C_{ECveh}$, because it is more representative of the vehicular fleet running around the city, containing both light and heavy duty vehicles, whereas the TJQ tunnel had restrictions for HDV and is therefore mainly representative of the LDV fleet.

OC is separated into primary and secondary OC, OC_{prim} and OC_{sec}, respectively:

$$OC = OC_{prim} + OC_{sec} \qquad (2.15)$$

Furthermore, OC_{prim} is determined as the sum of vehicular ($OC_{veh,prim}$) and biomass burning ($OC_{bb,prim}$) contributions:

$$OC_{prim} = OC_{veh,prim} + OC_{bb,prim,} \qquad (2.16)$$

where $OC_{bb,prim}$ is obtained from a typical ratio of OC/EC in biomass burning given by the literature (5, Table 2.8), and $OC_{veh,prim}$ can be estimated from the $(OC/EC)_{veh}$ ratio found in TRA campaign. Then OC_{sec} can be estimated by combining eq 2.15 and 2.16.

The modern carbon factions of OC_{prim} and OC_{sec} ($F^{14}C_{OC,prim}$ and $F^{14}C_{OC,sec}$, respectively) are important to estimate the sources of OC_{sec}. $F^{14}C_{OC,prim}$ can be estimated as follows:

$$F^{14}C_{OC\ prim} = \frac{F^{14}C_{bb} \cdot OC_{bb,prim} + F^{14}C_{OC,veh} \cdot OC_{veh,prim}}{OC_{prim}} \qquad (2.17)$$

Where: $F^{14}C_{OC\ veh}$ was determined from the tunnel samples.

Furthermore, $F^{14}C_{OC,sec}$ is given by the equation:

$$F^{14}C_{OC\ sec} = \frac{F^{14}C_{OC} \cdot OC - F^{14}C_{OC,prim} \cdot OC_{prim}}{OC_{sec}} \qquad (2.18)$$

OC_{sec} sources can be estimated by a simple division into vehicular ($OC_{veh,sec}$) and contributions from other possible sources ($OC_{other,sec}$):

$$OC_{sec} = OC_{veh,sec} + OC_{other,sec} \qquad (2.19)$$

Additionally, $OC_{other,sec}$ can be estimated from:

$$OC_{other,sec} = \frac{(F^{14}C_{OCsec} - F^{14}_{veh})}{(F^{14}C_{other} - F^{14}_{veh})} \cdot OC_{sec} \qquad (2.20)$$

Where: $F^{14}C_{other}$ is the modern carbon fraction of other sources (Table 2.8), such as biogenic emission, industrial activities, cooking processes. Then $OC_{veh,sec}$ is calculated from equation 2.19. Therefore, the total OC concentration from vehicles (OC_{veh}) can be calculated from the sum of $OC_{veh,prim}$ and $OC_{veh,sec}$.

The aerosols collected during the ambient campaign had a strong influence from the surrounding vegetation. The sampling point was surrounded by parks, containing forests, characterized by C3 plants, which did not lose their leaves during winter. Additionally, the

agricultural activities around the city of Sao Paulo mainly produce sugarcane, and the emission (either biogenic or from biomass burning) from these plants can affect the aerosol properties in the city. Therefore, a better understanding of possible contributions from vegetation is necessary. The source apportionment considering C3 and C4 plants (primary and secondary) takes also vehicular emissions into account, where OC_{veh} is estimated as described above. Then, OC_{C4} can be calculated from:

$$OC = OC_{C3} + OC_{C4} + OC_{veh} \qquad (2.21)$$

$$OC_{C4} = \frac{OC\left(\delta^{13}C - \delta^{13}C_{C3}\right) - OC_{veh}\left(\delta^{13}C_{veh} - \delta^{13}C_{C3}\right)}{\left(\delta^{13}C_{C4} - \delta^{13}C_{C3}\right)} \qquad (2.22)$$

Where: $\delta^{13}C$ and $\delta^{13}C_{veh}$ are the average of $\delta^{13}C$ measured by IRMS analyses for ambient and tunnel campaigns, respectively, and $\delta^{13}C_{C3}$ and $\delta^{13}C_{C4}$ are estimated from literature values (Table 2.8).

Table 2.8 summarizes the constants used for the source apportionment. The value used for $F^{14}C_b$ considered that biofuels are made of recent living material being in equilibrium with the atmosphere. The value $F^{14}C_{other,sec}$ represents contributions from other sources, such as biomass burning ($F^{14}C = 1.15$, Gelencsér et al., 2007) and BSOA ($F^{14}C = 1.04$, Genberg et al., 2011), and is in line with the approaches discussed in Gelencsér et al. (2007). There, the authors also considered a source apportionment using two sources: fossil and non-fossil sources. The $(OC/EC)_{bb}$ ratio showed large variability as discussed by Szidat et al. (2006), where the ratio was assumed to be equal to 5. However, different values are presented in the discussion section 3.4.1. The $\delta^{13}C_{C4}$ values assume that the contribution from particles during combustion of C4 plants were approximately 3.5‰ lighter than the unburned plants.

3. Results

3.1. Trace elements and particulate matter measured in the tunnel campaigns

Figure 3.1 and Figure 3.2 present the mass concentrations of $PM_{2.5}$ and BC, and the number of vehicles (LDV and HDV) for the TJQ and TRA campaigns, taken in May and July 2011, respectively. The concentrations are correlated to the number of vehicles: higher concentrations were observed during the occurrence of intense vehicle traffic. In general, lower values were observed during the early mornings and weekends. The relation between concentration and traffic was not linear because the emissions were higher during the traffic congestions. The TRA $PM_{2.5}$ average concentration was one order of magnitude higher than the TJQ average concentration, indicating that HDV emit more fine particles than LDV. Pérez-Martínez et al. (2014) confirmed this finding by calculating the emission factors for both type of vehicles. During the TJQ campaign, average BC represented 50% of $PM_{2.5}$, with a maximum of 90%, found on 11th May 2011; 20h. BC (TRA) concentrations were too high to provide the accuracy to perform a reflectance analysis, thus only the EC concentration is presented later with the other results from the TOT method. Nevertheless, it is clearly shown that HDV emit higher amounts of BC than LDV, especially for periods characterized by the presence of a large fleet of heavy duty diesel.

Figure 3.3 presents the average concentrations of $PM_{2.5}$, BC, OC, EC and trace elements, being the last measured by X-Ray Fluorescence, for the samples collected in TRA and TJQ. In general, the concentrations observed on the TRA campaign were higher than on TJQ campaign, related to the fact that HDV emit more particulate matter than LDV. However for some trace elements, such as iron (Fe) and copper (Cu), the highest concentrations were observed during the TJQ campaign. Table A.7 and Table A.8, in the Appendix, present the Pearson Correlation Coefficients among the trace elements and $PM_{2.5}$ for the two tunnel campaigns. The results of these analyses indicate the presence of two dominant sources discussed below. Differences among specific compound correlations between the campaigns can be attributed to different use of brakes. For example, in the TJQ campaign, breaks were used more often likely due to the lower speed limit in the city center and also to the higher number density of vehicles running only on two lanes. Besides this, traffic congestions are observed more often in the city than in the outskirts, where the TRA is located.
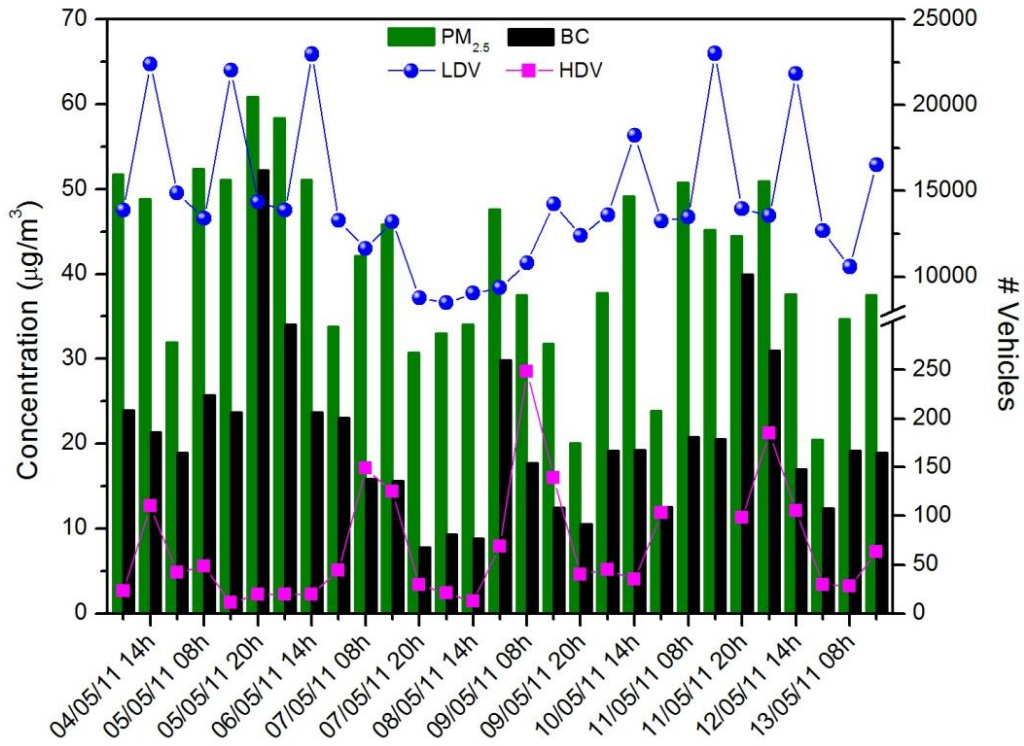
Figure 3.1: Concentrations of PM$_{2.5}$ and BC (both in μg/m^3), and total numbers of LDV and HDV during the TJQ campaign.
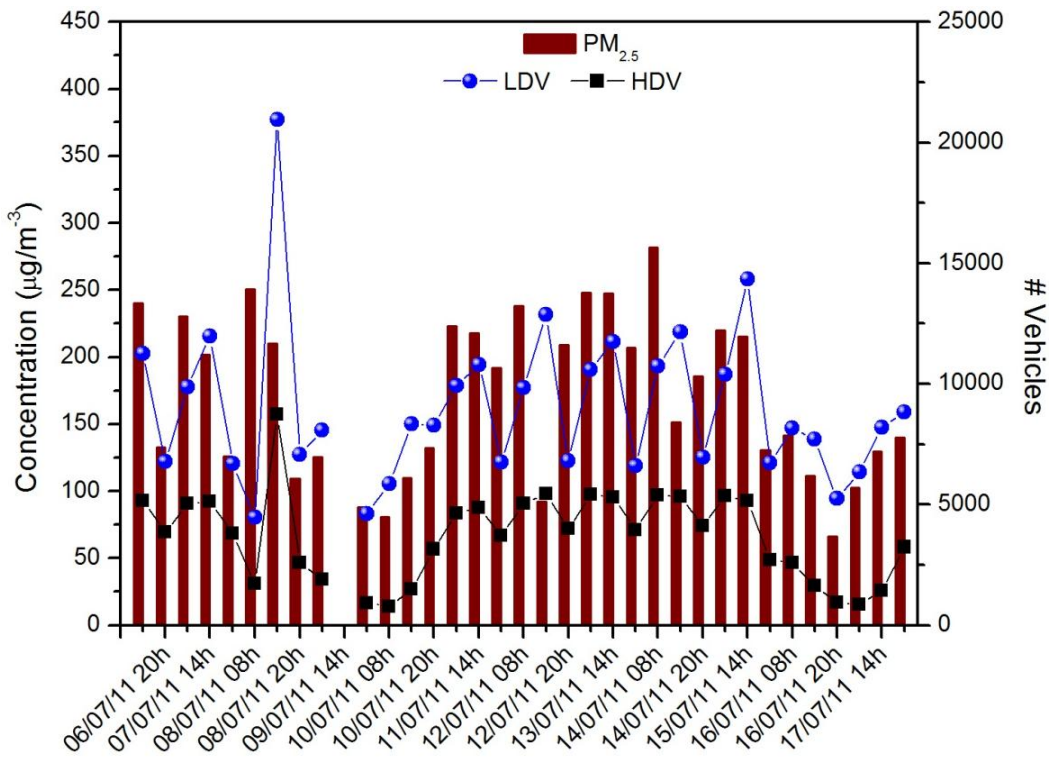
Figure 3.2: Concentrations of PM$_{2.5}$ (in μg/m^3), and total number of LDV and HDV during the TRA campaign.

Pio et al. (2013) distinguished two groups of sources using Pearson correlation analysis: one was associated to soil resuspension and the other to mechanical abrasion of engine and car parts. Although such clear distinction was not found here, it was possible to identify the same two groups by considering the trace elements that are characteristic for resuspended soil dust and vehicles in Table A.7. The group comprising Al, Si, K, Ca and Ti indicates soil source, while the group containing Cu, Fe, Mn, Cr and Zn is associated to the wear of vehicular brakes and tires.
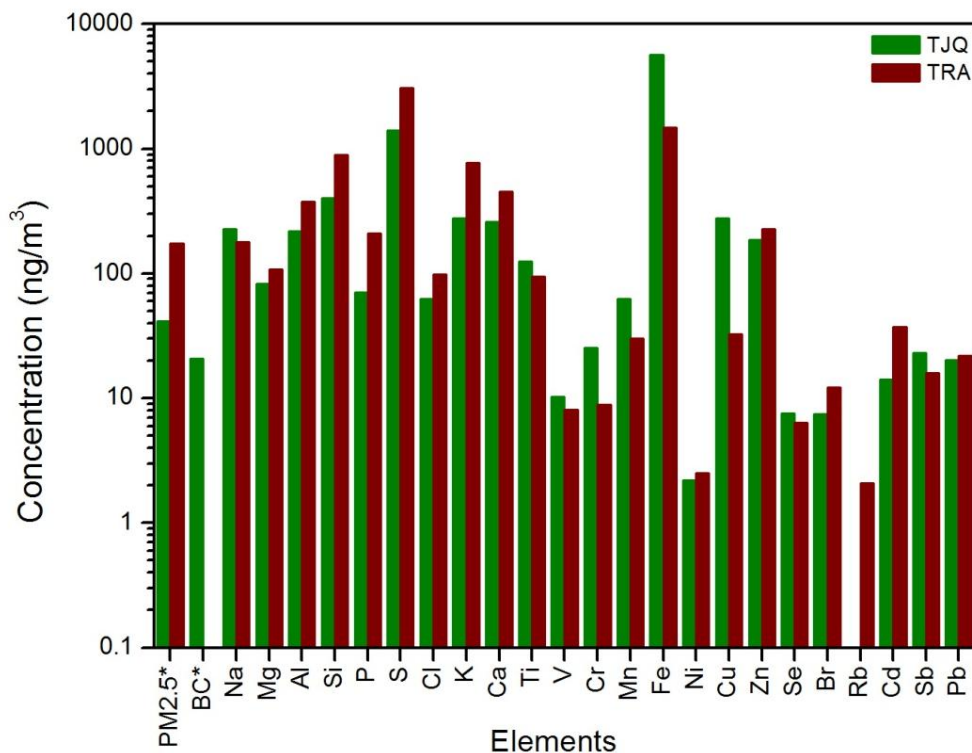
Figure 3.3: Average concentrations of $PM_{2.5}$ and BC (both in $\mu g/m^3$), trace elements and ions (in ng/m^3) for the TJQ and TRA campaign, respectively.

Table 3.1 shows the concentrations of $PM_{2.5}$, BC, OC, EC and inorganic compounds in their more frequent oxidized form measured in TJQ and TRA, which are also discussed in Hetem (2014). Detailed discussions of these campaigns and the analytical procedure for the tunnel measurements were presented by Brito et al. (2013) and Pérez-Martínez et al. (2014).

Although it was not possible to determine the BC concentration at TRA, Table 3.1 clearly shows that there is a significant fraction of $PM_{2.5}$ mass that is not explained by the inorganic fraction of the aerosols. This result illustrates the importance of studying the particulate organic fraction.

Table 3.1: Average concentrations and their respective standard deviations of $PM_{2.5}$, BC, EC and OC (all in $\mu g/m^3$) and inorganic species (in ng/m^3), partly in their oxidized form (modified from Hetem, 2014).

	TJQ	TRA
$PM_{2.5}$	41.2 ± 11.0	172.6 ± 60.6
BC	10.7 ± 4.1	--
EC	9.2 ± 3.3	123.5 ± 18.5
OC	13.3 ± 3.7	60.8 ± 15.2
Na	223.4 ± 126.0	180.0 ± 86.7
MgO	136.7 ± 73.9	176.7 ± 67.5
Al_2O_3	863.8 ± 525.8	1415.5 ± 558.1
SiO_2	918.5 ± 434.9	1909.1 ± 740.8
P	76.8 ± 40.3	216.0 ± 63.8
$(NH_4)_2SO_4$	6081.6 ± 2670.3	13430.3 ± 4622.4
Cl	60.7 ± 76.5	93.3 ± 89.0
KO_2	546.1 ± 303.9	1361.3 ± 641.2
$CaCO_3$	593.4 ± 230.3	1009.7 ± 483.4
TiO	206.3 ± 79.3	156.5 ± 54.1
V_2O_5	18.0 ± 10.4	13.6 ± 7.9
Cr	24.5 ± 11.7	8.9 ± 4.7
MnO_2	97.1 ± 40.2	47.1 ± 16.4
Fe_2O_3	7808.7 ± 3427.8	2102.6 ± 576.7
NiO	2.7 ± 2.0	3.2 ± 2.6
CuO	300.4 ± 144.7	36.8 ± 13.3
ZnO	232.3 ± 195.5	282.6 ± 112.9
As	2.2 ± 3.0	2.8 ± 1.9
Se	7.5 ± 5.0	6.2 ± 6.3
Br	8.0 ± 7.1	11.8 ± 6.2
Rb	1.1 ± 1.4	2.9 ± 3.5
Sr	5.4 ± 5.2	9.4 ± 8.2
Cd	14.2 ± 10.4	38.4 ± 31.4
Sb	23.2 ± 21.5	18.7 ± 14.9
Pb	20.9 ± 8.4	20.6 ± 16.4
Total mass explained (%)*	**18.3**	**22.6**

* summing up all compounds except BC, EC and OC (these last two were obtained from TOT analysis)

3.2. Source apportionment for the ambient campaign

Figure 3.4 presents the variation of $PM_{2.5}$ concentration during the ambient campaign. The highest concentrations occurred during the night, under conditions of low relative humidity (around 60%) and relatively high pressure (925 mmHg, see Figure 2.3). Thermal radiative inversions also collaborated to these high concentrations(CETESB, 2013b). Lower concentrations were observed during the days when the city was under the influence of cold fronts (Figure 2.2), and at periods with precipitation (Figure 2.3). The average concentration was around 20 $\mu g/m^3$, close to the value of 28 $\mu g/m^3$ found by Andrade et al. (2012) during a campaign performed between winter 2007 and winter 2008, next to an avenue with an intense traffic of vehicles.
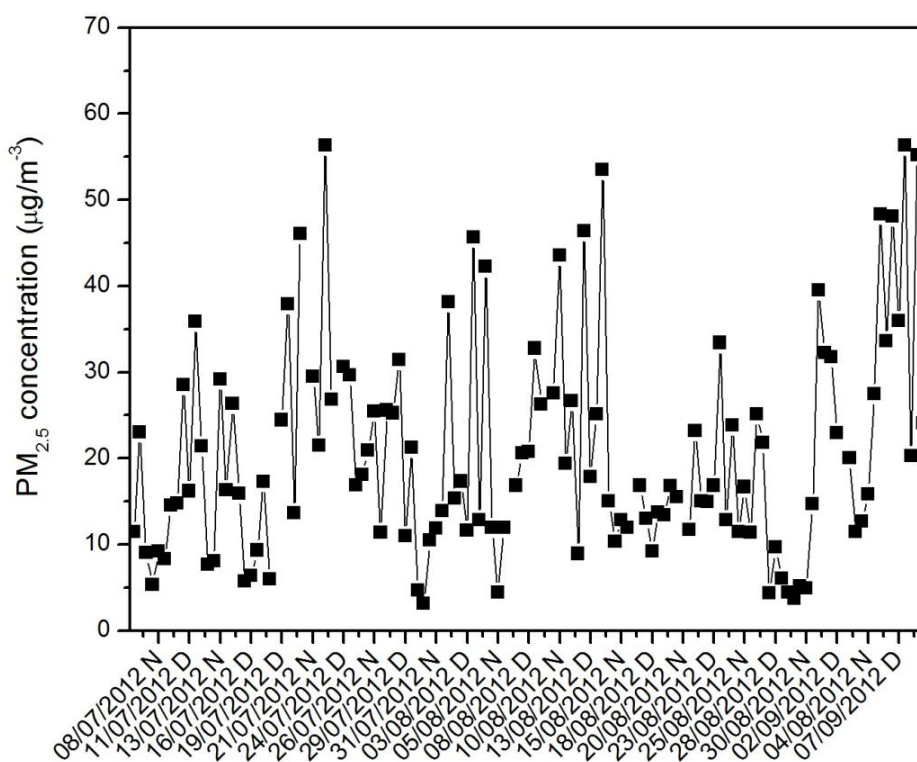
Figure 3.4: Variation of the $PM_{2.5}$ concentration during the ambient campaign (from 6th July to 9th September 2012). The indexes '*D*' and '*N*' correspond to day and night samples, respectively.

The trace element average concentrations for the present study is compared with the values found by Andrade et al. (2012) and are shown in Figure 3.5. No significant difference was found between the two campaigns with significant differences for Al and Si. These trace elements are usually associated to soil dust resuspension, indicating a local interference related to the sampling point. Trace elements emitted preferentially by vehicles and

vegetation, e.g. P, K and Cl, did not show significant differences between the campaigns. Once the vehicular emissions are the main source in the city of Sao Paulo, the source apportionment during the ambient campaign is now discussed.
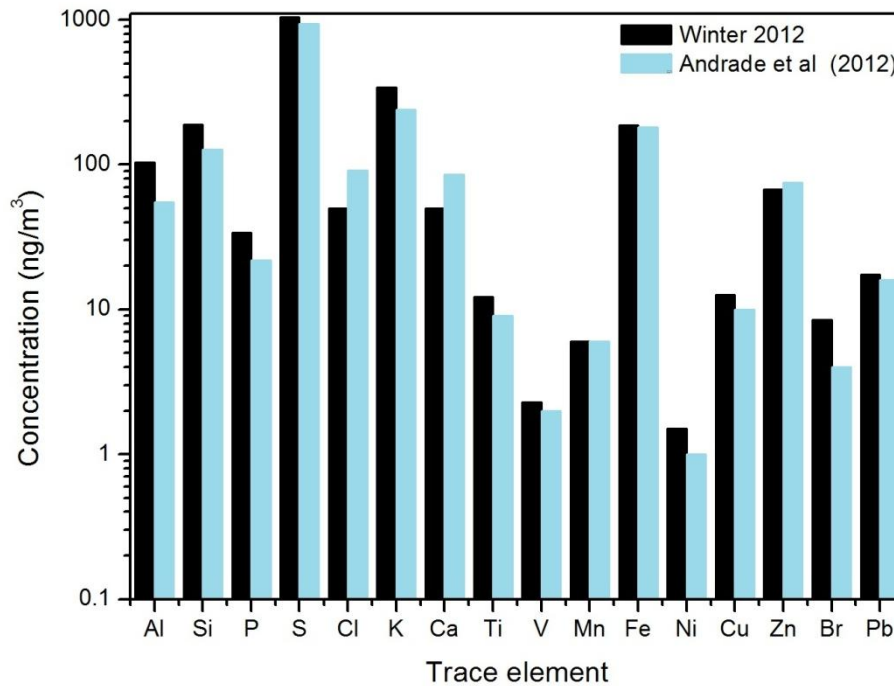
Figure 3.5: Trace element average concentrations (in ng/m^3) during the ambient campaign (2012) and results from Andrade et al. (2012).

Receptor models are an important tool to determine temporal and special variation patterns and to identify and quantify sources. Principal Components Analysis (PCA) is a very common receptor model used for source apportionment with many examples for Sao Paulo (ANDRADE et al., 2012; SÁNCHEZ-CCOYLLO; ANDRADE, 2002). The principle is to reduce a set of measurements comprising a large number of variables, often dependent to each other, to a much smaller set of new independent variables, called principal components. Details about this analytical method can be found in Thurston and Spengler (1985). The condition used here to retain the number of factors was based on the explained variance (eigenvalues) to be higher than 0.8, after varimax rotation. Table 3.2 shows the descriptive statistic, the factor loadings of the 4 retained factors and their respective communality. The 4 retained factors explained more than 80% of the total variance of the data. Additionally, the communalities showed high values (above 0.60), indicating a good adjustment. The high factor loadings were highlighted in Table 3.2.

Table 3.3 presents the 4 factors identified for the ambient campaign, characterized by the trace elements clustered by PCA. Regression analysis of the absolute factor scores for the

PM$_{2.5}$ concentrations was performed to estimate the source contribution. Factor 1 was related to soil dust resuspension/constructions, due to the high loadings of Al, Si, Ca, Ti, Mn, and Fe. Factor 2 represented vehicular emission as a possible source, showing high loadings of P and S. Additionally, PM$_{2.5}$ contributed also significantly to this factor, which means that factor 2 can also be associated to secondary aerosol formation. Factor 3 was related to vehicular emissions due to the presence of PM$_{2.5}$, BC, Cl, K, Cu, Zn, Br and Pb. Finally, V and Ni, associated to oil fuel burning, were found exclusively in factor 4. Although Fe was mainly characterized by Factor 1, this trace element also presents contribution in Factor 3, as well as Cu and Zn, which indicates vehicular tire wear, as discussed previously in the tunnel campaign sections.

Table 3.2: Descriptive statistic for concentrations of trace elements [ng/m^3] and PM$_{2.5}$ [µg/m^3], their respective factor loadings (*varimax* rotation), and communality [h^2] for ambient PCA analysis.

Element	Cases	Mean (SD)	Min	Max	F 1	F 2	F 3	F 4	h^2
PM$_{2.5}$	124	20.6 (12.4)	3.1	56.3	0.28	**0.55**	**0.71**	0.12	0.90
BC	116	3.3 (2.2)	1.0	11.7	0.54	0.11	**0.70**	0.08	0.81
Al	123	103.7 (75.6)	2.9	458.9	**0.85**	-0.14	0.27	-0.16	0.84
Si	122	191.3 (147.8)	0.6	985.3	**0.91**	0.01	0.12	0.02	0.84
P	120	33.9 (26.0)	1.1	127.6	0.03	**0.94**	0.11	0.13	0.92
S	124	1056.1 (719.3)	155.8	3998.6	-0.09	**0.96**	0.00	0.17	0.96
Cl	124	50.4 (90.6)	0.9	722.6	-0.02	-0.12	**0.86**	0.14	0.77
K	124	345.4 (251.9)	20.4	1468.7	0.58	0.17	**0.70**	-0.03	0.85
Ca	124	50.3 (29.6)	3.1	161.1	**0.87**	-0.18	0.08	-0.06	0.81
Ti	122	12.3 (7.7)	0.0	39.5	**0.86**	-0.01	0.28	-0.18	0.85
V	97	2.3 (1.9)	0.0	9.6	-0.10	0.27	0.22	**0.69**	0.61
Mn	114	6.1 (4.0)	0.1	18.5	**0.67**	0.28	0.08	0.37	0.67
Fe	124	190.7 (112.8)	8.4	490.6	**0.81**	0.26	0.39	0.17	0.90
Ni	112	1.5 (1.1)	0.0	4.8	0.01	0.06	0.09	**0.85**	0.74
Cu	124	12.8 (10.9)	0.3	75.1	0.33	0.08	**0.73**	0.22	0.69
Zn	124	68.7 (57.5)	1.3	343.6	0.26	-0.13	**0.81**	0.02	0.75
Br	108	8.6 (8.8)	0.1	49.4	0.21	0.07	**0.77**	0.02	0.64
Pb	119	17.6 (12.6)	0.4	54.5	0.03	0.30	**0.82**	0.14	0.78
		Eigenvalues			5.1	2.6	5.1	1.6	**Total**
		Varience explained (%)			28.4	14.3	28.2	8.8	79.7

In order to estimate relative contributions of the trace elements and BC to the PM$_{2.5}$ concentration, a regression mass balance was performed on ambient campaign data and the results are shown on Figure 3.6. The fraction of soil dust resuspension/construction was approximately 20% higher than the 13% contribution estimated by Andrade et al. (2012). Oil fuel burning represented less than 6%, while Andrade et al. (2012) reported 13%. Such differences can be explained by the different sampling points and sampling periods. On the

other hand, the vehicular emissions was the main source to $PM_{2.5}$ for both source apportionments: more than 60% (including the mixed source) and more 50% in Andrade et al. (2012).

Table 3.3: Source apportionment for the present study and Andrade et al. (2012)

Factor	Present work		Andrade et al. (2012)	
	Trace-elements	Source	Trace-elements	Source
1	Al, Si, Ca, Ti, Mn, Fe	soil / constructions	Al, Si, Ca, Ti, Fe	soil / construction
2	P, S, $PM_{2,5}$	Vehicular/ Secondary Aerosol	Cr, Ni, Cl, Mn, Cu	LDV
3	$PM_{2,5}$, BC, Cl, K, Cu, Zn, Br, Pb	Vehicular	Pb, BC, Cu, Zn, Br	HDV
4	V, Ni	oil fuel burning	NO_3^-, SO_4^{2-}, NH_4^+	oil fuel burning

Present work

- Not explained
- Soil dust resuspension/ contructions
- Vehicular/ Secondary Aerosol
- Vehicular
- Oil Fuel burning

1.1 µg/m³   0.9 µg/m³
4.1 µg/m³
7.6 µg/m³
6.7 µg/m³

Andrade et al. (2012)

- Soil / contructions
- LDV
- HDV
- Oil Fuel burning

3.8 µg/m³   3.8 µg/m³
3.5 µg/m³
8.0 µg/m³
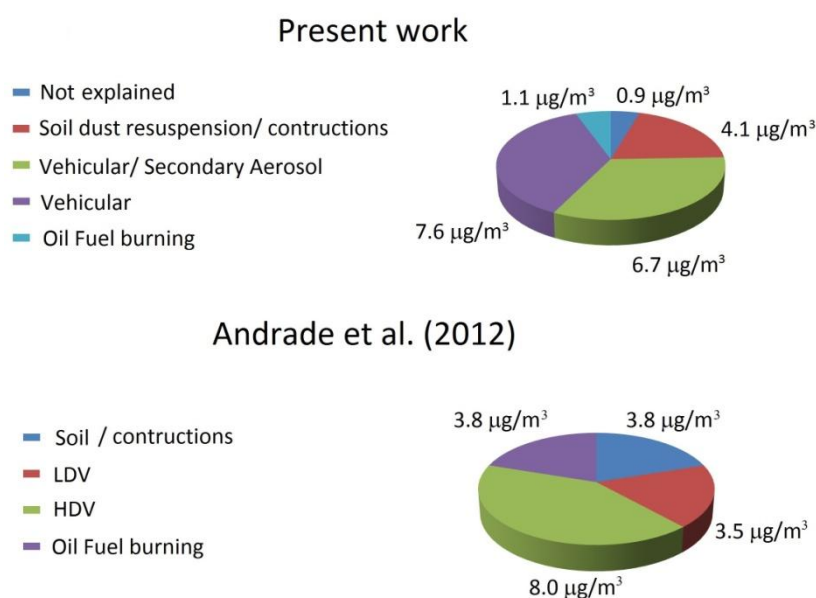
Figure 3.6: Source apportionment of total mass concentrations [µg/m³]during ambient campaign, using trace element and BC concentration for the mass regression, obtained from regression analyses of the absolute factor scores for the $PM_{2.5}$, for the present study and Andrade et al. (2012)

In summary, the present component analysis using trace elements concentrations confirmed that vehicular emissions are the main source of $PM_{2.5}$ in the city of Sao Paulo. Hetem, (2014) estimated that the total trace element contributions to the $PM_{2.5}$ concentration during the ambient campaign was around 30%, and BC corresponded to 15%, while more than 50% was not explained, possibly associated to organic contributions, which was also significant in other studies performed at Sao Paulo (ALBUQUERQUE; ANDRADE; YNOUE, 2012; BRITO et al., 2013). Considering that the OC average during the ambient campaign was 7.9 ± 3.6 µg/m³

(calculated from values presented on Table A.6, in the Appendix), the organic aerosol represented at least 40% of $PM_{2.5}$. Brito et al. (2013) found in tunnel measurements a contribution of OC to $PM_{2.5}$ of around 40%, while Albuquerque et al. (2012) attributed 30-60% of the remaining mass of the source apportionment to OC.

3.3. Emission factors of LDV and HDV

Table 3.4 shows EFs (in mg of pollutant per kg of burned fuel) for OC, OA, and total $PM_{2.5}$, as obtained by TOT, TD-PTR-MS, and gravimetrical analyses (Pérez-Martínez et al. 2014), respectively. All EF's were higher for HDV than for LDV. The OA emission factor calculated from PTR analysis is presented for all ions considering all temperatures and also separately for the compounds that contain oxygen atoms (O).

The EF of OC represented 36% and 43% of the EF of $PM_{2.5}$ for LDV and HDV, respectively. Brito et al. (2013) estimated OA/OC ratios of 1.6 and 1.5 for the TJQ and TRA campaigns, respectively. The use of these ratios and measured OC (TOT, up to $310^{o}C$) and OA concentrations (TD-PTR-MS, up to $300^{o}C$) indicate that the TD-PTR-MS quantified ~90% and ~75% of LDV and HDV emissions, respectively, which is in line with known loss processes in the TD-PTR-MS as discussed by Holzinger et al. (2010 and 2013).

Table 3.4: OA (TD-PTR-MS), OC (TOT) and $PM_{2.5}$ average emission factors (in mg/kg of burned fuel) and their standard deviations of the filters for LDV and HDV, respectively

	PTR-MS (OA)			TOT (OC)		Gravimetry[b]
	up to $300^{o}C$	Total[a]		at $310^{o}C$	From 310- $870^{o}C$	$PM_{2.5}$
		All compounds	Compounds with O			
LDV	27.4 ± 10.4	30.9 ± 12.2	21.0 ± 8.8	28.0 ± 7.9	108.3 ± 35.7	300 ± 100[b]
HDV	69.1 ± 15.0	74.5 ± 15.0	50.0 ± 11.0	58.6 ± 8.9	304.0 ± 81.4	700 ± 300[b]

[a] The sum of all EF over all temperature steps (from 100 to $350^{o}C$)

[b] Values obtained from Pérez-Martínez et al. (2014)

Table 3.4 also presents the EF of compounds containing oxygen for LDV and HDV. High contributions from oxygenated compounds were found to be around 70% for both LDV and HDV. This indicates that the fraction of oxygenated compounds in particulate matter is substantially higher than that found in the fuel. This can be associated to significant oxidation during the combustion, since photochemical processes are negligible inside tunnels due to the absence of sunlight.

Figure 3.7 shows the average EF (in mg/kg of fuel) mass spectra profiles for LDV and HDV, obtained from the TD-PTR-MS. As discussed above, HDV emitted higher concentrations of organic particulate compounds than the vehicles using gasohol. Differences between LDV and HDV are also seen from the chemical composition of the emitted particles. Several ions above 475 Da were detected from LDV emissions with the TD-PTR-MS, and only two compounds exceeded EF's of 0.250 mg/kg of fuel. In contrast, many compounds emitted by HDV exceeded 0.250 mg/kg of fuel, especially at m/z's at around 200 Da, however, no ions above 475 Da were detected.
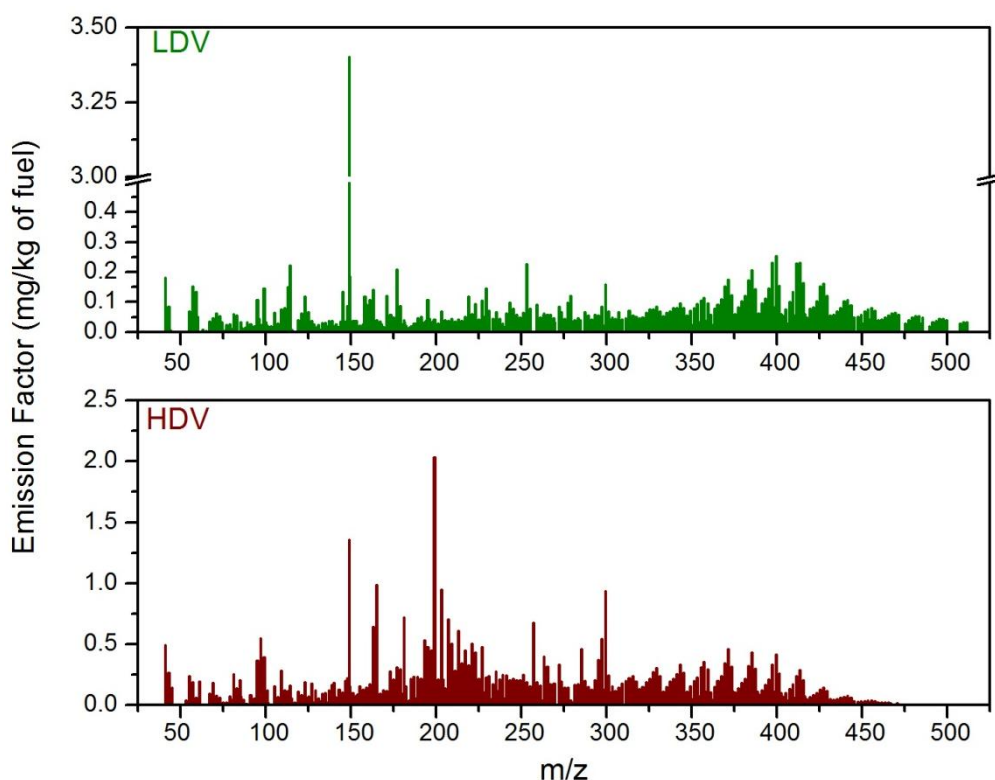
Figure 3.7: Average emission factor (mg/kg of fuel burned) mass spectra identified by the TD-PTR-MS for (a) LDV and (b) HDV.

Table 3.5 and Table 3.6 show the ten highest average EF values for both type of vehicles, as well as their m/z, their estimated empirical formula, the median, maximum and minimum EF values. The complete list of all compounds is shown in the Appendix (Table A.9). By using improved routines described in Holzinger et al. (2010), it was possible to attribute empirical formulas to the m/z's identified by the TD-PTR-MS, namely compounds with up to 16 atoms of oxygen and 2 atoms of nitrogen.

Table 3.5: The ten highest EF's (in mg/kg of fuel) for LDV.

m/z	Empirical Formula	Average ± SD	Median (Min, Max)
149.024	$C_8H_4O_3H^+$	3.403 ± 0.861	3.221 (2.252, 4.500)
399.391	$C_{25}H_{50}O_3H^+$	0.255 ± 0.043	0.261 (0.170, 0.305)
397.377	$C_{29}H_{48}H^+$	0.231 ± 0.038	0.234 (0.154, 0.277)
413.405	$C_{26}H_{52}O_3H^+$	0.231 ± 0.040	0.237 (0.155, 0.283)
411.39	$C_{26}H_{50}O_3H^+$	0.230 ± 0.054	0.226 (0.143, 0.327)
253.102	$C_{13}H_{16}O_5H^+$	0.227 ± 0.066	0.218 (0.128, 0.355)
114.091	$C_6H_{11}ONH^+$	0.223 ± 0.224	0.104 (0.046, 0.603)
177.055	$C_{10}H_8O_3H^+$	0.208 ± 0.174	0.173 (0.039, 0.586)
385.375	$C_{24}H_{48}O_3H^+$	0.206 ± 0.038	0.210 (0.133, 0.255)
149.131	$C_{11}H_{16}H^+$	0.187 ± 0.053	0.164 (0.119, 0.257)

Table 3.6: The ten highest EF's (in mg/kg of fuel) for HDV.

m/z	Empirical Formula	Average ± SD	Median (Min, Max)
199.041	$C_{12}H_6O_3H^+$	2.035 ± 0.351	2.013 (1.558 2.780)
149.024	$C_8H_4O_3H^+$	1.363 ± 0.493	1.181 (0.902 2.578)
165.02	$C_8H_4O_4H^+$	0.990 ± 0.210	0.965 (0.674 1.398)
203.087	$C_9H_{14}O_5H^+$	0.947 ± 0.181	0.905 (0.761 1.424)
299.289	$C_{19}H_{38}O_2H^+$	0.938 ± 0.242	0.884 (0.691 1.538)
181.08	$C_5H_{12}O_5N_2H^+$	0.722 ± 0.144	0.693 (0.557 1.076)
207.117	$C_{16}H_{14}H^+$	0.706 ± 0.144	0.684 (0.523 1.030)
257.246	$C_{16}H_{32}O_2H^+$	0.678 ± 0.474	0.475 (0.128 1.559)
163.04	$C_9H_6O_3H^+$	0.641 ± 0.137	0.630 (0.449 0.920)
213.06	$C_6H_{12}O_8H^+$	0.607 ± 0.108	0.613 (0.476 0.851)

The highest average EF was found for m/z 149.024 for the LDV with a value of 3.4 mg/kg of fuel. This compound was identified as $C_8H_4O_3$, tentatively attributed to phthalic anhydride. This compound is known for its use as plasticizers (responsible for the flexibility, resilience and transparency of the plastic) and it is also present in the plastic bags in which the filters (wrapped in aluminum foil) have been stored. Therefore, this peak potentially indicates a positive artifact due to the handling of the filters, however the blank filters that were also stored in plastic bags did not show a significant signal on this mass. Other speculation is the ion source contamination. However, there is no publication until now discussing this issue for measurements performed with the TD-PTR-MS. Decarlo et al. (2006), using the High-Resolution Time-of-Flight Aerosol Mass Spectrometer (HR-ToF-AMS), stated that the m/z 149 (phthalates) peak showed only little influence of real AMS measurements. Although these considerations could indicate that m/z 149.024 as a possible contamination/artifact, it is important to point out that the instrumental background, field blank, and ambient air

background subtractions were performed before calculating the emission factors. Therefore, this ion is most likely originating from real emissions. Furthermore, phthalic anhydride has been identified in the atmosphere. Another possibility would be that this compound is produced from octane present in gasoline. Higher values of octane in the fuel results in a higher resistance to auto ignition and consequently a lower chance for engine knocking (CERRI; D'ERRICO; ONORATI, 2013; WESTBROOK et al., 2011). However, this dataset does not suggest that m/z 149.024 might be a unique tracer for gasohol because this compound was also substantially emitted from HDV (1.363 mg/g of fuel, see Table 3.6). This can be due to the procedure used for the calculation of the HDV EF, which considers the subtraction of the LDV EF. It can be cautiously argued that m/z 149.024 may be a general tracer for aerosols emitted by vehicle exhausts. However, more research is necessary to clarify the origin of this compound.

The ion detected at m/z 149.131 ($C_{11}H_{16}H^+$), as presented in Table 3.5, was tentatively attributed to pentyl benzene. Pentyl benzene is a potential unique tracer for gasoline, as this compound is a known constituent of gasoline, e.g. Ramadhan and Al-Hyali (1999) used pentyl benzene to calculate the octane number in the fuel. The m/z 299.289 is potentially an unique tracer for HDV emissions. This ion was attributed to the formula $C_{19}H_{38}O_2H^+$, and tentatively attributed to methyl stearate, which is one of the main components found in biodiesel (NAIK et al., 2011). The emission factor for LDV was approximately a factor of 6 lower (see Table A.9, in the Appendix) than for HDV and this signal might originate from the low number of diesel fueled vehicles moving in the TJQ tunnel.
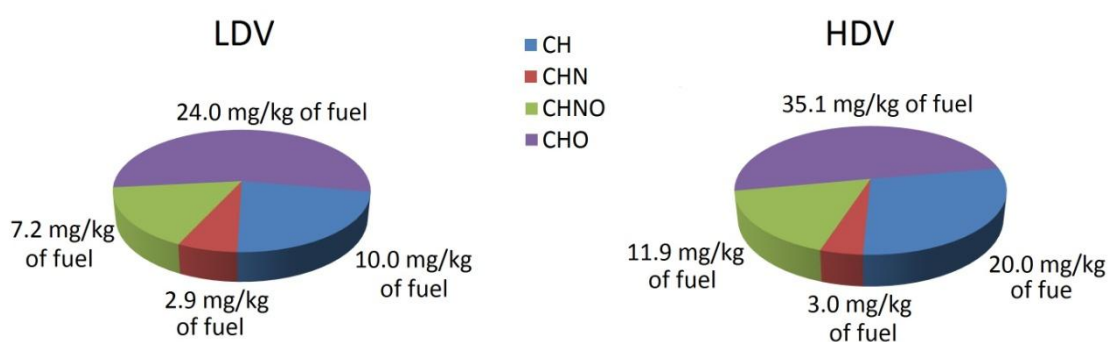
Figure 3.8: Total average emission factors calculated for LDV and HDV divided in groups containing CH, CHO, CHN, and CHON.

Figure 3.8 shows the average EF for LDV and HDV divided in groups containing: CH, CHO, CHON, and CHN. The hydrocarbon group (CH) presented an important contribution to the total EF. Contributions of nearly 25% for the LDV and 33% for HDV were observed.

Oxygenated hydrocarbons (CHO) showed highest contribution to emissions for both vehicle types, where LDV exhibited a slightly larger fraction than HDV. The nitrogen-containing groups contributed more than 20% to the measured OA. Since the presence of nitrogen in the fuels is insignificantly lower than in the aerosol, such a high percentage in the aerosol can be attributed to NO_x chemistry during the combustion process (thermal effect).

Figure 3.9 shows the relation between the atomic ratios H/C and O/C (Van Krevelen Diagram). The average O/C ratio calculated from the ambient air samples (ambient campaign) was higher than that measured in the tunnels. This can be associated to photochemical reactions in presence of sunlight producing oxygenated aerosol. The high H/C ratios found for tunnel samples indicated that fresh aerosols were collected on the filters due to primary emissions from vehicle exhausts, as expected.
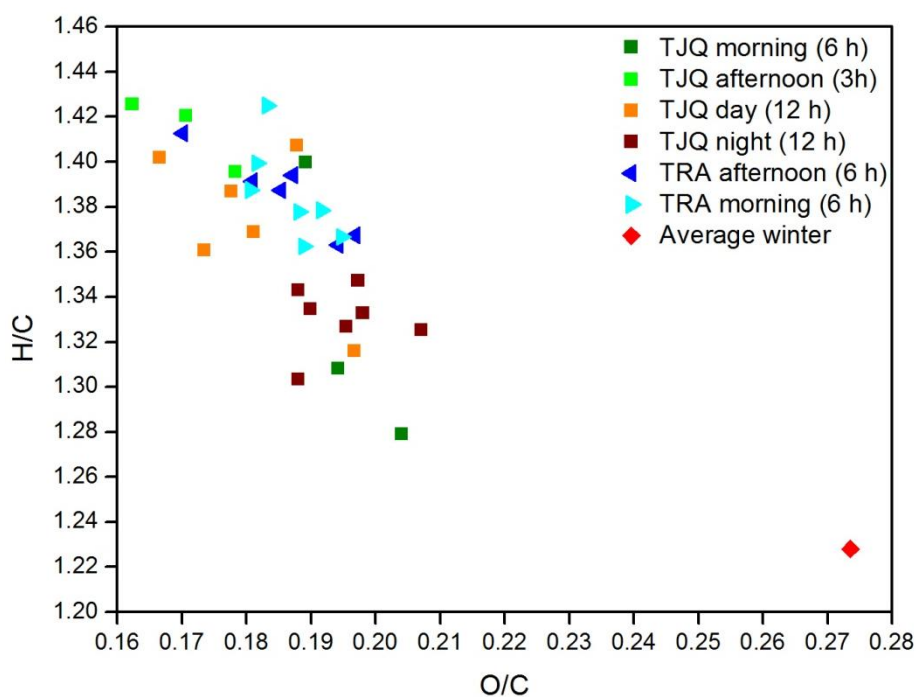
Figure 3.9: Scatter plot of the atomic ratios H/C against O/C (van Krevelen diagram) from TD-PTR-MS data for the TRA, TJQ and ambient campaigns.

The O/C and H/C ratios varied more for the samples collected during the TJQ campaign than for the samples collected in TRA, possibly due to the different sampling times (Table A.1 Table A.3). In general, the samples collected during the morning (for 6 h) and at night (for 12 h) were more oxidized than the others. This can be related to a smaller number of cars and consequently to less POA emissions. As a result, the contribution of external air was more significant during these times. The afternoon samples (sampled for 3 h) were collected during the traffic congestion periods (between 5 and 8 pm - Brito et al., 2013) suggesting that POA

dominated the burden sampled on the filters. Samples collected during the day (for 12 h) were mainly dominated by afternoon traffic congestion profile. Consequently, the 12h-day samples and the afternoon samples from the TJQ tunnel were used to calculate LDV emission factors.

The O/C ratios considered for EF calculation ranged between 0.16 and 0.20 (O/C), indicating a higher amount of oxygen in POA than reported in previous studies. Chirico et al. (2011) found O/C ratios ranging between 0.073 (workday) and 0.199 (weekend). Collier et al. (2015) estimated O/C ratios around 0.19 for low particulate matter concentrations, measured from vehicles in a dynamometer. Given the fact that O/C ratios measured with the TD-PTR-MS are biased low (HOLZINGER et al., 2013), the values found here indicate a more oxidized aerosol originated from the fuels used in Brazil, which may be related to the use of ethanol (NOGUEIRA et al., 2014).

The distribution of the total emissions over the different desorption temperatures is presented in Figure 3.10. This analysis indicated that OA produced from HDV were more volatile than OA from LDV. This can be seen by the higher amounts of HC and HCO ions derived from HDV at desorption temperatures up to 200°C.
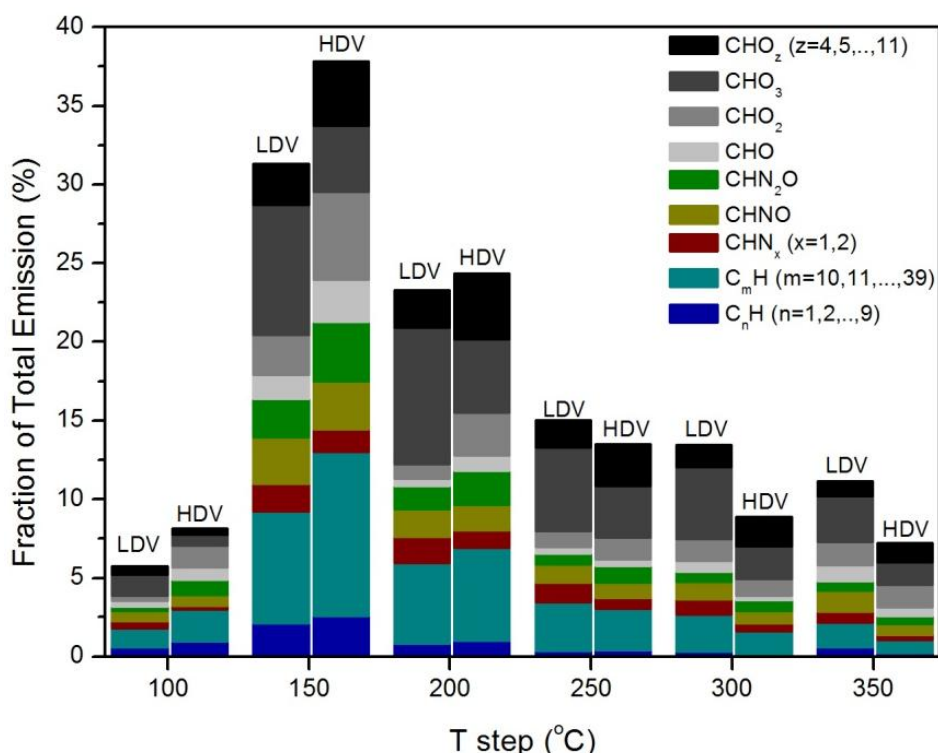
Figure 3.10: Fraction of total average emission (in %) divided into groups containing CH, CHO, CHON, and CHN, considering different numbers of carbon and oxygen atoms in the compounds, for LDV and HDV at each temperature step.

Hydrocarbons (HC) represented the most volatile group. As expected, their volatility was related to the number of carbons present in molecules: short-chain hydrocarbons (up to 9 carbon atoms) were more volatile than the long-chain ones (more than 9 carbon atoms). The short-chain HC contribution was substantially low at 250°C and higher temperatures while the long-chain HC contribution was still significant at 350°C.

HDV emitted more volatile nitrogen compounds than LDV. Such distinction between the two categories of vehicular fleet was not observed in previous studies.

The oxygenated hydrocarbon compounds containing up to 2 oxygen atoms emitted by HDV were more volatile, as can be seen by the histogram at the 150-200°C temperature steps. LDV emitted more volatile compounds containing three oxygen atoms due probably to the high contribution of phthalic anhydride ($C_8H_4O_3$), as presented in Table 3.5. Compounds containing more than 4 oxygen atoms were less volatile than compounds from other groups.

3.4. Source apportionment results

The values obtained from IRMS analyses were averaged over the whole campaign and the results are shown on Figure 3.11. The peak areas normalized by the area of the analyzed filter piece (in Vs/cm^2) were averaged for all filters analyzed, per each temperature step per campaign. For a better comparison among the campaigns, these average peak areas were presented as percentage of the total peak area summed over the temperature steps in Figure 3.11a. At 100°C, less than 5% of carbon was desorbed both in the tunnels and the ambient air. At 150 and 250°C, the normalized peak areas from the tunnel samples were higher than from the ambient samples, indicating that the ambient OC was less volatile than OC emitted by vehicles. More than 20% of the ambient OC during the ambient campaigns was desorbed at 350 and 400°C. Weekday samples had less material on these last two temperature steps than weekend samples. A comparison between the tunnels showed that in TJQ where found more volatile aerosol than in TRA, mainly observed at 200°C, which is not in line to the findings of the previous section. This could be due to the fact that PTR-MS measures the mass of the total organic compound (including compounds containing oxygen and nitrogen), whereas IRMS peak is related to the total mass of carbon (the organic material was converted to CO_2 during the IRMS analysis), besides that the thermal desorption may produce CO_2, which is not measured by PTR-MS.

Figure 3.11b presents the average δ^{13}C values for tunnels and ambient campaigns per temperature step. Since there is an amount of material that was not evaporating at 100°C, the

$\delta^{13}C$ values for the first temperature step have large uncertainties, and therefore the discussion will focus on the temperature steps ranging from 150 to 400°C. For all campaigns, more enriched values were related to higher temperatures. Considering all temperature steps, the $\delta^{13}C$ values for the ambient winter aerosol ranged from -25.6 and -22.8‰, $\delta^{13}C$ for tunnels ranged from -24.6 and -27‰. That means that the ambient samples were enriched compared to the tunnel samples. One potential reason is the contribution from C4 plants, as the city of Sao Paulo is surrounded by sugarcane fields. Martinelli et al. (2002) found delta values from organic aerosol in the sugarcane field areas ranging from -20.0 to -22.8‰. A comparison between the weekends and weekdays during the ambient campaign shows that weekdays are associated with lighter $\delta^{13}C$ values than weekend (Figure 3.11b). The reason for this difference can be related to vehicular emissions, since higher contributions from vehicles decrease $\delta^{13}C$ values with respect to ambient values.
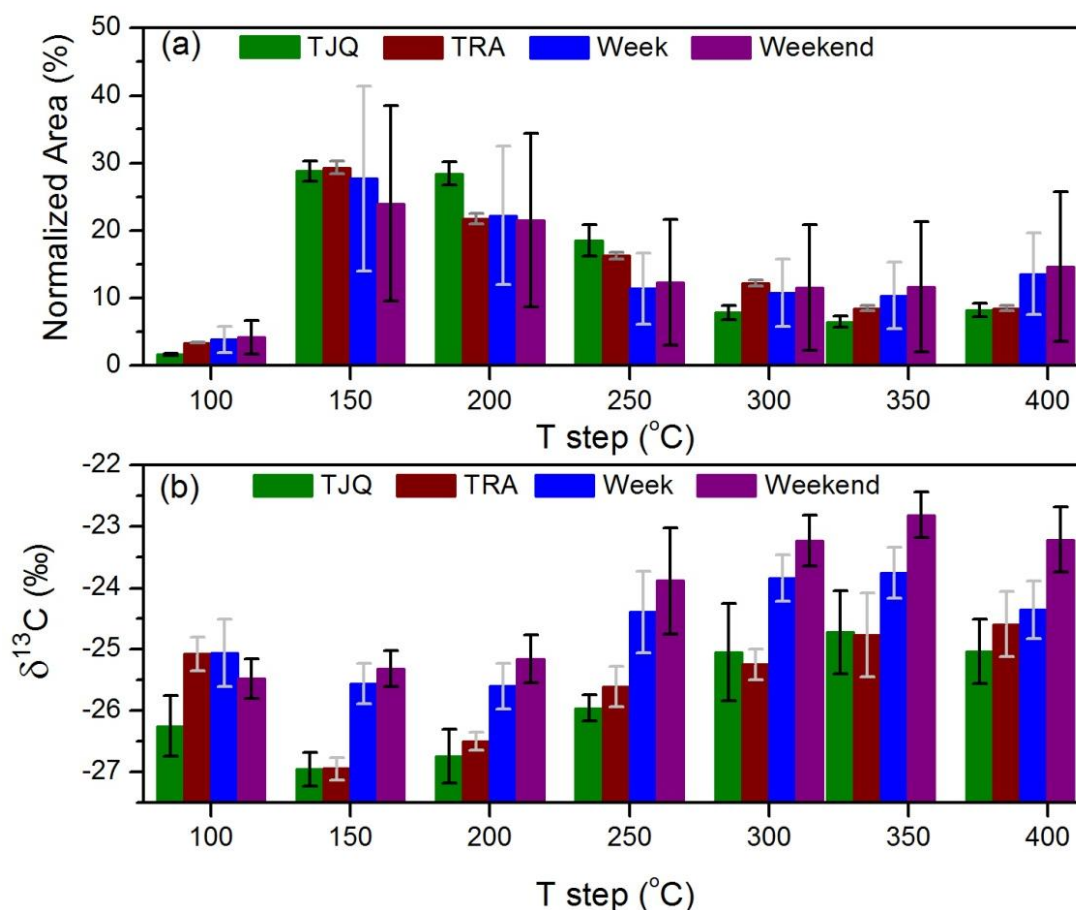
Figure 3.11: (a) IRMS average peak areas normalized and (b) average $\delta^{13}C$ values per temperature step for tunnels (TJQ and TRA) and ambient (split in weekday and weekend) campaigns. The error bars refer to standard errors of the means.

A comparison between the tunnel campaigns did not show significant differences, in spite of the significant presence of HDV in TRA (Figure 3.11b). It can be due to the fact that LDV still represented a high fraction (70%) of total vehicles running inside TRA. Furthermore, the use of ethanol in TJQ was not well characterized, since the sugarcane burning and its derivate (such as ethanol fuel) would expect to enrich the aerosol samples (MARTINELLI et al., 2002), however only a slightly enrichment on the δ^{13}C values of the aerosols sampled was observed in TJQ relatively to the TRA campaign. Therefore, there are two possible conclusions for this: (i) the amount of aerosols emitted by vehicles using ethanol is lower than by vehicles using gasoline; and (ii) the preferential fuel used by LDV was gasohol, other than the ethanol. However previous studies showed that the use of ethanol as fuel reduced the emission of particles. And the use of ethanol or gasohol in flex vehicles is not only function of relative prices between the fuels but also related to the personal decisions of the drivers (SALVO; HUSE, 2013).

In a review of studies from different parts of the world, Masalaite et al. (2012) presented δ^{13}C values measured in fossil fuels. They reported variations between -31.7 and -26.8‰, for gasoline, and between -31.9 and -27.4‰, for diesel. These ^{13}C-values are lower than the values showed in Figure 3.11b. This can be related not only to the different methodology (these authors investigated fuels directly, while this study focused on atmospheric particles) and different fuels, but also to the influence of biofuel burning in the tunnels (mainly ethanol and a lower contribution of biodiesel, which corresponded to 5% of diesel).

Given that biogenic and vehicular emissions have an important impact on the OC concentrations, the source apportionment is an essential tool to estimate their contribution. In this study, the sources were determined by using δ^{13}C values associated to ^{14}C measurements performed on OC and EC separately, and the results are discussed hereafter.

Table 3.7 shows F^{14}C values for the TRA and TJQ tunnels as well as the ambient ambient campaign before and after blank correction for OC and EC. The low amount of material collected on the blank filters implies higher uncertainties in F^{14}C blank, e.g. the ambient blank filter (0.12 μg/cm^2) did not have enough material to determine F^{14}C, so the $F^{14}C_{corr}$ (EC) for ambient samples was performed only considering the area of the filter.

Lower F^{14}C (OC) values were observed more in the tunnels than during the ambient campaign. This is due to high contribution of fossil fuel burning (gasoline and diesel) to OC formation inside the tunnels. The fraction of diesel vehicles is much higher in the TRA than in the TJQ tunnel, which explains the lower F^{14}C (OC) values in TRA. During the ambient

campaign, $F^{14}C$ (OC) was lower on weekdays, indicating a lower fraction of modern carbon, it can be probably due to the reduced number of vehicles running around the sampling point.

Table 3.7 also presents $F^{14}C$ (EC) values. These values were lower than $F^{14}C$ (OC), especially in the tunnels. Notably, EC emissions mostly originate from fossil fuels (diesel and gasoline, $F^{14}C$=0), even in the TJQ tunnel, where a high number of flex-fuel vehicles is expected. It seems that the ethanol contained in the flex fuels does not contribute significantly to the EC formation. Higher values of $F^{14}C$ (EC) for the ambient samples indicate other sources for EC formation beside vehicles, such as biomass burning (e.g. Heal et al., 2014).

Table 3.7: OC and EC average concentrations for each campaign. $F^{14}C_{raw}$ and $F^{14}C_{corr}$ refer to $F^{14}C$ values before and after blank correction, for OC and EC, respectively

Campaign	OC			EC		
	OC* ($\mu g/m^3$)	$F^{14}C$ raw	$F^{14}C$ corr	EC* ($\mu g/m^3$)	$F^{14}C$ raw	$F^{14}C$ corr
TJQ	14.3	0.47	0.46	9.2	0.08	0.04
TRA	61.5	0.20	0.19	121.0	0.05	0.04
Ambient						
Weekday	10.2	0.58	0.57	4.1	0.17	0.17
Weekend	8.3	0.69	0.68	2.3	0.27	0.27

* Average concentrations (TOT method) calculated for the same filters analyzed by AMS

Average OC and EC concentrations by using the TOT method are shown in Table 3.7. TRA had significantly higher EC and OC concentrations than TJQ due to higher HDV emissions. The main difference between the tunnels can be seen at the OC/EC ratios. A higher ratio is observed for TJQ, where the OC emissions are higher due to the combustion of mainly gasohol and ethanol, and the emission of EC is lower than in the TRA tunnel, which is more impacted by HDV. Since the fossil fuel burning is the main source of EC, a low OC/EC ratio of 0.5 was obtained in the TRA campaign.

Table 3.8 presents the relative contributions of the source apportionment estimated for the tunnel campaigns. Large contributions from fossil fuel were observed for OC and EC concentrations. This can be related to gasoline, present in gasohol and diesel (fossil fuels) used by the vehicles. The biofuel burning represented 44.5% of OC measured in TJQ, however this contribution was lower in TRA (18%), where HDV corresponded to 30% of the vehicular fleet. The low values of EC_b and high values of EC_f confirm that fossil fuel burning is the main source for EC concentrations in the tunnels.

Table 3.8: Relative contributions (in %) of biofuel (b) and fossil fuel (f) burning to the total carbon for the tunnel campaigns.

Campaign	OC		EC	
	OC_b	OC_f	EC_b	EC_f
TJQ	44.5	55.5	3.7	96.3
TRA	18.3	81.7	4.3	95.7

Table 3.9 presents the source apportionment for the ambient campaign. EC and OC_{prim} sources were divided into biomass burning (EC_{bb}) and vehicular (EC_{veh}) emissions, and OC_{sec} in $OC_{other,sec}$ and $OC_{veh,sec}$, as described in section 2.5. OC_{sec} represented around 60% of the total OC, showing that SOA formation is an important OC source. Furthermore, vehicular emissions were the main source for EC and OC. On average, EC_{bb}, $OC_{bb,prim}$ and $OC_{other,sec}$ did not differ strongly between weekday and weekend, indicating relatively constant sources. In contrast, vehicular emissions were higher during the week, with concentrations more than double of that found during the weekend. This is due to more intensive traffic of vehicles during workdays. The biomass burning had higher contribution of OC_{prim} than vehicles.

Table 3.9: Source apportionment of EC and OC concentrations for the ambient campaign.

Ambient	EC [µg/m³]		OC_{prim} [µg/m³]		OC_{sec} [µg/m³]	
	EC_{veh}	EC_{bb}	$OC_{veh,prim}$	$OC_{bb,prim}$	$OC_{other,sec}$	$OC_{veh,sec}$
Weekday	3.7	0.5	1.9	2.4	1.9	4.0
Weekend	1.8	0.5	0.9	2.5	2.1	2.8

It is possible to refine the source apportionment of OC from sources other than traffic, using ^{13}C results. For this, contributions from vehicles (OC_{veh}, the sum of $OC_{veh,prim}$ and $OC_{veh,sec}$) and from biogenic and biomass burning emissions of C3 (OC_{C3}) and C4 (OC_{C4}) plants are considered. The results of this source apportionment are presented in Table 3.10. OC_{C3} was higher than OC_{C4} and showed similar concentrations during weekday and weekend. This is not surprising as the sampling point and the immediate outskirts of Sao Paulo are surrounded by C3 plants. OC_{C4} concentrations were around 2.0 µg/m³, mainly related to the sugarcane fields located around the city, emissions from plants and biomass burning, and ethanol fuel burning. In order to estimate the contribution of C4 plants to biomass burning, a rough estimation considered all mixed sources in $OC_{other,sec}$ originated from biomass burning and the values are presented on Table 3.10. The ratios are lower than 1, indicating that OC_{C4} cannot account for all biomass burning. However, it has an important contribution to this process. Additionally, a

comparison between weekend and weekday shows no reliable distinction due to the slight differences between this two periods in $OC_{bb,prim}$, $OC_{other,sec}$ (Table 3.9) and OC_{C4} concentrations.

Table 3.10: OC concentrations from C4 and C3 plants and vehicles (in $\mu g/m^3$) during the ambient campaign and the OC relative contribution of C4 plants to the OC from primary biomass burning and secondary formation from other sources.

Ambient	OC_{veh}	OC_{C4}	OC_{C3}	$OC_{C4}/(OC_{bb.prim} + OC_{other,sec})$
Weekday	5.8	1.7	2.6	0.40
Weekend	3.7	1.9	2.6	0.43

3.4.1. Source apportionment discussion

The methods for the source apportionments used simplifications, excluded contributions such as cooking processes (including burning of wood and charcoal), industrial activities, and biogenic processes for primary OC. Bauer et al. (2008) estimated the fungus contribution around 3-8% of OC_{prim} in the coarse mode, and Matthias-Maser et al. (2000) found that primary biological aerosols, including pollen, spores, and plant debris, correspond to 25% of the total number of particles. It is important to point out that these contributions to primary biogenic aerosols were excluded because they contribute mainly to the coarse mode of the particles, and much less to the fine mode, the size of the samples collected in this study. The methods presented here only considered the main sources: biomass burning, BSOA and vehicular emissions.

The OC/EC ratios and modern carbon fractions found in the tunnel campaigns were related to primary emissions, since photochemical processes were restricted due to the absence of sunlight. Furthermore, the OC/EC ratio used to estimate the vehicular emission was obtained from TRA campaign, which implied in an overestimation, once EC concentrations are considerable higher in this tunnel. A possible solution for this is to try values ranging from the highest (TRA campaign) to the lowest (TJQ campaign) ratios. For the source apportionment on ambient samples, it was assumed that modern carbon fractions were the same for primary and secondary vehicular emissions. No publication discussed a potential variability of these fractions until now. As a first approach of source apportionment, this approximation was sufficient to estimate vehicular emission contributions, since differences between weekends and weekdays were observed.

Another important approximation was the $(OC/EC)_{bb,prim}$ ratio. Table 3.11 shows different ratios and their impact on the OC_{sec} source apportionment. Since $OC_{bb,prim}$ is

calculated directly from the $(OC/EC)_{bb,prim}$ ratio (eq 2.16), higher ratios implied lower OC_{sec} concentrations. Furthermore, this sensitivity study shows that different ratios do not have significant impact on the vehicular contribution. $(OC/EC)_{bb,prim}$ ratios of eight and above lead to unrealistically low or even negative $OC_{other,sec}$ concentrations and even though such values are reported in the literature, they do not seem appropriate for the type of burning in the region of Sao Paulo.

Table 3.11: Sensitivity test of $(OC/EC)_{bb,prim}$ ratios and their impact on the OC_{sec} source apportionment, by using three-source and two-source methods.

$(OC/EC)_{bb}$	Weekday		Weekend	
	$OC_{other,sec}$	$OC_{veh,sec}$	$OC_{other,sec}$	$OC_{veh,sec}$
1	3.93	3.91	4.11	2.75
2	3.42	3.93	3.60	2.76
3	2.92	3.95	3.10	2.78
4	2.41	3.96	2.59	2.80
5	1.91	3.98	2.08	2.81
6	1.40	4.00	1.57	2.83
7	0.90	4.01	1.07	2.85
8	0.40	4.03	0.56	2.86
9	-0.11	4.05	0.05	2.88
10	-0.61	4.06	-0.46	2.90

4. Conclusions

Since the vehicular emissions have a strong impact on air pollution in big cities, the focus of this work was to characterize the particulate matter chemical composition originated from this source in the city of Sao Paulo. Three field campaigns were performed in the city, sampling $PM_{2.5}$ on filters: two in tunnels (in the Janio Quadros (TJQ), , and the Rodoanel Mario Covas (TRA) tunnels). , and an ambient campaign was performed on the roof of the IAG building on the University of Sao Paulo campus during the Southern Hemisphere Winter. A complete analysis of particulate matter included the very known techniques used for determination of mass, trace-elements, BC, OC and EC concentrations, furthermore, it is important to highlight that for the first time, the organic fraction of particle filter samples collected in the city of Sao Paulo were analyzed by: (i) a *Thermal-Desorption Proton-Transfer-Reaction Time-of-Flight Mass Spectrometer* (TD-PTR-ToF-MS) to identify and quantify organic compounds, (ii) an *Isotope-Ratio Mass Spectrometry* (IRMS) and (iii) an *Accelerator Mass Spectrometry* (AMS) were used to identify the carbon isotopes ^{13}C and ^{14}C, respectively.

The source apportionment using the concentrations of mass, trace elements and BC during the ambient campaign identified four possible sources: soil/ construction, vehicular/ secondary aerosol, vehicular and fuel oil burning. This analysis showed that vehicular emission is the main source of $PM_{2.5}$ in the city of Sao Paulo; it was also shown that the identified sources did not have significant differences from previous studies. The organic matter contribution was estimated to be at least 40% of $PM_{2.5}$ in ambient samples.

The emission factors characterized the OA emitted from LDV and HDV. OA represented 36% and 43% of $PM_{2.5}$ emissions, respectively from LDV and HDV. Additionally, for both type of fleet a high amount of compounds containing oxygen (70%) were observed, suggesting that the oxygenation occurs during fuel combustion. Nitrogen-containing compounds contributed around 20% to the EF values for both types of vehicles, possibly associated with incomplete fuel combustion. The vehicular fleet was not distinguished only by the mass spectra, obtained by the TD-PTR-MS, where compounds with higher m/z ratios were emitted by LDV, but also by the more volatile compounds originated from HDV. Furthermore, some compounds were possibly related as tracers for gasoline (m/z 149.131, $C_{11}H_{16}H^+$, pentylbenzene), biodiesel (m/z 299.289, $C_{19}H_{38}O_2H^+$, methyl stearate) and vehicle engine combustions (149.024, $C_8H_4O_3H^+$, phthalic anhydride). Results from isotopic analyses were used to determine differences between tunnel and ambient samples, besides differences between weekdays and weekends. Compounds observed in tunnel samples were more volatile than in ambient ambient samples.

Additionally, δ^{13}C values obtained from the tunnel measurements were lower than that measured during ambient campaign. A comparison between the two tunnels did not show significant differences regarding the volatility and δ^{13}C values, although both tunnels showed different vehicular fleets. On the other hand, aerosols with less volatile compounds were more frequent during the weekend than on weekdays, probably associated to the lower number of vehicles. However, to investigate this hypothesis, a quantitative source apportionment study is necessary.

The source apportionment for the tunnel campaigns indicated that the vehicular emissions of OC and EC are dominated by the fossil fuel burning (gasohol and diesel-containing 5% of biodiesel). In a source apportionment study applied to the ambient samples, the vehicular emissions were higher during the weekday than in the weekend and they were identified as the main source of OC (also OC$_{sec}$) and EC, representing more than 50% and 80% of total OC and EC, respectively. Additionally, biomass burning was found to be the dominant source (65%) of OC$_{prim}$ concentrations. The estimative contributions from C3 and C4 plants were approximately constant in the city of Sao Paulo, where the main contribution came from C3 plants due to the fact that the sampling point is surrounded by parks.

This thesis presented original results concerning the emission inventory of the organic fraction from the PM$_{2.5}$ and the identification of tracers for fossil and bio fuels. Furthermore the source apportionment for OC and EC is not only relevant information for models related to the air quality, but also for studies of biological influence of vegetation. Also, all the results will be applied in the description of aerosols in Chemical Transport Models and biosphere-atmosphere exchanges modeling.

5. Perspectives

The work presented here showed the necessity of a better understanding of the vehicular contribution to organic aerosols. For future studies, two main points are suggested:

(i) Ambient aerosol contains hundreds of thousands of organic compounds, which are difficult to analyze separately. A common receptor model, called *Positive Matrix Factorization* (PMF), has been successfully used in ambient studies apportioning the measured organics in terms of source/process-related components. This statistical tool uses constrained, weighted least squares estimations to determine source profiles and strengths. PMF is often performed on data measured by the *Aerodyne Aerosol Mass Spectrometer* and due to the large number of studies, which reported its application in different case studies, a consolidated mass spectral library was established[1]. However, the same library cannot be used to the TD-PTR-ToF-MS data, since this method uses soft chemical ionization in contrast to the electron impact ionization used in the Aerosol Mass Spectrometer, resulting in different fragmentation patterns of the same factors. On the other hand, as the mass spectra obtained by the TD-PTR-MS (from the emission factor study in the tunnels) represent vehicular emissions for LDV and HDV, associated to the thermal desorption information per compound these spectra can be used as references for PMF studies using the ambient campaign data. In this way, factors deriving from LDV and HDV may be identified and separated from potential other sources contributing to $PM_{2.5}$ during the winter in Sao Paulo.

(ii) A large number of studies exist in the literature regarding source apportionment using carbon isotopes, and they present different values of modern carbon fractions and signatures of $\delta^{13}C$. A complete source study should consider these variations, and analyze their impact on the final results, called sensitive tests. The next step of this study will perform these tests and then estimate the deviation to the results presented here.

---

[1] http://cires.colorado.edu/jimenez-group/AMSsd/

6. References

ALBUQUERQUE, T. A.; ANDRADE, M. F.; YNOUE, R. Y. Characterization of atmospheric aerosols in the city of Sao Paulo, Brazil: Comparisons between polluted and unpolluted periods. **Environmental Monitoring and Assessment**, v. 184, n. 2, p. 969–984, 2012.

ALMEIDA, G. P. et al. Measured and modelled cloud condensation nuclei (CCN) concentration in São Paulo, Brazil: the importance of aerosol size-resolved chemical composition on CCN\hack{
} concentration prediction. **Atmospheric Chemistry and Physics**, v. 14, n. 14, p. 7559–7572, 2014.

ANDERSON, J. O.; THUNDIYIL, J. G.; STOLBACH, A. Clearing the Air: A Review of the Effects of Particulate Matter Air Pollution on Human Health. **Journal of Medical Toxicology**, v. 8, n. 2, p. 166–175, 2012.

ANDRADE, M. F. et al. Vehicle emissions and PM2.5 mass concentrations in six Brazilian cities. **Air Quality, Atmosphere & Health**, v. 5, n. 1, p. 79–88, 2012.

ANP. **Boletim Mensal do Biodiesel- Fevereiro 2015 Agência Nacional do Petróleo, Gás Natural e Biocombustíveis.**São Paulo, 2015.

BAUER, H. et al. Significant contributions of fungal spores to the organic carbon and to the aerosol mass balance of the urban atmospheric aerosol. **Atmospheric Environment**, v. 42, n. 22, p. 5542–5549, 2008.

BRITO, J. et al. Physical–chemical characterisation of the particulate matter inside two road tunnels in the São Paulo Metropolitan Area. **Atmospheric Chemistry and Physics**, v. 13, n. 24, p. 12199–12213, 17 dez. 2013.

BRITO, J. M. et al. Acute Cardiovascular and Inflammatory Toxicity Induced by Inhalation of Diesel and Biodiesel Exhaust Particles. **Toxicological Sciences**, v. 116, n. 1, p. 67–78, 2010.

CACHIER, H. et al. Source terms and source strengths of the carbonaceous aerosol in the tropics. **Journal of Atmospheric Chemistry**, v. 3, n. 4, p. 469–489, 1985.

CACHIER, H.; BREMOND, M.-P.; BUAT-MÉNARD, P. Determination of atmospheric soot carbon with a simple thermal method. **Tellus B**, v. 41, n. 3, p. 379–390, 1989.

CARVALHO, V. S. B. et al. Air quality status and trends over the Metropolitan Area of São Paulo, Brazil as a result of emission control policies. **Environmental Science & Policy**, v. 47, p. 68–79, 2015.

CASTANHO, D. A.; ARTAXO, P. Wintertime and summertime São Paulo aersol source apportionment study. **Atmospheric Environment**, v. 35, p. 4889–4902, 2001.

CEBURNIS, D. et al. Quantification of the carbonaceous matter origin in submicron marine aerosol by ^{13}C and ^{14}C isotope analysis. **Atmospheric Chemistry and Physics**, v. 11, n. 16, p. 8593–8606, 23 ago. 2011.

CERRI, T.; D'ERRICO, G.; ONORATI, A. Experimental investigations on high octane number gasoline formulations for internal combustion engines. **Fuel**, v. 111, p. 305–315, 2013.

CETESB. **Relatório anual de Qualidade do Ar no estado de São Paulo 2011.**São Paulo, 2012. Disponível em: <http://ar.cetesb.sp.gov.br/publicacoes-relatorios/>

CETESB. **Inventário nacional de emissões Atmosféricas por veículos automotores rodoviários**São Paulo, 2013a. Disponível em: <http://ar.cetesb.sp.gov.br/publicacoes-relatorios/>

CETESB. **Operação inverno – 2012 Qualidade do Ar.**São Paulo, 2013b. Disponível em: <http://ar.cetesb.sp.gov.br/publicacoes-relatorios/>

CETESB. **Relatório de Qualidade do Ar no Estado de São Paulo 2012.**São Paulo, 2013c. Disponível em: <http://ar.cetesb.sp.gov.br/publicacoes-relatorios/>

CETESB. **Relatório de Qualidade do Ar no Estado de São Paulo 2013.**São Paulo, 2014. Disponível em: <http://ar.cetesb.sp.gov.br/publicacoes-relatorios/>

CHARLSON, R. J. et al. Climate forcing by anthropogenic Aerosols. **Science**, v. 255, n. January, p. 423– 430, 1992.

CHIRICO, R. et al. Aerosol and trace gas vehicle emission factors measured in a tunnel using an Aerosol Mass Spectrometer and other on-line instrumentation. **Atmospheric Environment**, v. 45, n. 13, p. 2182–2192, 2011.

COLLIER, C. G. The impact of urban areas on weather. **Quarterly Journal of the Royal Meteorological Society**, v. 132, n. 614, p. 1–25, 2006.

COLLIER, S. et al. Organic PM Emissions from Vehicles: Composition, O/C Ratio, and Dependence on PM Concentration. **Aerosol Science and Technology**, v. 49, n. 2, p. 86–97, 2015.

CPTEC. **Centro de Previsão de Tempo e Estudos Climáticos - CPTEC/INPE**. Disponível em: <http://www.cptec.inpe.br/>. Acesso em: 4 nov. 2014.

CURRIE, L. A. The remarkable metrological history of radiocarbon dating [II]. **Journal of Research of the National Institute of Standards and Technology**, v. 109, n. 2, p. 185, 2004.

DE ROOIJ, M.; VAN DER PLICHT, J.; MEIJER, H. A. J. Porous iron pellets for AMS 14C analysis of small samples down to ultra-microscale size (10–25μgC). **Nuclear Instruments and Methods in Physics Research Section B: Beam Interactions with Materials and Atoms**, v. 268, n. 7-8, p. 947–951, 2010.

DECARLO, P. F. et al. Field-Deployable, High-Resolution, Time-of-Flight Aerosol Mass Spectrometer. **Analytical Chemistry**, v. 78, n. 24, p. 8281–8289, 2006.

DUSEK, U. et al. The contribution of fossil sources to the organic aerosol in the Netherlands. **Atmospheric Environment**, v. 74, p. 169–176, 2013a.

DUSEK, U. et al. A thermal desorption system for measuring δ13C ratios on organic aerosol. **Journal of Aerosol Science**, v. 66, p. 72–82, dez. 2013b.

DUSEK, U. et al. Evaluation of a two-step thermal method for separating organic and elemental carbon for radiocarbon analysis. **Atmospheric Measurement Techniques**, v. 7, n. 7, p. 1943–1955, 2014.

FINLAYSON-PITTS, B. J.; PITTS, J. N. J. **Chemistry of the Upper and Lower Atmosphere Theory, Experiments, and Applications**. 1st. ed. San Diego: Academic Press, 2000.

GELENCSÉR, A. et al. Source apportionment of PM2.5 organic aerosol over Europe: Primary/secondary, natural/anthropogenic, and fossil/biogenic origin. **Journal of Geophysical Research: Atmospheres**, v. 112, n. 23, p. 1–12, 2007.

GENBERG, J. et al. Source apportionment of carbonaceous aerosol in southern Sweden. **Atmospheric Chemistry and Physics**, v. 11, n. 22, p. 11387–11400, 16 nov. 2011.

GLASIUS, M.; LA COUR, A.; LOHSE, C. Fossil and nonfossil carbon in fine particulate matter: A study of five European cities. **Journal of Geophysical Research: Atmospheres**, v. 116, n. 11, p. 1–11, 2011.

GRAUS, M.; MÜLLER, M.; HANSEL, A. High resolution PTR-TOF: Quantification and Formula Confirmation of VOC in Real Time. **Journal of the American Society for Mass Spectrometry**, v. 21, p. 1037–1044, 2010.

GUENTHER, A. B. et al. The Model of Emissions of Gases and Aerosols from Nature version 2.1 (MEGAN2.1): an extended and updated framework for modeling biogenic emissions. **Geoscientific Model Development**, v. 5, n. 6, p. 1471–1492, 2012.

GUENTHER, A. et al. A global model of natural volatile organic compound emissions. **Journal of Geophysical Research**, v. 100, n. D5, p. 8873–8892, 1995.

HANSEL, A. et al. Proton transfer reaction mass spectrometry: on-line trace gas analysis at the ppb level. **International Journal of Mass Spectrometry and Ion Processes**, v. 149-150, n. 95, p. 609–619, 1995.

HEAL, M. R. et al. Application of 14C analyses to source apportionment of carbonaceous PM2.5 in the UK. **Atmospheric Environment**, v. 45, n. 14, p. 2341–2348, 2011.

HEAL, M. R. The application of carbon-14 analyses to the source apportionment of atmospheric carbonaceous particulate matter: a review. **Analytical and bioanalytical chemistry**, v. 406, n. 1, p. 81–98, jan. 2014.

HETEM, I. G. **Quantificação da contribuição veicular para as cocnentrações atmosféricas de material particulado fino e Black Carbon em São Paulo**. [s.l.] University of Sao Paulo, 2014.

HOLZINGER, R. et al. Analysis of the chemical composition of organic aerosol at the Mt. Sonnblick observatory using a novel high mass resolution thermal-desorption proton-transfer-reaction mass-spectrometer (hr-TD-PTR-MS). **Atmospheric Chemistry and Physics**, v. 10, n. 6, p. 13969–14011, 27 out. 2010.

HOLZINGER, R. et al. Chemical evolution of organic aerosol in Los Angeles during the CalNex 2010 study. **Atmospheric Chemistry and Physics**, v. 13, n. 19, p. 10125–10141, 15 out. 2013.

HOLZINGER, R. PTRwid: a new widget-tool for processing PTR-TOF-MS data. **Atmospheric Measurement Techniques Discussions**, v. 8, n. 2, p. 1629–1669, 2015.

HOSHI, J. et al. Investigation and estimation of emission sources of 54 volatile organic compounds in ambient air in Tokyo. **Atmospheric Environment**, v. 42, n. 10, p. 2383–2393, 2008.

INFOCIDADE. **Infocidade**. Disponível em: <http://infocidade.prefeitura.sp.gov.br/>. Acesso em: 23 maio. 2015.

JIMENEZ, J. L. et al. Evolution of organic aerosols in the atmosphere. **Science (New York, N.Y.)**, v. 326, n. 5959, p. 1525–1529, 11 dez. 2009.

JORDAN, A. et al. A high resolution and high sensitivity proton-transfer-reaction time-of-flight mass spectrometer (PTR-TOF-MS). **International Journal of Mass Spectrometry**, v. 286, p. 122–128, 2009.

KANAKIDOU, M. et al. Organic aerosol and global climate modelling: a review. **Atmospheric Chemistry and Physics**, v. 5, n. 4, p. 1053–1123, 2005.

KIRCHSTETTER, T. W. et al. On-road measurement of fine particle and nitrogen oxide emissions from light- and heavy-duty motor vehicles. **Atmospheric Environment**, v. 33, p. 2955 – 2968, 1999.

KOPPMANN, R. **Volatile Organic Compounds in the Atmosphere**. 1 st ed. Oxford: Blackwell Publishing Ltd, 2007.

KROLL, J. H.; SEINFELD, J. H. Chemistry of secondary organic aerosol: Formation and evolution of low-volatility organics in the atmosphere. **Atmospheric Environment**, v. 42, p. 3593 – 3624, 2008.

LEWIS, C. W.; KLOUDA, G. A.; ELLENSON, W. D. Radiocarbon measurement of the biogenic contribution to summertime PM-2.5 ambient aerosol in Nashville, TN. **Atmospheric Environment**, v. 38, n. 35, p. 6053–6061, 2004.

LINDINGER, W.; HANSEL, A.; JORDAN, A. On-line monitoring of volatile organic compounds at pptv levels by means of proton-transfer-reaction mass spectrometry (PTR-MS) medical applications, food control and environmental research. **International Journal of Mass Spectrometry and Ion Processes**, v. 173, n. 3, p. 191–241, 1998.

LÓPEZ-VENERONI, D. The stable carbon isotope composition of PM2.5 and PM10 in Mexico City Metropolitan Area air. **Atmospheric Environment**, v. 43, n. 29, p. 4491–4502, set. 2009.

MARTINELLI, L. A. et al. Stable carbon and nitrogen isotopic composition of bulk aerosol particles in a C4 plant landscape of southeast Brazil. **Atmospheric Environment**, v. 36, n. 14, p. 2427–2432, maio 2002.

MARTINS, L. D. et al. Emission factors for gas-powered vehicles traveling through road tunnels in São Paulo, Brazil. **Environmental science & technology**, v. 40, n. 21, p. 6722–6729, 2006.

MASALAITE, A.; GARBARAS, A.; REMEIKIS, V. Stable isotopes in environmental investigations. **Lithuanian Journal of Physics**, v. 52, n. 3, p. 261–268, 2012.

MATTHIAS-MASER, S.; BOGS, B.; JAENICKE, R. The size distribution of primary biological aerosol particles in cloud water on the mountain Kleiner Feldberg/Taunus (FRG). **Atmospheric Research**, v. 54, n. 1, p. 1–13, 2000.

MIGUEL, A. H. et al. On-road emissions of particulate polycyclic aromatic hydrocarbons and black carbon from gasoline and diesel vehicles. **Environmental Science and Technology**, v. 32, n. 4, p. 450–455, 1998.

MIRANDA, R. M. et al. Characterisation of aerosol particles in the São Paulo Metropolitan Area. **Atmospheric Environment**, v. 36, p. 345–352, 2002.

MIRANDA, R. M.; ANDRADE, M. F. Physicochemical characteristics of atmospheric aerosol during winter in the São Paulo Metropolitan area in Brazil. **Atmospheric Environment**, v. 39, n. 33, p. 6188–6193, 2005.

MME. **Ministério de Minas e Energia**. Disponível em: <http://www.mme.gov.br/programas/biodiesel/menu/programa/objetivos_diretrizes.html>. Acesso em: 23 mar. 2015.

NAIK, C. V. et al. Detailed chemical kinetic reaction mechanism for biodiesel components methyl stearate and methyl oleate. **Proceedings of the Combustion Institute**, v. 33, n. 1, p. 383–389, 2011.

NAKAJIMA, T. et al. A possible correlation between satellite-derived cloud and aerosol

microphysical parameters. **Geophysical Research Letters**, v. 28, n. 7, p. 1171–1174, 2001.

NOAA. **Air Resources Laboratory - HYSPLIT - Hybrid Single Particle Lagrangian Integrated Trajectory model**. Disponível em: <https://ready.arl.noaa.gov>. Acesso em: 26 abr. 2013.

NOGUEIRA, T. et al. Formaldehyde and acetaldehyde measurements in urban atmosphere impacted by the use of ethanol biofuel: Metropolitan Area of Sao Paulo (MASP), 2012–2013. **Fuel**, v. 134, p. 505–513, 2014.

PAATERO, P. A weighted non-negative least squares algorithm for three-way "PARAFAC" factor analysis. **Chemometrics and Intelligent Laboratory Systems**, v. 38, n. 2, p. 223–242, out. 1997.

PAATERO, P.; TAPPERT, U. Positve Matrix Factorization: a non-negative factor model with optimal utilization of error estimates of data values. v. 5, n. April 1993, p. 111–126, 1994.

PENG, R. D. et al. Emergency Admissions for Cardiovascular and Respiratory Diseases and the Chemical Composition of Fine Particle Air Pollution. **Environmental Health Perspectives**, v. 117, n. 6, p. 957–963, 2009.

PÉREZ-MARTÍNEZ, P. J. et al. Emission factors of air pollutants from vehicles measured inside road tunnels in São Paulo: case study comparison. **International Journal of Environmental Science and Technology**, 9 abr. 2014.

PIERSON, W. R. et al. Real-world automotive emissions - summary of studies in the Fort McHenry and Tuscarora Mountain Tunnels. **Atmospheric Environment**, v. 30, n. 12, p. 2233–2256, 1996.

PIO, C. et al. Size-segregated chemical composition of aerosol emissions in an urban road tunnel in Portugal. **Atmospheric Environment**, v. 71, p. 15–25, 2013.

POPE, C. A. et al. Lung Cance, Cardiopulmoary Mortality, and Long-term Exposure to Fine Particulate Air Pollution. **Journal of the American Medical Association**, v. 287, n. 9, 2002.

RAES, F. et al. Formation and cycling of aerosols in the global troposphere. **Atmospheric Environment**, v. 34, n. 25, p. 4215–4240, jul. 2000.

RAMADHAN, O. M.; AL-HYALI, E. A. New Experimental and Theoretical Relation To Determine the Research Octane Number (Ron) of Authentic Aromatic Hydrocarbons Could Be

Present in the Gasoline Fraction. **Petroleum Science and Technology**, v. 17, n. February 2015, p. 623–635, 1999.

RAMANATHAN, V. et al. Atmospheric brown clouds: Hemispherical and regional variations in long-range transport, absorption, and radiative forcing. **Journal of Geophysical Research**, v. 112, n. D22, p. D22S21, 2007.

REIMER, P. J.; BROWN, T. A; REIMER, R. W. Discussion: Reporting and Calibration of Post-Bomb 14C Data. **Radiocarbon**, v. 46, n. 3, p. 1299–1304, 2004.

RICO, J. A. P.; SAUER, I. L. A review of Brazilian biodiesel experiences. **Renewable and Sustainable Energy Reviews**, v. 45, p. 513–529, 2015.

SALVO, A.; GEIGER, F. M. Reduction in local ozone leves in urban São Paulo due to a shift from ethanol to gasoline use. **Nature Geoscience**, v. 7, n. 6, p. 450–458, 2014.

SALVO, A.; HUSE, C. Build it, but will they come? Evidence from consumer choice between gasoline and sugarcane ethanol. **Journal of Environmental Economics and Management**, v. 66, n. 2, p. 251–279, 2013.

SÁNCHEZ-CCOYLLO, O. R.; ANDRADE, M. F. The influence of meteorological conditions on the behavior of pollutants concentrations in São Paulo, Brazil. **Environmental Pollution**, v. 116, n. 2, p. 257–63, jan. 2002.

SCHWARTZ, S. E. Does fossil combustion lead to global warming? **Energy**, v. 18, n. 12, p. 1229–1248, 1993.

SEINFELD, J. H.; PANDIS, S. N. **Atmospheric Chemistry and Physics: From Air Pollution to Climate Change**. 2nd. ed. New Jersey: John Wiley & Sons, Inc, 2006. v. 2nd

SMITH, B. N.; EPSTEIN, S. Two categories of c/c ratios for higher plants. **Plant physiology**, v. 47, n. 3, p. 380–384, 1971.

SOUZA, D. Z. et al. Composition of PM2.5 and PM10 collected at Urban Sites in Brazil. **Aerosol and Air Quality Research**, v. 14, n. 1, p. 168–176, 2014.

SPOLNIK, Z. et al. Optimization of Measurement Conditions of an Energy Dispersive X-ray Fluorescence Spectrometer with High-Energy Polarized Beam Excitation for Analysis of Aerosol Filters. **Applied Spectroscopy**, v. 59, n. 12, p. 1465–1469, 2005.

STATTMAN, S. L.; HOSPES, O.; MOL, A. P. J. Governing biofuels in Brazil: A comparison of ethanol and biodiesel policies. **Energy Policy**, v. 61, p. 22–30, 2013.

SZIDAT, S. et al. Radiocarbon (14C)-deduced biogenic and anthropogenic contributions to organic carbon (OC) of urban aerosols from Zürich, Switzerland. **Atmospheric Environment**, v. 38, n. 24, p. 4035–4044, ago. 2004.

SZIDAT, S. et al. Contributions of fossil fuel, biomass-burning, and biogenic emissions to carbonaceous aerosols in Zurich as traced by 14C. **Journal of Geophysical Research: Atmospheres**, v. 111, n. 7, p. 1–12, 2006.

SZIDAT, S. et al. Dominant impact of residential wood burning on particulate matter in Alpine valleys during winter. **Geophysical Research Letters**, v. 34, n. 5, p. 1–6, 2007.

SZIDAT, S. et al. Fossil and non-fossil sources of organic carbon (OC) and elemental carbon (EC) in Göteborg, Sweden. **Atmospheric Chemistry and Physics Discussions**, v. 8, n. 4, p. 16255–16289, 2008.

SZWARCFITER, L.; MENDES, F. E.; LA ROVERE, E. L. Enhancing the effects of the Brazilian program to reduce atmospheric pollutant emissions from vehicles. **Transportation Research Part D: Transport and Environment**, v. 10, n. 2, p. 153–160, 2005.

THURSTON, G. D.; SPENGLER, J. D. A quantitative assessment of source contributions to inhalable particulate matter pollution in metropolitan Boston. **Atmospheric Environment (1967)**, v. 19, n. 1, p. 9–25, 1985.

TIMKOVSKY, J. et al. Offline thermal-desorption proton-transfer-reaction mass spectrometry to study composition of organic aerosol. **Journal of Aerosol Science**, v. 79, p. 1–14, jan. 2015.

TUREKIAN, V. C. et al. Causes of bulk carbon and nitrogen isotopic fractionations in the products of vegetation burns: laboratory studies. **Chemical Geology**, v. 152, n. 1-2, p. 181–192, out. 1998.

ULBRICH, I. M. et al. Interpretation of organic components from positive matrix factorization of aerosol mass spectrometric data. **Atmospheric Chemistry and Physics Discussions**, v. 8, n. 2, p. 6729–6791, 2008.

VAN DER PLICHT, J. et al. Status report: The Groningen AMS facility. **Nuclear Instruments and**

Methods in Physics Research Section B: Beam Interactions with Materials and Atoms, v. 172, n. 1-4, p. 58–65, 2000.

WANG, G. et al. Source Apportionment of Carbonaceous Particulate Matter in a Shanghai Suburb Based on Carbon Isotope Composition. **Aerosol Science and Technology**, v. 47, n. 3, p. 239–248, mar. 2013.

WESTBROOK, C. K. et al. Detailed chemical kinetic reaction mechanisms for primary reference fuels for diesel cetane number and spark-ignition octane number. **Proceedings of the Combustion Institute**, v. 33, n. 1, p. 185–192, 2011.

WHITBY, K. T. The physical characteristics sulfur aerosols. **Atmospheric Environment**, v. 12, p. 135 – 159, 1978.

WIDORY, D. et al. The origin of atmospheric particles in Paris: a view through carbon and lead isotopes. **Atmospheric Environment**, v. 38, n. 7, p. 953–961, mar. 2004.

YNOUE, R. Y.; ANDRADE, M. F. Size-Resolved Mass Balance of Aerosol Particles over the São Paulo Metropolitan Area of Brazil. **Aerosol Science and Technology**, v. 38, n. sup2, p. 52–62, jan. 2004.

YTTRI, K. E. et al. Source apportionment of the carbonaceous aerosol in Norway – quantitative estimates based on ^{14}C, thermal-optical and organic tracer analysis. **Atmospheric Chemistry and Physics**, v. 11, n. 17, p. 9375–9394, 9 set. 2011.

Appendix

Table A.1: Filter identification, sampling time start, sampling duration, volume sampled (low volume sampler), vehicle counts, OA concentrations and average CO and CO_2 concentrations inside and outside the tunnel during sampling in TJQ in the year 2011.

Filter #	Start Sampling	Sampling duration (h)	Volume sampled (m^3)	# vehicles		OA ($\mu g/m^3$)	Inside		Outside	
				LDV	HDV		CO_2	CO	CO_2	CO
							(ppm)			
TJQ 01	4th May 08:16	5.8	5.5	13920	29	4.7	513.6	5.10	403.2	1.33
TJQ 02	4th May 17:00	2.7	2.6	12856	34	4.2	526.3	6.15	401.1	1.14
TJQ 03	4th May 20:28	11.7	11.0	13584	36	1.9	456.0	2.66	416.2	1.09
TJQ 04	5th May 08:22	5.4	5.1	14759	49	4.0	513.6	5.47	403.2	1.33
TJQ 05	5th May 17:00	3.0	3.0	12252	6	4.4	526.3	7.06	401.1	1.14
TJQ 06	5th May 20:10	11.7	11.0	13538	18	4.2	456.0	4.42	416.2	1.09
TJQ 08	6th May 08:13	5.9	5.4	13338	19	4.9	513.6	7.25	403.2	1.33
TJQ 09	6th May 17:00	2.5	2.5	12660	6	5.8	526.3	7.37	401.1	1.14
TJQ 10	6th May 20:15	11.6	10.8	12363	43	2.6	456.0	3.58	405.1	1.09
TJQ 11	7th May 08:05	11.7	10.8	24510	272	2.4	510.5	3.47	400.4	1.24
TJQ 12	9th May 08:10	11.9	11.0	25067	387	2.2	511.0	5.04	394.5	1.26
TJQ 13	9th May 20:10	11.8	10.7	11546	36	1.8	425.9	2.05	390.5	0.75
TJQ 14	10th May 08:11	11.7	11.0	31258	79	2.7	498.9	5.41	405.4	1.45
TJQ 15	10th May 20:15	11.9	11.1	13113	111	2.1	437.5	2.50	392.5	0.49
TJQ 16	11st May 08:22	11.9	11.2	--	--	2.9	507.3	5.45	395.7	0.73
TJQ 17	11st May 20:33	12.0	11.1	13274	86	3.6	488.1	3.32	458.5	1.88
TJQ 18	12nd May 08:37	11.1	10.3	32800	283	3.2	512.2	5.79	393.9	1.29
TJQ 19	12nd May 19:45	12.6	11.9	14209	35	2.1	436.3	2.40	393.2	0.76
TJQ 20	13rd May 08:25	11.8	11.1	27162	87	2.4	510.0	5.35	403.1	1.35

Table A.2: Filter identification, sampling time start, sampling duration, volume sampled (mini volume sampler), vehicle counts, OC and EC concentrations and average CO and CO_2 concentrations inside and outside the tunnel during sampling in TJQ in the year 2011.

Filter #	Start Sampling	Sampling duration (h)	Volume sampled (m^3)	# vehicles		OC ($\mu g/m^3$)	EC ($\mu g/m^3$)	Inside		Outside	
				LDV	HDV			CO_2	CO	CO_2	CO
								(ppm)			
MV JQ01	4th May 08:00	11.9	3.57	36288	133	17.6	10.8	510.5	5.28	400.1	1.20
MV JQ02	5th May 19:56	12.5	3.75	14879	42	10.2	7.8	456.0	2.66	416.2	1.09
MV JQ03	5th May 08:31	11.4	3.42	35428	59	14.7	9.1	510.5	5.65	400.1	1.20
MV JQ04	6th May 20:00	11.8	3.54	14367	19	20.7	17.6	456.0	4.42	416.2	1.09
MV JQ05	6th May 07:54	12.4	3.72	36850	38	18.0	13.0	510.5	6.75	400.1	1.20
MV JQ06	7th May 20:21	11.5	3.45	13282	44	12.9	9.7	456.0	3.58	405.1	1.09
MV JQ07	7th May 07:50	12.1	3.63	24879	274	12.8	8.2	510.5	3.47	400.4	1.24
MV JQ08	9th May 08:18	11.6	3.48	25067	387	10.5	6.4	511.0	5.04	394.5	1.26
MV JQ09	10th May 20:00	12.4	3.72	12394	40	8.2	4.2	425.9	2.05	390.5	0.75
MV JQ10	10th May 08:24	11.5	3.45	31871	80	12.5	8.3	498.9	5.41	405.4	1.45
MV JQ11	11st May 19:54	12.7	3.81	13266	103	8.3	6.6	437.5	2.50	392.5	0.49
MV JQ12	11st May 08:36	11.4	3.42	--	--	14.7	8.4	506.5	5.46	395.3	0.75
MV JQ13	12nd May 20:04	12	3.60	14247	98	15.2	13.0	490.7	3.56	454.7	1.79
MV JQ14	12nd May 08:02	11.5	3.45	36192	290	15.3	10.1	525.3	5.95	402.0	1.46
MV JQ15	13rd May 19:35	12.9	3.87	12790	29	8.3	5.7	436.3	2.40	393.2	0.76
MV JQ16	13rd May 08:31	11.6	3.48	27090	91	12.3	8.3	510.0	5.35	403.1	1.35

Table A.3: Filter identification, sampling time start, sampling duration, volume sampled (low volume sampler), vehicle counts, OA concentration and average CO and CO_2 concentrations inside and outside the tunnel during sampling in TRA in the year 2011.

Filter #	Start Sampling	Sampling duration (h)	Volume sampled (m^3)	# vehicles		OA (µg/m^3)	Inside		Outside	
				LDV	HDV		CO_2	CO	CO_2	CO
							(ppm)			
TRA 01	7th July 16:30	6	6	10497	4189	10.3	671.5	3.90	405.7	0.78
TRA 02	8th July 08:45	6	5	8406	4401	11.2	681.7	3.49	415.5	0.83
TRA 03	8th July 14:20	6	6	14432	5171	10.5	661.9	3.91	416.8	0.74
TRA 04	11st July 08:53	5	5	7675	3960	11.4	678.1	4.56	417.1	1.49
TRA 05	11st July 14:26	7	6	10807	4865	9.6	689.4	3.91	416.8	0.91
TRA 06	12nd July 08:18	6	5	9836	5030	12.1	746.5	5.35	417.6	2.09
TRA 07	12nd July 14:19	6	6	12860	5441	11.5	679.1	3.85	416.8	0.96
TRA 08	13rd July 08:10	6	5	10585	5426	14.8	696.1	4.79	417.6	1.01
TRA 09	13rd July 14:10	7	8	11739	5311	8.9	678.8	4.62	416.8	1.04
TRA 10	14th July 08:28	6	5	10751	5386	13.6	754.1	6.68	417.6	2.43
TRA 11	14th July 14:28	6	5	11795	5112	11.5	683.5	4.31	416.8	1.15
TRA 15	15th July 08:10	6	5	10400	5354	15.1	694.4	4.83	417.6	1.15
TRA 12	15th July 14:10	5	6	14351	5142	11.6	689.0	3.62	416.8	1.00

Table A.4: Filter identification, sampling time start, sampling duration, volume sampled (mini volume sampler), vehicle counts, OC and EC concentrations and average CO and CO_2 concentrations inside and outside the tunnel during sampling in TRA in the year 2011.

Filter #	Start sampling	Sampling duration (h)	Volume sampled (m^3)	# vehicles		OC (µg/m^3)	EC (µg/m^3)	Inside		Outside	
				LDV	HDV			CO_2	CO	CO_2	CO
								(pm)			
MV RA06	7th July 14:53	17	5.22	17198	8029	32.5	76.0	594.8	2.83	408.3	0.67
MV RA07	8th July 08:19	6	1.71	10972	5272	57.9	123.6	681.1	3.65	415.2	0.83
MV RA08	8th July 14:13	6	1.77	14432	5171	54.3	107.5	661.9	3.91	416.8	0.74
MV RA09	11st July 08:40	6	1.77	9924	4639	71.4	113.0	699.6	4.97	417.6	1.72
MV RA10	11st July 08:40	5	1.62	9319	4229	57.8	125.5	686.6	3.62	416.5	0.79
MV RA11	12nd July 08:07	6	1.77	9836	5030	98.1	116.9	746.5	5.35	417.6	2.09
MV RA12	12nd July 14:03	6	1.77	12860	5441	54.1	133.5	679.1	3.85	416.8	0.96
MV RA13	13rd July 07:55	6	1.89	10585	5426	60.2	146.2	696.1	4.79	417.6	1.01
MV RA14	13rd July 14:10	6	1.74	11739	5311	63.9	131.5	678.8	4.62	416.8	1.04
MV RA15	14th July 08:06	6	1.74	10751	5386	68.2	149.4	754.1	6.68	417.6	2.43
MV RA16	14th July 14:03	6	1.8	11795	5112	70.0	130.4	683.5	4.31	416.8	1.15
MV RA17	15th July 08:16	6	1.8	10400	5354	54.2	122.2	694.4	4.83	417.6	1.15
MV RA18	15th July 14:22	6	1.68	14351	5142	47.8	129.3	689.0	3.62	416.8	1.00

Table A.5: Filter identification, sampling time start, sampling duration, volume sampled (high volume sampler), OA concentrations during winter in the year 2012.

Filter #	Start sampling	Sampling duration (h)	Volume sampled (m^3)	AO (µg/m^3)	Filter #	Start sampling	Sampling duration (h)	Volume sampled (m^3)	AO (µg/m^3)
HV-01	8th August 09:00	24	1624.49	1.34	HV-17	24th August 09:13	23	1587.20	1.30
HV-02	9th August 09:06	24	1617.03	2.79	HV-18	25th August 08:43	25	1668.56	1.03
HV-03	10th August 09:06	24	1608.89	2.33	HV-19	26th August 09:33	23	1592.62	1.30
HV-04	11st August 08:57	24	1622.45	1.48	HV-20	27th August 09:07	24	1615.00	1.03
HV-05	12nd August 08:59	24	1626.52	1.90	HV-21	28th August 09:03	23	1576.35	0.67
HV-06	13rd August 09:05	24	1645.51	1.22	HV-22	29th August 08:25	24	1615.67	0.41
HV-07	14th August 09:28	23	1580.42	1.01	HV-23	30th August 08:26	24	1610.25	0.46
HV-08	15th August 08:53	24	1641.44	0.85	HV-24	31st August 08:21	24	1604.83	1.64
HV-09	16th August 09:13	24	1603.47	1.15	HV-25	1st September 08:10	24	1626.52	1.93
HV-10	17th August 08:59	24	1612.28	1.15	HV-26	2nd September 08:17	25	1662.46	2.20
HV-11	18th August 08:55	23	1591.94	0.93	HV-27	3rd September 08:57	23	1577.71	0.98
HV-12	19th August 08:31	24	1643.47	1.06	HV-28	4th September 08:26	24	1618.39	0.89
HV-13	20th August 08:52	23	1577.71	1.41	HV-29	5th September 08:26	25	1679.41	2.17
HV-14	21st August 08:14	25	1674.66	1.23	HV-30	6th September 09:22	22	1500.41	1.99
HV-15	22nd August 09:01	24	1597.37	1.16	HV-32	8th September 08:54	24	1632.62	2.70
HV-16	23rd August 08:41	24	1655.68	1.25					

Table A.6: Filter identification, sampling time start, sampling duration, volume sampled (mini volume sampler), OC and EC concentrations during ambient campaign in the year 2012.

Filter #	Start sampling	Sampling duration (h)	Volume sampled (m^3)	OC (µg/m^3)	EC (µg/m^3)	Filter #	Start sampling	Sampling duration (h)	Volume sampled (m^3)	OC (µg/m^3)	EC (µg/m^3)
MV02	8th August 10:00	24	7.20	8.3	2.5	MV15	23rd August 10:00	24	7.17	7.4	3.0
MV03	9th August 10:00	24	7.20	17.5	7.3	MV16	24th August 10:00	24	7.20	8.5	3.2
MV04	10th August 10:00	24	7.17	14.1	4.3	MV17	25th August 10:00	24	7.20	5.5	1.3
MV05	11st August 10:00	24	7.20	9.1	2.3	MV18	27th August 10:00	24	7.20	5.0	1.6
MV06	13rd August 10:00	24	7.20	8.1	2.2	MV19	28th August 10:00	22	6.48	4.1	1.5
MV07	14th August 10:00	24	7.20	5.5	2.0	MV20	29th August 10:00	24	7.20	2.8	0.9
MV08	15th August 10:00	24	7.20	5.4	2.0	MV21	30th August 10:00	24	7.20	2.9	0.7
MV09	16th August 10:00	24	7.20	6.3	2.9	MV22	31st August 10:00	24	7.20	12.0	5.8
MV10	17th August 10:00	24	7.20	5.5	1.9	MV23	1st September 10:00	24	7.20	11.6	4.4
MV11	18th August 10:00	24	7.20	6.9	1.2	MV24	3rd September 10:00	24	7.20	4.3	1.0
MV12	20th August 10:00	24	7.20	8.7	4.0	MV25	4th September 10:00	23	7.02	5.4	1.9
MV13	21st August 10:00	20	6.00	9.1	3.6	MV26	5th September 10:00	24	7.20	13.7	7.2
MV14	22nd August 10:00	24	7.20	7.5	2.6	MV27	6th September 10:00	24	7.20	11.2	5.2

Table A.7: Pearson correlation coefficients for the TJQ campaign.

TJQ	PM$_{2.5}$	Na	Mg	Al	Si	P	S	Cl	K	Ca	Ti	V	Cr	Mn	Fe	Ni	Cu	Zn	Se	Br	Sb	Pb
PM$_{2.5}$	1.00	0.42	0.61	0.88	0.81	0.77	0.51	0.69	0.73	0.69	0.61	0.56	0.60	0.62	0.56	0.38	0.55	0.75	0.27	0.56	0.26	0.66
Na	0.42	1.00	0.09	0.24	0.12	0.20	0.17	0.74	0.37	-0.02	-0.02	-0.23	0.04	0.16	-0.09	0.12	-0.13	0.78	0.09	0.66	-0.62	0.59
Mg	0.61	0.09	1.00	0.69	0.83	0.63	0.19	0.06	0.02	0.86	0.92	0.82	0.92	0.87	0.92	0.54	0.91	0.21	0.81	-0.09	0.60	0.01
Al	0.88	0.24	0.69	1.00	0.92	0.67	0.46	0.54	0.53	0.74	0.68	0.73	0.62	0.62	0.65	0.46	0.64	0.69	0.19	0.49	0.48	0.51
Si	0.81	0.12	0.83	0.92	1.00	0.55	0.18	0.41	0.32	0.91	0.86	0.90	0.83	0.84	0.86	0.55	0.86	0.52	0.39	0.22	0.62	0.21
P	0.77	0.20	0.63	0.67	0.55	1.00	0.82	0.19	0.44	0.58	0.60	0.36	0.58	0.42	0.48	0.29	0.50	0.37	0.50	0.22	0.26	0.57
S	0.51	0.17	0.19	0.46	0.18	0.82	1.00	0.16	0.45	0.15	0.11	0.00	0.08	-0.13	-0.02	-0.12	0.02	0.33	0.08	0.39	0.04	0.62
Cl	0.69	0.74	0.06	0.54	0.41	0.19	0.16	1.00	0.75	0.17	0.02	0.11	0.05	0.22	0.00	0.05	-0.03	0.94	-0.25	0.88	-0.27	0.65
K	0.73	0.37	0.02	0.53	0.32	0.44	0.45	0.75	1.00	0.09	-0.02	0.09	-0.05	0.05	-0.06	-0.05	-0.09	0.69	-0.24	0.82	-0.07	0.79
Ca	0.69	-0.02	0.86	0.74	0.91	0.58	0.15	0.17	0.09	1.00	0.94	0.88	0.96	0.87	0.94	0.49	0.96	0.28	0.60	-0.10	0.68	-0.01
Ti	0.61	-0.02	0.92	0.68	0.86	0.60	0.11	0.02	-0.02	0.94	1.00	0.81	0.98	0.92	0.98	0.69	0.98	0.17	0.72	-0.23	0.62	0.00
V	0.56	-0.23	0.82	0.73	0.90	0.36	0.00	0.11	0.09	0.88	0.81	1.00	0.80	0.78	0.88	0.38	0.89	0.17	0.44	-0.06	0.86	-0.17
Cr	0.60	0.04	0.92	0.62	0.83	0.58	0.08	0.05	-0.05	0.96	0.98	0.80	1.00	0.93	0.97	0.60	0.98	0.17	0.78	-0.23	0.59	-0.06
Mn	0.62	0.16	0.87	0.62	0.84	0.42	-0.13	0.22	0.05	0.87	0.92	0.78	0.93	1.00	0.95	0.71	0.92	0.27	0.69	-0.10	0.50	0.00
Fe	0.56	-0.09	0.92	0.65	0.86	0.48	-0.02	0.00	-0.06	0.94	0.98	0.88	0.97	0.95	1.00	0.66	0.99	0.11	0.71	-0.25	0.71	-0.11
Ni	0.38	0.12	0.54	0.46	0.55	0.29	-0.12	0.05	-0.05	0.49	0.69	0.38	0.60	0.71	0.66	1.00	0.61	0.16	0.36	-0.13	0.24	0.24
Cu	0.55	-0.13	0.91	0.64	0.86	0.50	0.02	-0.03	-0.09	0.96	0.98	0.89	0.98	0.92	0.99	0.61	1.00	0.09	0.70	-0.28	0.73	-0.14
Zn	0.75	0.78	0.21	0.69	0.52	0.37	0.33	0.94	0.69	0.28	0.17	0.17	0.17	0.27	0.11	0.16	0.09	1.00	-0.14	0.86	-0.23	0.73
Se	0.27	0.09	0.81	0.19	0.39	0.50	0.08	-0.25	-0.24	0.60	0.72	0.44	0.78	0.69	0.71	0.36	0.70	-0.14	1.00	-0.40	0.33	-0.19
Br	0.56	0.66	-0.09	0.49	0.22	0.22	0.39	0.88	0.82	-0.10	-0.23	-0.06	-0.23	-0.10	-0.25	-0.13	-0.28	0.86	-0.40	1.00	-0.30	0.77
Sb	0.26	-0.62	0.60	0.48	0.62	0.26	0.04	-0.27	-0.07	0.68	0.62	0.86	0.59	0.50	0.71	0.24	0.73	-0.23	0.33	-0.30	1.00	-0.32
Pb	0.66	0.59	0.01	0.51	0.21	0.57	0.62	0.65	0.79	-0.01	0.00	-0.17	-0.06	0.00	-0.11	0.24	-0.14	0.73	-0.19	0.77	-0.32	1.00

Table A.8: Pearson correlation coefficients for the TRA campaign.

TRA	PM$_{2.5}$	Na	Mg	Al	Si	P	S	Cl	K	Ca	Ti	V	Cr	Mn	Fe	Ni	Cu	Zn	Se	Br	Rb	Pb
PM$_{2.5}$	1.00	0.96	0.52	0.95	0.96	0.90	0.54	0.67	0.92	0.99	0.89	0.74	0.99	1.00	0.97	0.12	0.94	0.99	0.97	0.69	0.03	0.29
Na	0.96	1.00	0.55	0.89	0.89	0.89	0.54	0.82	0.95	0.92	0.86	0.89	0.96	0.96	0.93	0.30	0.96	0.98	0.97	0.80	0.20	0.45
Mg	0.52	0.55	1.00	0.51	0.54	0.78	0.90	0.79	0.61	0.49	0.59	0.62	0.47	0.56	0.55	0.80	0.73	0.54	0.36	0.88	0.75	0.03
Al	0.95	0.89	0.51	1.00	1.00	0.79	0.41	0.62	0.94	0.97	0.98	0.71	0.97	0.95	0.99	0.04	0.85	0.90	0.91	0.63	0.07	0.40
Si	0.96	0.89	0.54	1.00	1.00	0.83	0.47	0.62	0.94	0.98	0.97	0.70	0.98	0.97	1.00	0.06	0.87	0.92	0.91	0.64	0.06	0.34
P	0.90	0.89	0.78	0.79	0.83	1.00	0.85	0.78	0.82	0.86	0.76	0.73	0.85	0.92	0.84	0.46	0.98	0.92	0.81	0.84	0.29	0.06
S	0.54	0.54	0.90	0.41	0.47	0.85	1.00	0.66	0.46	0.49	0.42	0.47	0.45	0.58	0.48	0.71	0.75	0.58	0.38	0.77	0.50	-0.28
Cl	0.67	0.82	0.79	0.62	0.62	0.78	0.66	1.00	0.83	0.60	0.70	0.96	0.67	0.69	0.69	0.76	0.85	0.73	0.65	0.99	0.73	0.52
K	0.92	0.95	0.61	0.94	0.94	0.82	0.46	0.83	1.00	0.91	0.97	0.90	0.95	0.92	0.96	0.29	0.90	0.91	0.91	0.81	0.32	0.59
Ca	0.99	0.92	0.49	0.97	0.98	0.86	0.49	0.60	0.91	1.00	0.91	0.68	0.99	0.99	0.98	0.03	0.90	0.96	0.95	0.62	-0.02	0.28
Ti	0.89	0.86	0.59	0.98	0.97	0.76	0.42	0.70	0.97	0.91	1.00	0.77	0.93	0.90	0.97	0.17	0.83	0.85	0.85	0.71	0.25	0.51
V	0.74	0.89	0.62	0.71	0.70	0.73	0.47	0.96	0.90	0.68	0.77	1.00	0.76	0.75	0.76	0.57	0.84	0.79	0.78	0.91	0.57	0.69
Cr	0.99	0.96	0.47	0.97	0.98	0.85	0.45	0.67	0.95	0.99	0.93	0.76	1.00	0.99	0.99	0.07	0.91	0.97	0.98	0.67	0.03	0.40
Mn	1.00	0.96	0.56	0.95	0.97	0.92	0.58	0.69	0.92	0.99	0.90	0.75	0.99	1.00	0.97	0.16	0.95	0.99	0.96	0.71	0.07	0.28
Fe	0.97	0.93	0.55	0.99	1.00	0.84	0.48	0.69	0.96	0.98	0.97	0.76	0.99	0.97	1.00	0.12	0.90	0.94	0.94	0.70	0.12	0.41
Ni	0.12	0.30	0.80	0.04	0.06	0.46	0.71	0.76	0.29	0.03	0.17	0.57	0.07	0.16	0.12	1.00	0.44	0.21	0.05	0.79	0.92	0.13
Cu	0.94	0.96	0.73	0.85	0.87	0.98	0.75	0.85	0.90	0.90	0.83	0.84	0.91	0.95	0.90	0.44	1.00	0.96	0.89	0.88	0.31	0.25
Zn	0.99	0.98	0.54	0.90	0.92	0.92	0.58	0.73	0.91	0.96	0.85	0.79	0.97	0.99	0.94	0.21	0.96	1.00	0.97	0.74	0.09	0.30
Se	0.97	0.97	0.36	0.91	0.91	0.81	0.38	0.65	0.91	0.95	0.85	0.78	0.98	0.96	0.94	0.05	0.89	0.97	1.00	0.63	-0.03	0.43
Br	0.69	0.80	0.88	0.63	0.64	0.84	0.77	0.99	0.81	0.62	0.71	0.91	0.67	0.71	0.70	0.79	0.88	0.74	0.63	1.00	0.73	0.39
Rb	0.03	0.20	0.75	0.07	0.06	0.29	0.50	0.73	0.32	-0.02	0.25	0.57	0.03	0.07	0.12	0.92	0.31	0.09	-0.03	0.73	1.00	0.35
Pb	0.29	0.45	0.03	0.40	0.34	0.06	-0.28	0.52	0.59	0.28	0.51	0.69	0.40	0.28	0.41	0.13	0.25	0.30	0.43	0.39	0.35	1.00
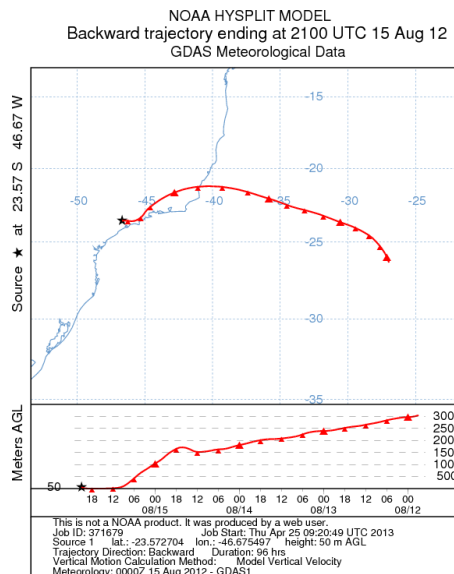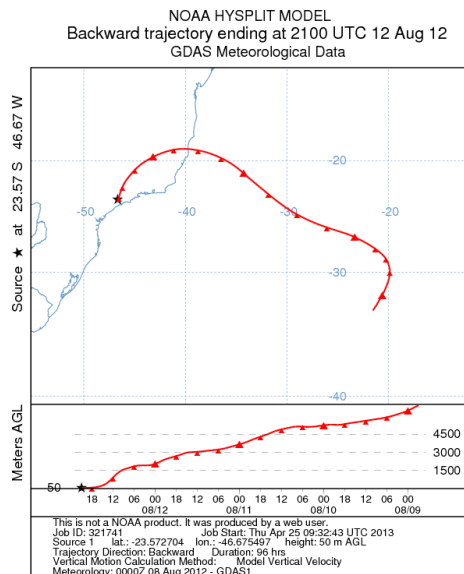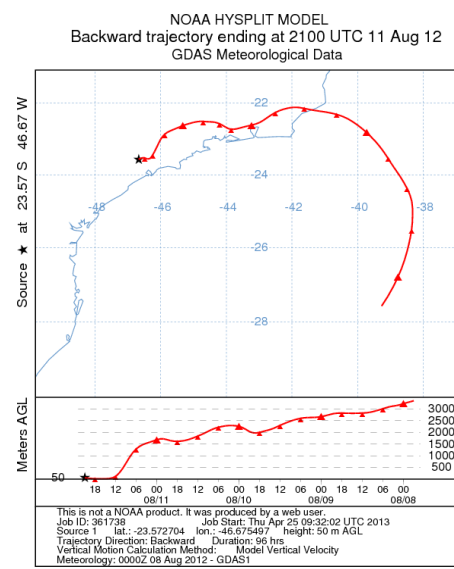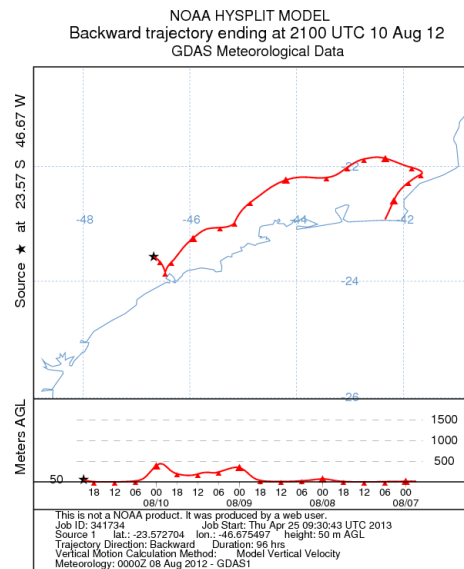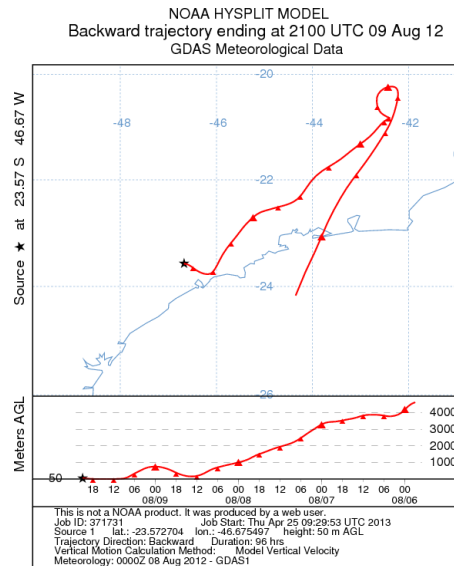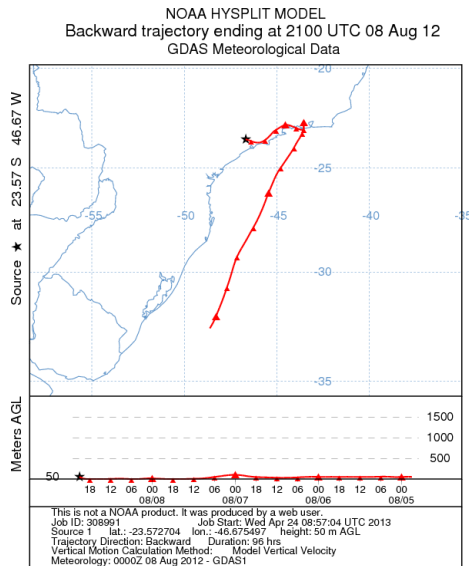
Figure A.1: 72 h back trajectories for the samples selected for IRMS analyses, Hysplit model (NOAA, 2014)
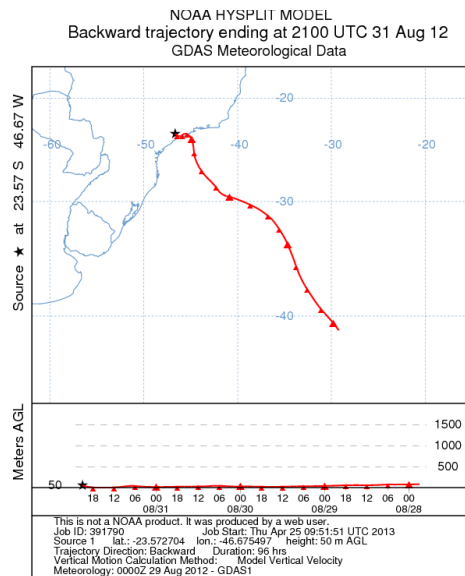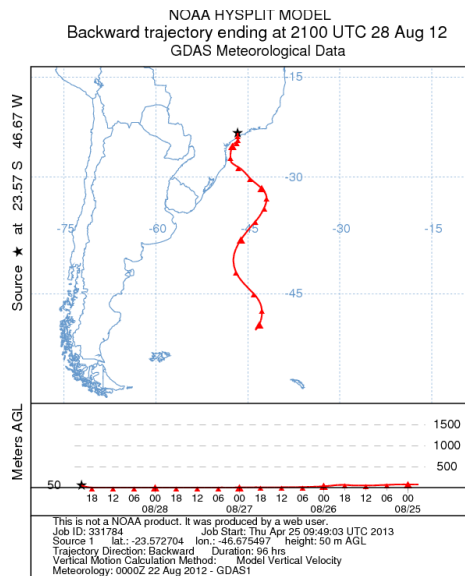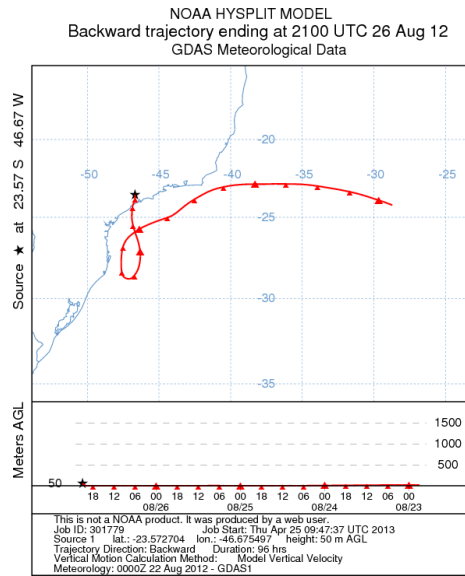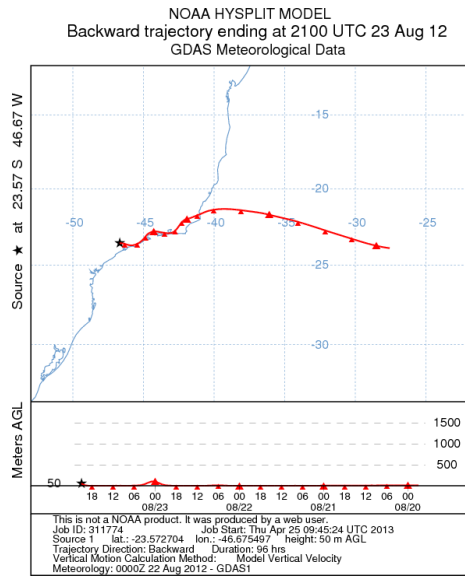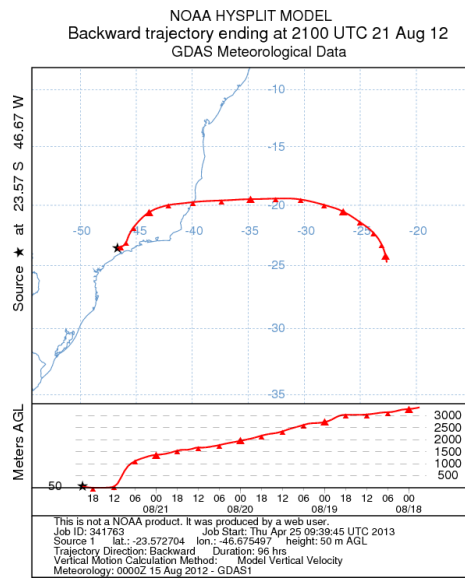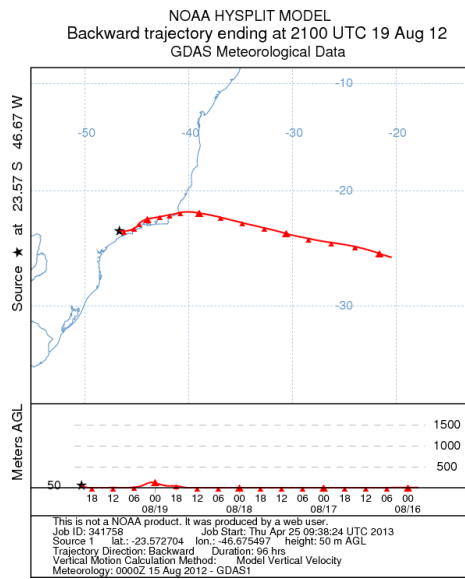
Figure A.1: continue
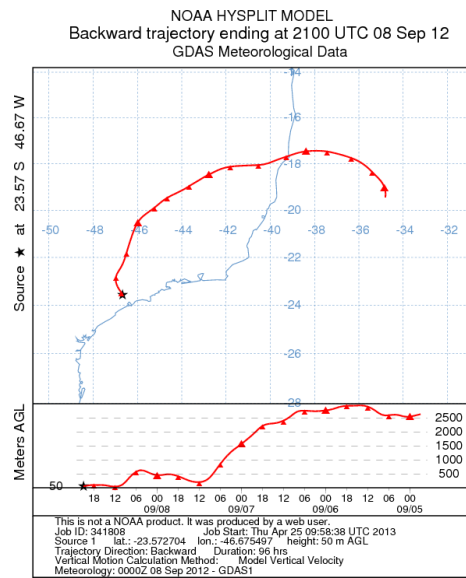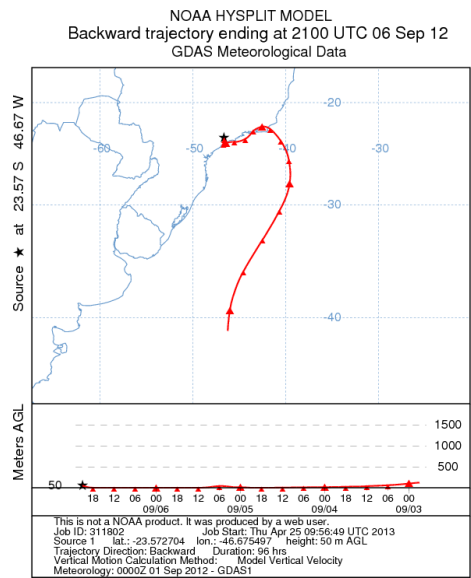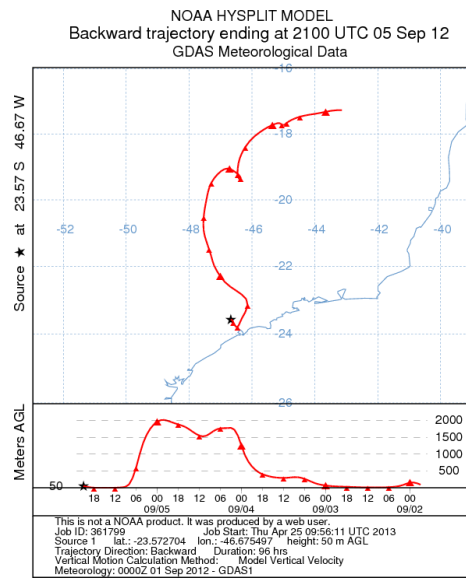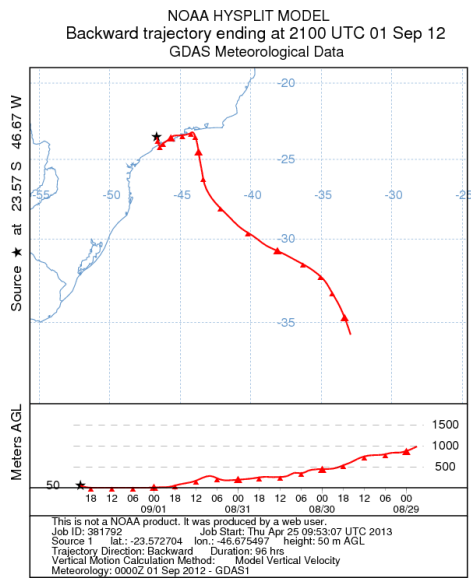
Figure A.1: continue

Table A.9: Emission factors (in mg/kg of fuel) for LDV and HDV for the m/z identified by PTR-MS and their respective empirical formulas.

m/z	Formula	LDV					HDV				
		Average	Std Dev	Med	Max	Min	Average	Std Dev	Med	Max	Min
41.038	C3H4H+	0.181	0.100	0.131	0.382	0.095	0.495	0.095	0.479	0.638	0.315
43.017	C2H2OH+	--	--	--	--	--	0.267	0.104	0.238	0.484	0.109
43.054	C3H6H+	0.085	0.066	0.056	0.228	0.034	0.185	0.034	0.180	0.239	0.123
44.013	CHONH+	--	--	--	--	--	0.025	0.018	0.023	0.072	0.005
44.049	C2H5NH+	0.006	0.012	0.003	0.035	0.000	0.016	0.016	0.014	0.063	0.000
45.033	C2H4OH+	--	--	--	--	--	0.146	0.044	0.144	0.243	0.096
53.038	C4H4H+	--	--	--	--	--	0.037	0.011	0.035	0.065	0.019
55.049	C4H6H+	0.070	0.046	0.048	0.142	0.024	0.240	0.047	0.231	0.307	0.165
56.050	C3H5NH+	--	--	--	--	--	0.010	0.003	0.010	0.017	0.005
57.070	C4H8H+	0.153	0.079	0.113	0.286	0.081	0.188	0.043	0.163	0.256	0.129
58.032	C2H3ONH+	0.000	0.000	0.000	0.000	0.000	0.005	0.003	0.004	0.010	0.002
58.066	C3H7NH+	0.013	0.012	0.008	0.041	0.005	0.006	0.003	0.006	0.010	0.002
59.013	C2H2O2H+	0.001	0.002	0.000	0.006	0.000	0.001	0.001	0.002	0.002	0.000
59.048	C3H6OH+	0.135	0.177	0.052	0.523	0.022	0.063	0.023	0.062	0.097	0.011
60.045	C2H5ONH+	0.051	0.034	0.037	0.125	0.023	0.041	0.015	0.047	0.063	0.021
60.079	C3H9NH+	0.003	0.007	0.000	0.019	0.000	0.004	0.004	0.003	0.012	0.000
61.028	C2H4O2H+	--	--	--	--	--	0.197	0.088	0.170	0.348	0.057
62.030	CH3O2NH+	--	--	--	--	--	0.007	0.003	0.008	0.014	0.002
63.043	C2H6O2H+	0.010	0.012	0.004	0.036	0.002	--	--	--	--	--
65.030	CH4O3H+	--	--	--	--	--	0.002	0.001	0.002	0.003	0.001
65.038	C5H4H+	0.003	0.004	0.002	0.010	0.000	0.005	0.002	0.005	0.010	0.003
67.054	C5H6H+	0.035	0.025	0.028	0.084	0.011	0.094	0.019	0.098	0.125	0.060
68.050	C4H5NH+	0.020	0.012	0.016	0.039	0.009	--	--	--	--	--
69.034	C4H4OH+	--	--	--	--	--	0.111	0.064	0.110	0.282	0.025
69.070	C5H8H+	0.048	0.039	0.027	0.124	0.013	0.182	0.039	0.173	0.240	0.110
70.034	C3H3ONH+	--	--	--	--	--	0.007	0.004	0.007	0.016	0.002
71.013	C3H2O2H+	--	--	--	--	--	0.008	0.007	0.005	0.022	0.002
71.049	C4H6OH+	--	--	--	--	--	0.048	0.019	0.044	0.082	0.021
71.086	C5H10H+	0.062	0.023	0.053	0.107	0.033	0.079	0.019	0.066	0.104	0.058
72.045	C3H5ONH+	0.009	0.012	0.001	0.034	0.001	0.013	0.008	0.011	0.028	0.002
72.081	C4H9NH+	0.009	0.010	0.002	0.025	0.001	0.005	0.004	0.004	0.016	0.000
73.029	C3H4O2H+	0.054	0.066	0.026	0.177	0.000	0.062	0.028	0.057	0.110	0.017
74.029	C2H3O2NH+	0.002	0.004	0.000	0.010	0.000	0.002	0.001	0.001	0.005	0.000
74.061	C3H7ONH+	0.014	0.015	0.012	0.033	0.000	--	--	--	--	--
74.096	C4H11NH+	0.032	0.039	0.008	0.113	0.006	0.007	0.005	0.005	0.021	0.001
75.026	C6H2H+	--	--	--	--	--	0.006	0.003	0.007	0.009	0.001
75.043	C3H6O2H+	--	--	--	--	--	0.024	0.016	0.027	0.061	0.003
76.026	C5HNH+	0.006	0.004	0.005	0.012	0.002	--	--	--	--	--
77.038	C6H4H+	0.024	0.016	0.016	0.056	0.012	0.021	0.006	0.021	0.036	0.011
79.054	C6H6H+	0.027	0.018	0.019	0.063	0.011	0.073	0.011	0.072	0.092	0.051
80.051	C5H5NH+	0.011	0.011	0.006	0.031	0.002	0.010	0.005	0.010	0.024	0.003

Table A.9: continue

m/z	Formula	LDV					HDV				
		Average	Std Dev	Med	Max	Min	Average	Std Dev	Med	Max	Min
81.034	C5H4OH+	0.000	0.000	0.000	0.000	0.000	0.052	0.031	0.043	0.124	0.012
81.070	C6H8H+	0.061	0.044	0.043	0.151	0.019	0.255	0.053	0.264	0.326	0.159
82.033	C4H3ONH+	--	--	--	--	--	0.006	0.003	0.004	0.012	0.002
82.067	13CC5H8H+	0.011	0.010	0.008	0.031	0.002	0.016	0.003	0.016	0.021	0.009
83.014	C4H2O2H+	--	--	--	--	--	0.005	0.005	0.004	0.014	0.000
83.049	C5H6OH+	0.042	0.051	0.022	0.136	0.000	0.089	0.039	0.090	0.154	0.027
83.086	C6H10H+	0.056	0.055	0.025	0.165	0.015	0.138	0.036	0.152	0.185	0.067
85.028	C4H4O2H+	--	--	--	--	--	0.207	0.141	0.142	0.550	0.040
85.064	C5H8OH+	0.026	0.041	0.006	0.098	0.000	0.039	0.016	0.036	0.069	0.009
85.102	C6H12H+	0.033	0.025	0.023	0.088	0.013	0.074	0.015	0.076	0.097	0.051
86.030	C3H3O2NH+	0.000	0.000	0.000	0.000	0.000	0.012	0.009	0.009	0.034	0.002
86.060	C4H7ONH+	0.014	0.019	0.000	0.042	0.000	0.007	0.005	0.007	0.019	0.002
86.097	C5H11NH+	0.007	0.009	0.003	0.027	0.001	0.004	0.002	0.004	0.009	0.002
87.008	C3H2O3H+	--	--	--	--	--	0.000	0.000	0.000	0.001	0.000
87.044	C4H6O2H+	0.000	0.000	0.000	0.000	0.000	0.044	0.026	0.037	0.085	0.011
88.023	C6HNH+	0.009	0.011	0.002	0.026	0.000	0.003	0.003	0.001	0.011	0.000
88.044	C3H5O2NH+	0.007	0.010	0.003	0.027	0.000	0.003	0.002	0.003	0.005	0.000
88.075	C4H9ONH+	0.014	0.007	0.014	0.026	0.004	0.012	0.006	0.012	0.020	0.003
89.024	C3H4O3H+	--	--	--	--	--	0.004	0.003	0.002	0.012	0.001
89.060	C4H8O2H+	0.033	0.031	0.016	0.081	0.006	0.012	0.009	0.010	0.036	0.002
91.054	C7H6H+	0.026	0.017	0.019	0.064	0.013	0.086	0.017	0.083	0.117	0.060
92.056	13CC6H6H+	0.005	0.005	0.002	0.015	0.001	0.009	0.002	0.009	0.013	0.004
93.037	C6H4OH+	0.000	0.000	0.000	0.000	0.000	0.013	0.004	0.012	0.025	0.007
93.070	C7H8H+	0.021	0.023	0.011	0.068	0.003	0.059	0.016	0.062	0.084	0.033
94.032	C5H3ONH+	0.012	0.008	0.009	0.027	0.006	0.012	0.003	0.012	0.020	0.009
94.066	C6H7NH+	0.019	0.019	0.013	0.050	0.000	0.025	0.007	0.026	0.036	0.012
95.015	C5H2O2H+	0.013	0.006	0.013	0.024	0.006	0.014	0.005	0.013	0.023	0.009
95.050	C6H6OH+	0.040	0.050	0.018	0.149	0.001	0.109	0.027	0.101	0.146	0.059
95.085	C7H10H+	0.108	0.056	0.087	0.232	0.064	0.365	0.072	0.372	0.458	0.221
96.046	C5H5ONH+	0.045	0.026	0.040	0.087	0.019	0.082	0.050	0.076	0.224	0.028
96.086	13CC6H10H+	0.017	0.013	0.010	0.043	0.006	0.031	0.007	0.030	0.048	0.015
97.029	C5H4O2H+	0.000	0.000	0.000	0.000	0.000	0.548	0.357	0.503	1.524	0.075
97.064	C6H8OH+	0.021	0.028	0.009	0.072	0.000	0.048	0.027	0.045	0.109	0.010
97.102	C7H12H+	0.024	0.016	0.017	0.055	0.009	0.138	0.030	0.126	0.185	0.079
98.060	C5H7ONH+	0.019	0.029	0.006	0.087	0.001	0.018	0.013	0.012	0.046	0.005
98.097	C6H11NH+	0.010	0.011	0.006	0.034	0.002	0.009	0.004	0.008	0.018	0.003
99.008	C4H2O3H+	0.145	0.137	0.123	0.331	0.001	0.394	0.089	0.375	0.546	0.267
99.044	C5H6O2H+	--	--	--	--	--	0.166	0.082	0.156	0.322	0.054
99.079	C6H10OH+	0.029	0.043	0.009	0.116	0.000	0.038	0.011	0.039	0.057	0.023
100.012	C7HNH+	0.007	0.010	0.003	0.028	0.000	0.016	0.005	0.015	0.025	0.009
100.041	C4H5O2NH+	--	--	--	--	--	0.027	0.013	0.023	0.047	0.009

m/z	Formula	LDV					HDV				
		Average	Std Dev	Med	Max	Min	Average	Std Dev	Med	Max	Min
100.075	C5H9ONH+	0.033	0.035	0.011	0.103	0.008	0.018	0.007	0.018	0.035	0.003
100.112	C6H13NH+	0.015	0.010	0.012	0.029	0.002	0.002	0.001	0.002	0.005	0.000
101.025	C4H4O3H+	0.021	0.031	0.011	0.091	0.000	0.120	0.044	0.103	0.199	0.052
101.058	C5H8O2H+	0.016	0.025	0.004	0.065	0.000	0.024	0.014	0.021	0.057	0.008
102.025	C3H3O3NH+	0.002	0.003	0.001	0.009	0.000	0.006	0.003	0.005	0.011	0.002
102.058	C4H7O2NH+	0.005	0.007	0.001	0.019	0.000	0.002	0.002	0.002	0.006	0.000
102.127	C6H15NH+	0.016	0.014	0.013	0.043	0.001	--	--	--	--	--
103.074	C5H10O2H+	0.019	0.020	0.013	0.065	0.002	0.006	0.004	0.006	0.015	0.001
104.048	C7H5NH+	0.000	0.000	0.000	0.000	0.000	0.009	0.002	0.009	0.011	0.005
105.035	C7H4OH+	0.013	0.014	0.005	0.042	0.003	0.020	0.006	0.020	0.029	0.008
105.070	C8H8H+	0.066	0.033	0.053	0.133	0.038	0.155	0.035	0.155	0.214	0.088
106.032	C6H3ONH+	0.006	0.008	0.001	0.021	0.000	0.003	0.002	0.002	0.006	0.002
106.070	13CC7H8H+	0.011	0.010	0.005	0.030	0.003	0.015	0.004	0.015	0.024	0.008
107.050	C7H6OH+	--	--	--	--	--	0.067	0.047	0.048	0.209	0.030
107.085	C8H10H+	0.030	0.040	0.009	0.109	0.000	0.065	0.027	0.063	0.137	0.030
108.048	C6H5ONH+	0.009	0.010	0.008	0.030	0.000	0.010	0.004	0.011	0.017	0.004
108.082	C7H9NH+	0.012	0.012	0.009	0.036	0.000	0.021	0.010	0.022	0.042	0.008
109.029	C6H4O2H+	0.000	0.000	0.000	0.000	0.000	0.075	0.050	0.063	0.221	0.022
109.066	C7H8OH+	0.045	0.044	0.032	0.107	0.000	0.078	0.021	0.081	0.109	0.038
109.101	C8H12H+	0.075	0.045	0.062	0.167	0.032	0.280	0.059	0.287	0.359	0.175
110.061	C6H7ONH+	0.031	0.023	0.023	0.076	0.010	0.026	0.012	0.022	0.050	0.011
110.103	13CC7H12H+	0.016	0.013	0.008	0.040	0.005	0.027	0.006	0.026	0.040	0.014
111.045	C6H6O2H+	0.079	0.098	0.045	0.271	0.000	0.124	0.057	0.109	0.248	0.068
111.080	C7H10OH+	0.036	0.046	0.023	0.113	0.000	0.046	0.018	0.052	0.070	0.014
111.117	C8H14H+	0.044	0.044	0.018	0.123	0.007	0.103	0.026	0.101	0.142	0.055
112.041	C5H5O2NH+	0.019	0.030	0.011	0.090	0.000	0.024	0.016	0.017	0.055	0.007
112.076	C6H9ONH+	0.023	0.027	0.011	0.083	0.005	0.009	0.006	0.007	0.019	0.000
113.024	C5H4O3H+	0.150	0.161	0.104	0.440	0.000	0.116	0.055	0.114	0.242	0.040
113.060	C6H8O2H+	0.080	0.104	0.042	0.281	0.000	0.047	0.022	0.037	0.096	0.023
113.133	C8H16H+	0.016	0.015	0.010	0.045	0.004	0.018	0.004	0.018	0.025	0.011
114.023	C4H3O3NH+	0.005	0.009	0.001	0.025	0.000	0.006	0.004	0.005	0.017	0.001
114.056	C5H7O2NH+	0.014	0.022	0.002	0.063	0.000	0.013	0.005	0.013	0.020	0.001
114.091	C6H11ONH+	0.223	0.224	0.104	0.603	0.046	0.160	0.068	0.144	0.293	0.051
115.016	C8H2OH+	--	--	--	--	--	0.014	0.007	0.011	0.027	0.004
115.040	C5H6O3H+	--	--	--	--	--	0.057	0.025	0.050	0.104	0.024
115.074	C6H10O2H+	0.009	0.019	0.000	0.054	0.000	0.026	0.008	0.025	0.038	0.010
116.038	C4H5O3NH+	0.004	0.007	0.001	0.019	0.000	0.006	0.004	0.005	0.014	0.002
117.088	C6H12O2H+	--	--	--	--	--	0.021	0.009	0.020	0.035	0.004
119.054	C8H6OH+	0.014	0.014	0.006	0.042	0.002	0.031	0.013	0.030	0.065	0.013
119.085	C9H10H+	0.040	0.023	0.028	0.087	0.015	0.113	0.025	0.114	0.159	0.074
120.046	C7H5ONH+	0.009	0.009	0.005	0.027	0.001	0.027	0.006	0.026	0.042	0.019

m/z	Formula	LDV					HDV				
		Average	Std Dev	Med	Max	Min	Average	Std Dev	Med	Max	Min
120.082	C8H9NH+	0.011	0.011	0.005	0.035	0.002	0.016	0.004	0.017	0.026	0.009
121.031	C7H4O2H+	0.009	0.008	0.005	0.024	0.001	0.047	0.013	0.044	0.081	0.029
121.065	C8H8OH+	0.062	0.055	0.042	0.156	0.012	0.068	0.030	0.066	0.143	0.026
121.101	C9H12H+	0.027	0.024	0.017	0.063	0.005	0.082	0.021	0.081	0.117	0.046
122.062	C7H7ONH+	0.017	0.017	0.007	0.050	0.002	0.020	0.007	0.020	0.038	0.010
122.097	C8H11NH+	0.017	0.017	0.009	0.052	0.004	0.020	0.009	0.018	0.035	0.004
123.044	C7H6O2H+	0.118	0.087	0.084	0.272	0.045	0.188	0.045	0.189	0.292	0.127
123.079	C8H10OH+	0.044	0.039	0.033	0.104	0.001	0.073	0.019	0.079	0.096	0.030
123.116	C9H14H+	0.044	0.028	0.033	0.101	0.019	0.168	0.035	0.161	0.212	0.102
124.043	C6H5O2NH+	0.033	0.013	0.030	0.053	0.019	0.045	0.010	0.042	0.073	0.036
124.076	C7H9ONH+	0.027	0.022	0.016	0.070	0.009	0.018	0.007	0.017	0.032	0.006
124.117	13CC8H14H+	0.013	0.013	0.006	0.036	0.003	0.022	0.005	0.022	0.031	0.011
124.992	C2H4O6H+	--	--	--	--	--	0.064	0.029	0.053	0.135	0.029
125.060	C7H8O2H+	0.068	0.085	0.040	0.226	0.000	0.067	0.023	0.067	0.103	0.028
125.095	C8H12OH+	0.032	0.042	0.013	0.113	0.000	0.036	0.015	0.040	0.054	0.011
125.134	C9H16H+	0.020	0.017	0.013	0.050	0.005	0.069	0.016	0.067	0.097	0.040
126.056	C6H7O2NH+	0.016	0.019	0.012	0.058	0.001	0.013	0.008	0.011	0.028	0.005
126.091	C7H11ONH+	0.023	0.023	0.009	0.069	0.005	0.008	0.004	0.006	0.016	0.000
127.040	C6H6O3H+	--	--	--	--	--	0.178	0.118	0.152	0.515	0.036
127.074	C7H10O2H+	0.039	0.050	0.021	0.141	0.000	0.059	0.022	0.057	0.102	0.027
128.040	C5H5O3NH+	0.007	0.008	0.006	0.024	0.001	0.018	0.011	0.014	0.044	0.003
128.068	C6H9O2NH+	0.011	0.012	0.008	0.035	0.001	0.016	0.006	0.014	0.032	0.008
128.107	C7H13ONH+	0.026	0.031	0.005	0.077	0.004	0.020	0.014	0.014	0.051	0.002
129.060	C6H8O3H+	0.009	0.016	0.006	0.048	0.000	0.121	0.022	0.116	0.170	0.086
130.051	C5H7O3NH+	0.009	0.011	0.004	0.033	0.000	0.037	0.011	0.037	0.056	0.022
130.158	C8H19NH+	0.018	0.010	0.014	0.037	0.007	0.003	0.002	0.003	0.007	0.000
131.043	C4H6O3N2H+	0.016	0.011	0.012	0.034	0.002	0.038	0.013	0.036	0.060	0.021
131.086	C10H10H+	0.024	0.026	0.009	0.070	0.002	0.060	0.015	0.062	0.083	0.032
132.047	C8H5ONH+	0.005	0.005	0.003	0.014	0.001	0.006	0.002	0.005	0.010	0.003
132.082	C9H9NH+	0.009	0.011	0.004	0.034	0.001	0.011	0.004	0.010	0.019	0.005
133.032	C8H4O2H+	0.002	0.003	0.002	0.009	0.000	0.041	0.017	0.037	0.070	0.018
133.065	C9H8OH+	0.021	0.017	0.018	0.056	0.005	0.056	0.016	0.054	0.089	0.029
133.100	C10H12H+	0.031	0.023	0.019	0.078	0.013	0.096	0.025	0.097	0.142	0.058
134.062	C8H7ONH+	0.022	0.012	0.019	0.048	0.011	0.029	0.010	0.027	0.056	0.015
135.046	C8H6O2H+	0.030	0.029	0.026	0.075	0.00	0.066	0.024	0.062	0.104	0.036
135.079	C9H10OH+	0.027	0.023	0.021	0.064	0.003	0.056	0.019	0.054	0.101	0.023
135.116	C10H14H+	0.032	0.023	0.017	0.075	0.014	0.104	0.025	0.102	0.148	0.059
136.024	C3H5O5NH+	0.004	0.006	0.001	0.018	0.000	0.015	0.006	0.014	0.027	0.007
136.043	C7H5O2NH+	0.010	0.009	0.007	0.028	0.001	0.021	0.009	0.019	0.046	0.012
136.076	C8H9ONH+	0.020	0.021	0.010	0.064	0.003	0.020	0.009	0.019	0.045	0.007
136.113	C9H13NH+	0.017	0.016	0.009	0.050	0.003	0.018	0.008	0.020	0.035	0.005

m/z	Formula	LDV					HDV				
		Average	Std Dev	Med	Max	Min	Average	Std Dev	Med	Max	Min
137.060	C8H8O2H+	0.036	0.042	0.025	0.124	0.000	0.119	0.036	0.107	0.211	0.070
137.095	C9H12OH+	0.030	0.030	0.018	0.084	0.003	0.055	0.018	0.057	0.086	0.022
137.132	C10H16H+	0.029	0.022	0.018	0.072	0.008	0.106	0.024	0.097	0.137	0.063
138.057	C7H7O2NH+	0.017	0.018	0.013	0.056	0.002	0.027	0.012	0.022	0.056	0.016
139.040	C7H6O3H+	0.017	0.022	0.009	0.063	0.000	0.166	0.048	0.161	0.270	0.114
139.076	C8H10O2H+	0.038	0.047	0.025	0.135	0.000	0.063	0.020	0.066	0.093	0.025
139.109	C9H14OH+	0.029	0.038	0.007	0.098	0.0000	0.027	0.014	0.027	0.049	0.005
139.149	C10H18H+	0.014	0.014	0.007	0.040	0.002	0.043	0.012	0.041	0.061	0.023
140.036	C6H5O3NH+	0.020	0.009	0.019	0.039	0.011	0.185	0.046	0.166	0.256	0.108
140.072	C7H9O2NH+	0.015	0.015	0.013	0.049	0.001	0.038	0.011	0.034	0.058	0.025
141.020	C6H4O4H+	0.010	0.008	0.011	0.021	0.001	0.060	0.018	0.057	0.096	0.038
141.058	C7H8O3H+	0.023	0.025	0.019	0.072	0.000	0.067	0.024	0.057	0.115	0.045
141.090	C8H12O2H+	0.026	0.032	0.016	0.094	0.001	0.046	0.015	0.043	0.073	0.026
142.054	C10H7NH+	0.008	0.009	0.007	0.029	0.001	0.017	0.006	0.016	0.027	0.011
143.035	C6H6O4H+	--	--	--	--	--	0.027	0.014	0.024	0.059	0.011
143.081	C6H10O2N2H+	0.016	0.027	0.008	0.082	--	0.126	0.024	0.121	0.176	0.094
144.081	C10H9NH+	0.035	0.034	0.026	0.109	0.003	0.038	0.016	0.036	0.065	0.012
145.049	C6H8O4H+	--	--	--	--	--	0.108	0.041	0.111	0.214	0.040
145.121	C8H16O2H+	0.136	0.199	0.019	0.559	0.014	0.046	0.014	0.043	0.075	0.024
146.060	C9H7ONH+	0.020	0.013	0.017	0.045	0.009	0.035	0.011	0.032	0.067	0.019
147.046	C9H6O2H+	0.021	0.020	0.017	0.053	0.001	0.200	0.042	0.196	0.273	0.141
147.078	C10H10OH+	0.036	0.024	0.031	0.085	0.015	0.092	0.021	0.092	0.122	0.054
147.115	C11H14H+	0.028	0.020	0.018	0.066	0.011	0.078	0.019	0.078	0.113	0.050
148.040	C8H5O2NH+	0.087	0.071	0.052	0.241	0.034	0.223	0.049	0.213	0.316	0.154
149.024	C8H4O3H+	3.403	0.861	3.221	4.500	2.252	1.363	0.493	1.181	2.578	0.902
149.131	C11H16H+	0.187	0.053	0.164	0.257	0.119	0.159	0.043	0.147	0.214	0.083
150.090	C9H11ONH+	0.033	0.025	0.021	0.078	0.009	0.033	0.011	0.033	0.059	0.014
150.129	C10H15NH+	0.032	0.017	0.023	0.060	0.012	0.024	0.008	0.024	0.042	0.009
151.037	C8H6O3H+	0.034	0.016	0.034	0.065	0.017	0.103	0.028	0.098	0.174	0.071
151.076	C9H10O2H+	0.038	0.038	0.028	0.116	0.004	0.100	0.035	0.094	0.185	0.058
151.109	C10H14OH+	0.037	0.044	0.014	0.117	0.002	0.051	0.019	0.055	0.082	0.021
151.147	C11H18H+	0.029	0.023	0.018	0.071	0.007	0.087	0.022	0.077	0.118	0.050
152.021	C3H5O6NH+	0.038	0.015	0.032	0.070	0.023	0.060	0.020	0.060	0.095	0.033
152.074	C8H9O2NH+	0.019	0.017	0.016	0.054	0.004	0.031	0.012	0.026	0.060	0.018
153.059	C8H8O3H+	0.022	0.027	0.013	0.080	0.000	0.077	0.032	0.062	0.157	0.045
153.092	C9H12O2H+	0.037	0.050	0.021	0.148	0.000	0.064	0.021	0.056	0.103	0.030
154.054	C11H7NH+	0.014	0.010	0.013	0.037	0.004	0.091	0.030	0.082	0.166	0.048
154.086	C8H11O2NH+	0.014	0.018	0.007	0.055	0.002	0.029	0.009	0.026	0.048	0.019
155.079	C7H10O2N2H+	0.023	0.028	0.018	0.086	0.000	0.156	0.034	0.148	0.226	0.107
156.081	C11H9NH+	0.015	0.014	0.011	0.046	0.003	0.031	0.010	0.028	0.053	0.019
157.058	C6H8O3N2H+	0.010	0.011	0.007	0.031	0.000	0.081	0.022	0.072	0.121	0.055

m/z	Formula	LDV					HDV				
		Average	Std Dev	Med	Max	Min	Average	Std Dev	Med	Max	Min
157.096	C7H12O2N2H+	0.026	0.040	0.013	0.123	0.005	0.128	0.026	0.122	0.177	0.094
158.097	C11H11NH+	0.075	0.030	0.074	0.127	0.032	0.034	0.013	0.035	0.066	0.012
158.154	C9H19ONH+	0.119	0.144	0.019	0.349	0.014	0.010	0.004	0.009	0.017	0.005
159.085	C11H10OH+	0.078	0.034	0.077	0.123	0.032	0.146	0.030	0.146	0.212	0.082
159.137	C9H18O2H+	0.093	0.112	0.031	0.316	0.018	0.056	0.019	0.053	0.088	0.027
160.081	C10H9ONH+	0.091	0.127	0.043	0.405	0.034	0.079	0.115	0.045	0.454	0.020
161.061	C10H8O2H+	0.051	0.041	0.036	0.129	0.014	0.170	0.044	0.166	0.259	0.107
161.094	C11H12OH+	0.108	0.049	0.085	0.219	0.076	0.100	0.035	0.096	0.158	0.039
162.058	C9H7O2NH+	0.034	0.021	0.026	0.076	0.014	0.072	0.020	0.070	0.122	0.045
162.093	C10H11ONH+	0.087	0.102	0.046	0.338	0.038	0.061	0.045	0.042	0.165	0.021
163.040	C9H6O3H+	0.141	0.087	0.146	0.247	0.014	0.641	0.137	0.630	0.920	0.449
163.074	C10H10O2H+	0.094	0.093	0.057	0.265	0.006	0.224	0.064	0.229	0.322	0.126
163.121	C10H14N2H+	0.075	0.047	0.063	0.154	0.030	0.063	0.020	0.062	0.092	0.031
163.147	C12H18H+	0.051	0.026	0.043	0.105	0.026	0.113	0.026	0.106	0.150	0.066
164.040	13CC8H6O3H+	0.023	0.014	0.024	0.045	0.005	0.156	0.031	0.149	0.210	0.110
164.146	C11H17NH+	0.027	0.018	0.018	0.060	0.010	0.026	0.008	0.027	0.043	0.011
165.020	C8H4O4H+	0.019	0.017	0.017	0.044	0.002	0.990	0.210	0.965	1.398	0.674
165.056	C9H8O3H+	0.019	0.020	0.015	0.056	0.000	0.260	0.058	0.251	0.386	0.166
165.089	C10H12O2H+	0.039	0.032	0.033	0.106	0.010	0.138	0.037	0.130	0.207	0.083
166.050	C8H7O3NH+	0.009	0.009	0.008	0.028	0.002	0.046	0.012	0.042	0.077	0.031
166.086	C9H11O2NH+	0.016	0.015	0.013	0.049	0.003	0.028	0.009	0.025	0.048	0.014
167.035	C8H6O4H+	0.018	0.014	0.015	0.041	0.004	0.094	0.038	0.093	0.173	0.019
167.073	C9H10O3H+	0.019	0.022	0.012	0.064	0.000	0.074	0.023	0.066	0.122	0.040
167.107	C10H14O2H+	0.036	0.051	0.016	0.154	0.001	0.090	0.028	0.089	0.149	0.043
168.070	C8H9O3NH+	0.028	0.013	0.026	0.058	0.017	0.060	0.014	0.057	0.086	0.042
168.100	C9H13O2NH+	0.016	0.021	0.008	0.065	0.002	0.029	0.008	0.026	0.048	0.019
169.056	C8H8O4H+	0.004	0.005	0.001	0.014	0.000	0.086	0.029	0.078	0.162	0.057
169.093	C9H12O3H+	0.018	0.024	0.015	0.074	0.001	0.124	0.027	0.118	0.180	0.080
170.063	C11H7ONH+	0.009	0.009	0.007	0.027	0.001	0.034	0.010	0.030	0.062	0.024
170.092	C12H11NH+	0.015	0.013	0.009	0.041	0.004	0.032	0.009	0.029	0.055	0.023
171.081	C12H10OH+	0.009	0.009	0.008	0.027	0.000	0.118	0.025	0.112	0.162	0.086
171.113	C8H14O2N2H+	0.024	0.025	0.011	0.077	0.005	0.091	0.021	0.088	0.127	0.050
171.146	C9H18ON2H+	0.122	0.151	0.077	0.486	0.031	0.079	0.130	0.020	0.484	0.008
172.044	C3H9O7NH+	0.012	0.004	0.011	0.019	0.007	0.038	0.008	0.036	0.058	0.028
172.075	C11H9ONH+	0.012	0.009	0.009	0.031	0.005	0.025	0.007	0.024	0.040	0.014
172.111	C12H13NH+	0.031	0.013	0.025	0.054	0.020	0.027	0.008	0.026	0.045	0.010
172.166	C10H21ONH+	0.033	0.034	0.013	0.100	0.007	0.012	0.018	0.005	0.068	0.001
173.061	C11H8O2H+	0.019	0.015	0.018	0.046	0.002	0.277	0.051	0.271	0.385	0.208
173.093	C12H12OH+	0.035	0.023	0.023	0.076	0.011	0.138	0.028	0.136	0.204	0.098
173.150	C10H20O2H+	0.058	0.051	0.031	0.152	0.019	0.084	0.019	0.079	0.119	0.061
174.023	C2H7O8NH+	0.011	0.004	0.011	0.019	0.007	0.063	0.013	0.061	0.086	0.047

m/z	Formula	LDV					HDV				
		Average	Std Dev	Med	Max	Min	Average	Std Dev	Med	Max	Min
174.060	C10H7O2NH+	0.031	0.012	0.028	0.055	0.018	0.072	0.014	0.071	0.101	0.049
175.041	C10H6O3H+	--	--	--	--	--	0.211	0.050	0.201	0.321	0.143
175.074	C11H10O2H+	0.048	0.043	0.031	0.126	0.011	0.199	0.053	0.199	0.321	0.124
176.040	C9H5O3NH+	0.008	0.007	0.007	0.021	0.002	0.054	0.011	0.052	0.079	0.036
176.073	C10H9O2NH+	0.030	0.015	0.025	0.059	0.014	0.061	0.018	0.060	0.106	0.037
177.055	C10H8O3H+	0.208	0.174	0.173	0.586	0.039	0.310	0.091	0.303	0.477	0.146
177.162	C13H20H+	0.070	0.033	0.053	0.128	0.034	0.132	0.033	0.131	0.194	0.072
178.059	13CC9H8O3H+	0.037	0.028	0.027	0.088	0.007	0.075	0.021	0.070	0.129	0.047
179.071	C10H10O3H+	0.036	0.026	0.034	0.077	0.005	0.297	0.068	0.271	0.489	0.233
179.104	C11H14O2H+	0.087	0.065	0.055	0.191	0.032	0.226	0.047	0.224	0.335	0.162
179.179	C13H22H+	0.035	0.023	0.024	0.077	0.011	0.118	0.027	0.112	0.168	0.076
180.087	C6H13O5NH+	0.028	0.016	0.023	0.058	0.011	0.093	0.024	0.088	0.158	0.073
181.080	C5H12O5N2H+	0.040	0.037	0.034	0.127	0.005	0.722	0.144	0.693	1.076	0.557
181.125	C11H16O2H+	0.033	0.041	0.012	0.117	0.002	0.164	0.042	0.167	0.258	0.107
182.072	C9H11O3NH+	0.021	0.018	0.014	0.062	0.005	0.154	0.032	0.146	0.234	0.115
184.081	C5H13O6NH+	0.016	0.016	0.011	0.051	0.003	0.042	0.012	0.039	0.073	0.030
185.062	C12H8O2H+	0.020	0.023	0.014	0.064	0.001	0.220	0.051	0.206	0.333	0.155
185.126	C9H16O2N2H+	0.021	0.021	0.012	0.063	0.003	0.151	0.034	0.149	0.213	0.101
187.076	C12H10O2H+	0.029	0.028	0.026	0.093	0.005	0.231	0.056	0.228	0.366	0.157
188.041	C3H9O8NH+	0.014	0.006	0.012	0.023	0.008	0.056	0.010	0.055	0.079	0.041
188.075	13CC11H10O2H+	0.030	0.014	0.024	0.061	0.019	0.049	0.012	0.047	0.082	0.031
189.023	C3H8O9H+	0.005	0.005	0.004	0.013	0.000	0.234	0.046	0.235	0.326	0.177
189.055	C11H8O3H+	0.016	0.012	0.016	0.041	0.005	0.158	0.036	0.157	0.236	0.111
189.088	C12H12O2H+	0.031	0.027	0.020	0.087	0.006	0.141	0.040	0.137	0.238	0.085
189.124	C13H16OH+	0.047	0.044	0.022	0.125	0.009	0.115	0.034	0.116	0.179	0.063
190.053	C10H7O3NH+	0.023	0.008	0.022	0.038	0.014	0.072	0.013	0.069	0.103	0.053
190.084	C11H11O2NH+	0.021	0.015	0.015	0.052	0.006	0.048	0.014	0.046	0.083	0.029
191.037	C10H6O4H+	0.007	0.006	0.008	0.016	0.000	0.185	0.042	0.192	0.264	0.130
191.072	C11H10O3H+	0.039	0.027	0.033	0.090	0.009	0.220	0.054	0.209	0.354	0.157
191.178	C14H22H+	0.052	0.026	0.039	0.092	0.020	0.138	0.035	0.136	0.207	0.080
192.035	C9H5O4NH+	0.009	0.010	0.005	0.029	0.001	0.050	0.012	0.049	0.068	0.030
192.072	C10H9O3NH+	0.016	0.012	0.013	0.043	0.004	0.062	0.017	0.056	0.107	0.043
193.015	C9H4O5H+	0.019	0.024	0.012	0.074	0.001	0.455	0.185	0.456	0.753	0.142
193.102	C15H12H+	0.034	0.024	0.034	0.083	0.008	0.533	0.101	0.519	0.767	0.410
194.019	C5H7O7NH+	0.019	0.011	0.016	0.042	0.008	0.073	0.022	0.072	0.116	0.039
194.104	13CC14H12H+	0.038	0.015	0.033	0.067	0.022	0.111	0.023	0.106	0.171	0.087
195.086	C7H14O6H+	0.108	0.040	0.101	0.198	0.061	0.476	0.093	0.447	0.715	0.390
196.093	C10H13O3NH+	0.044	0.019	0.036	0.085	0.025	0.124	0.029	0.112	0.204	0.097
197.063	C13H8O2H+	0.023	0.018	0.024	0.060	0.004	0.448	0.089	0.428	0.666	0.354
197.126	C10H16O2N2H+	0.024	0.024	0.015	0.069	0.003	0.231	0.049	0.226	0.337	0.162
198.059	C5H11O7NH+	0.035	0.013	0.031	0.059	0.021	0.169	0.033	0.165	0.252	0.132

m/z	Formula	LDV					HDV				
		Average	Std Dev	Med	Max	Min	Average	Std Dev	Med	Max	Min
199.041	C12H6O3H+	0.041	0.018	0.048	0.057	0.009	2.035	0.351	2.013	2.780	1.558
200.198	C12H25ONH+	0.018	0.014	0.010	0.039	0.006	0.024	0.007	0.023	0.043	0.013
201.058	C12H8O3H+	0.009	0.009	0.006	0.027	0.001	0.114	0.028	0.111	0.187	0.080
201.087	C13H12O2H+	0.029	0.022	0.021	0.074	0.006	0.131	0.038	0.123	0.219	0.073
201.184	C12H24O2H+	--	--	--	--	--	0.213	0.133	0.176	0.606	0.118
202.087	C12H11O2NH+	0.021	0.019	0.013	0.062	0.006	0.055	0.016	0.051	0.097	0.035
202.187	13CC11H24O2H+	0.025	0.018	0.018	0.060	0.011	0.035	0.017	0.028	0.081	0.021
203.087	C9H14O5H+	0.070	0.037	0.061	0.140	0.025	0.947	0.181	0.905	1.424	0.761
203.176	C15H22H+	0.035	0.028	0.020	0.085	0.007	0.164	0.039	0.163	0.245	0.106
204.089	C8H13O5NH+	0.035	0.020	0.030	0.077	0.011	0.212	0.044	0.201	0.333	0.165
205.135	C12H16ON2H+	0.029	0.009	0.026	0.045	0.019	0.054	0.013	0.052	0.087	0.042
205.089	C12H12O3H+	0.015	0.009	0.011	0.029	0.005	0.046	0.011	0.046	0.069	0.028
205.193	C15H24H+	0.039	0.026	0.027	0.085	0.011	0.139	0.034	0.132	0.195	0.087
206.061	C10H7O4NH+	0.009	0.009	0.007	0.026	0.001	0.056	0.011	0.054	0.086	0.042
206.093	C8H15O5NH+	--	--	--	--	--	0.060	0.016	0.055	0.104	0.046
207.063	C11H10O4H+	--	--	--	--	--	0.039	0.012	0.037	0.070	0.023
207.032	C10H6O5H+	0.013	0.004	0.013	0.021	0.008	0.048	0.012	0.046	0.080	0.034
207.117	C16H14H+	0.037	0.027	0.037	0.096	0.007	0.706	0.144	0.684	1.030	0.523
208.118	13CC15H14H+	0.026	0.017	0.018	0.056	0.008	0.144	0.030	0.139	0.217	0.106
209.020	C8H4O5N2H+	0.012	0.016	0.005	0.048	0.002	0.128	0.029	0.119	0.203	0.098
209.096	C15H12OH+	0.038	0.034	0.030	0.109	0.004	0.507	0.104	0.499	0.767	0.398
209.156	C13H20O2H+	0.045	0.046	0.023	0.150	0.012	0.271	0.056	0.267	0.385	0.199
210.128	C15H15NH+	0.019	0.015	0.013	0.052	0.006	0.096	0.020	0.093	0.149	0.076
210.147	C12H19O2NH+	0.017	0.017	0.010	0.058	0.006	0.051	0.012	0.048	0.080	0.038
211.088	C13H10ON2H+	0.020	0.014	0.019	0.048	0.004	0.195	0.044	0.191	0.307	0.153
211.141	C11H18O2N2H+	0.034	0.030	0.022	0.091	0.007	0.280	0.061	0.278	0.419	0.196
212.069	C13H9O2NH+	0.033	0.014	0.029	0.062	0.019	0.093	0.021	0.086	0.148	0.070
213.060	C6H12O8H+	0.043	0.014	0.042	0.067	0.020	0.607	0.108	0.613	0.851	0.476
214.062	C5H11O8NH+	0.025	0.007	0.024	0.040	0.016	0.090	0.017	0.085	0.135	0.069
214.085	C13H11O2NH+	0.033	0.012	0.035	0.054	0.016	0.075	0.020	0.072	0.125	0.049
215.036	C12H6O4H+	0.020	0.012	0.018	0.038	0.005	0.344	0.061	0.316	0.490	0.272
215.193	C13H26O2H+	0.037	0.018	0.031	0.075	0.020	0.129	0.031	0.129	0.189	0.076
216.036	C4H9O9NH+	0.021	0.010	0.018	0.040	0.010	0.089	0.017	0.083	0.130	0.067
217.015	C11H4O5H+	0.014	0.012	0.011	0.037	0.002	0.447	0.083	0.428	0.629	0.332
217.104	C10H16O5H+	0.053	0.026	0.052	0.103	0.018	0.399	0.091	0.385	0.644	0.292
217.190	C11H24O2N2H+	0.043	0.032	0.025	0.102	0.009	0.158	0.041	0.148	0.244	0.100
218.012	C10H3O5NH+	0.011	0.017	0.004	0.050	0.000	0.174	0.043	0.171	0.251	0.111
218.104	C9H15O5NH+	0.027	0.019	0.019	0.066	0.009	0.091	0.022	0.083	0.153	0.062
219.047	C8H10O7H+	0.005	0.005	0.004	0.012	0.000	0.149	0.042	0.148	0.253	0.095
219.110	C12H14O2N2H+	0.120	0.035	0.131	0.154	0.065	0.327	0.091	0.288	0.568	0.241
219.173	C15H22OH+	0.082	0.092	0.040	0.294	0.013	0.162	0.045	0.158	0.259	0.099

m/z	Formula	LDV					HDV				
		Average	Std Dev	Med	Max	Min	Average	Std Dev	Med	Max	Min
221.080	C12H12O4H+	0.027	0.013	0.024	0.052	0.009	0.230	0.054	0.213	0.376	0.172
221.134	C10H20O5H+	0.061	0.022	0.064	0.088	0.024	0.508	0.112	0.487	0.778	0.371
222.068	C11H11O4NH+	0.027	0.010	0.025	0.049	0.016	0.064	0.014	0.063	0.105	0.048
222.135	C9H19O5NH+	0.022	0.013	0.018	0.048	0.007	0.112	0.025	0.108	0.173	0.087
223.062	C11H10O5H+	0.094	0.016	0.094	0.123	0.066	0.203	0.046	0.188	0.333	0.159
223.143	C12H18O2N2H+	0.057	0.026	0.050	0.106	0.025	0.429	0.091	0.415	0.635	0.311
225.048	C9H8O5N2H+	0.043	0.011	0.044	0.062	0.027	0.218	0.046	0.201	0.338	0.167
227.084	C13H10O2N2H+	0.105	0.022	0.110	0.129	0.068	0.480	0.099	0.474	0.744	0.376
227.175	C17H22H+	0.036	0.026	0.022	0.086	0.010	0.156	0.038	0.157	0.244	0.106
228.088	C10H13O5NH+	0.052	0.013	0.051	0.078	0.033	0.109	0.026	0.102	0.184	0.081
229.102	C6H16O7N2H+	0.125	0.027	0.125	0.162	0.082	0.215	0.064	0.213	0.399	0.128
229.214	C14H28O2H+	0.146	0.064	0.133	0.288	0.088	0.225	0.061	0.214	0.370	0.159
230.106	C10H15O5NH+	0.050	0.017	0.045	0.084	0.029	0.061	0.018	0.060	0.110	0.036
230.215	13CC13H28O2H+	0.040	0.017	0.032	0.075	0.023	0.047	0.011	0.043	0.076	0.036
231.084	C10H14O6H+	0.072	0.015	0.076	0.088	0.040	0.153	0.046	0.148	0.282	0.087
231.112	C13H14O2N2H+	0.068	0.017	0.067	0.096	0.035	0.238	0.055	0.224	0.383	0.168
231.205	C12H26O2N2H+	0.046	0.025	0.034	0.091	0.015	0.155	0.041	0.152	0.242	0.095
232.079	C9H13O6NH+	--	--	--	--	--	0.052	0.018	0.048	0.104	0.024
233.108	C10H16O6H+	0.027	0.029	0.022	0.097	0.004	0.111	0.030	0.104	0.196	0.079
233.133	C13H16O2N2H+	0.028	0.015	0.029	0.056	0.008	0.173	0.041	0.164	0.277	0.130
233.223	C17H28H+	0.044	0.029	0.029	0.095	0.011	0.145	0.037	0.134	0.212	0.091
235.149	C18H18H+	0.047	0.031	0.040	0.101	0.011	0.276	0.058	0.260	0.416	0.219
235.202	C16H26OH+	0.067	0.062	0.031	0.180	0.019	0.123	0.040	0.106	0.185	0.073
237.117	C13H16O4H+	0.045	0.014	0.043	0.070	0.022	0.179	0.041	0.164	0.285	0.140
237.160	C18H20H+	0.026	0.016	0.022	0.057	0.006	0.214	0.050	0.204	0.328	0.148
237.215	C16H28OH+	0.032	0.026	0.019	0.086	0.008	0.107	0.027	0.106	0.163	0.074
239.039	C7H10O9H+	0.022	0.012	0.018	0.042	0.008	0.206	0.042	0.202	0.312	0.150
239.176	C18H22H+	0.029	0.019	0.023	0.068	0.006	0.247	0.057	0.242	0.373	0.169
240.038	C6H9O9NH+	0.017	0.008	0.014	0.033	0.008	0.055	0.012	0.053	0.089	0.040
241.102	C7H16O7N2H+	0.063	0.017	0.062	0.095	0.035	0.243	0.060	0.226	0.404	0.190
241.193	C18H24H+	0.028	0.020	0.021	0.069	0.005	0.159	0.038	0.160	0.242	0.104
242.103	C11H15O5NH+	0.037	0.012	0.035	0.062	0.023	0.059	0.015	0.056	0.102	0.043
243.119	C12H18O5H+	0.098	0.019	0.097	0.132	0.063	0.146	0.042	0.136	0.263	0.093
243.228	C15H30O2H+	0.085	0.042	0.073	0.184	0.048	0.204	0.043	0.187	0.313	0.162
244.229	C14H29O2NH+	0.031	0.013	0.027	0.060	0.016	0.046	0.010	0.044	0.073	0.036
245.129	C14H16O2N2H+	0.078	0.018	0.081	0.105	0.041	0.203	0.055	0.192	0.352	0.139
245.223	C18H28H+	0.053	0.025	0.044	0.099	0.019	0.218	0.059	0.223	0.358	0.147
247.149	C14H18O2N2H+	0.045	0.020	0.046	0.084	0.014	0.206	0.052	0.198	0.341	0.149
247.237	C13H30O2N2H+	0.058	0.035	0.041	0.124	0.020	0.181	0.047	0.176	0.288	0.120
249.061	C9H12O8H+	0.050	0.015	0.049	0.076	0.027	0.098	0.030	0.090	0.175	0.054
249.168	C12H24O5H+	0.043	0.022	0.039	0.085	0.014	0.206	0.052	0.191	0.336	0.156

m/z	Formula	LDV					HDV				
		Average	Std Dev	Med	Max	Min	Average	Std Dev	Med	Max	Min
251.037	C8H10O9H+	0.019	0.018	0.011	0.057	0.004	0.099	0.025	0.098	0.162	0.062
251.090	C13H14O5H+	0.066	0.085	0.040	0.275	0.018	0.091	0.028	0.084	0.170	0.057
251.176	C19H22H+	0.042	0.028	0.033	0.103	0.011	0.250	0.058	0.237	0.388	0.180
252.163	C14H21O3NH+	0.060	0.079	0.024	0.247	0.013	0.071	0.022	0.071	0.123	0.043
253.102	C13H16O5H+	0.227	0.066	0.218	0.355	0.128	0.046	0.022	0.040	0.106	0.021
253.192	C19H24H+	0.063	0.037	0.047	0.127	0.019	0.189	0.047	0.180	0.304	0.132
254.103	C12H15O5NH+	0.076	0.024	0.071	0.111	0.044	0.016	0.008	0.015	0.039	0.006
255.086	C12H14O6H+	0.079	0.021	0.079	0.112	0.043	0.089	0.026	0.083	0.159	0.059
255.176	C18H22OH+	0.012	0.007	0.009	0.021	0.004	0.023	0.007	0.022	0.041	0.015
255.115	C15H14O2N2H+	0.011	0.009	0.007	0.031	0.002	0.021	0.006	0.018	0.037	0.014
255.213	C19H26H+	0.055	0.050	0.031	0.154	0.009	0.155	0.037	0.150	0.242	0.115
257.246	C16H32O2H+	--	--	--	--	--	0.678	0.474	0.475	1.559	0.128
258.250	13CC15H32O2H+	--	--	--	--	--	0.122	0.081	0.085	0.273	0.023
259.242	C19H30H+	0.092	0.033	0.078	0.155	0.052	0.190	0.045	0.179	0.294	0.129
261.165	C13H24O5H+	0.046	0.017	0.044	0.081	0.024	0.161	0.039	0.153	0.257	0.116
261.251	C14H32O2N2H+	0.050	0.026	0.038	0.097	0.021	0.165	0.041	0.158	0.253	0.110
263.089	C14H14O5H+	0.058	0.016	0.057	0.087	0.035	0.048	0.018	0.044	0.099	0.023
263.237	C18H30OH+	0.063	0.023	0.058	0.114	0.032	0.399	0.123	0.362	0.715	0.259
264.240	13CC17H30OH+	0.018	0.010	0.015	0.040	0.006	0.091	0.027	0.080	0.160	0.061
265.104	C14H16O5H+	0.050	0.014	0.050	0.074	0.028	0.066	0.021	0.062	0.125	0.042
265.250	C18H32OH+	0.059	0.027	0.053	0.120	0.028	0.318	0.090	0.288	0.558	0.225
266.258	13CC17H32OH+	0.018	0.014	0.014	0.049	0.007	0.074	0.021	0.069	0.127	0.052
267.118	C14H18O5H+	0.059	0.017	0.058	0.080	0.029	0.068	0.023	0.061	0.128	0.043
267.206	C20H26H+	0.033	0.017	0.031	0.064	0.008	0.170	0.039	0.165	0.262	0.127
269.009	C7H8O11H+	0.014	0.019	0.007	0.056	0.001	0.036	0.011	0.038	0.065	0.020
269.134	C14H20O5H+	0.048	0.019	0.044	0.079	0.021	0.094	0.027	0.086	0.167	0.066
269.226	C20H28H+	0.033	0.025	0.022	0.076	0.005	0.176	0.045	0.174	0.277	0.117
272.264	C16H33O2NH+	0.084	0.065	0.052	0.226	0.037	0.334	0.122	0.315	0.626	0.168
273.178	C13H24O4N2H+	0.067	0.017	0.069	0.096	0.040	0.112	0.030	0.101	0.189	0.082
273.254	C20H32H+	0.060	0.030	0.047	0.117	0.024	0.192	0.050	0.185	0.306	0.132
275.179	C16H22O2N2H+	0.034	0.015	0.033	0.064	0.013	0.127	0.031	0.120	0.198	0.093
275.268	C20H34H+	0.045	0.023	0.035	0.079	0.017	0.147	0.036	0.143	0.223	0.105
277.101	C10H16O7N2H+	0.099	0.089	0.073	0.315	0.038	--	--	--	--	--
277.196	C14H28O5H+	0.049	0.020	0.046	0.090	0.022	0.146	0.038	0.138	0.242	0.105
278.103	C14H15O5NH+	0.050	0.033	0.040	0.127	0.025	--	--	--	--	--
279.154	C16H22O4H+	0.121	0.062	0.095	0.224	0.056	0.040	0.027	0.032	0.115	0.012
280.159	13CC15H22O4H+	0.036	0.021	0.027	0.077	0.015	0.019	0.010	0.016	0.046	0.007
281.050	C9H12O10H+	0.018	0.010	0.013	0.040	0.009	0.006	0.003	0.005	0.014	0.003
281.228	C21H28H+	0.041	0.015	0.039	0.066	0.018	0.166	0.040	0.166	0.259	0.121
282.130	C14H19O5NH+	0.002	0.002	0.002	0.006	0.001	0.001	0.001	0.001	0.002	0.000
282.050	C8H11O10NH+	0.002	0.002	0.002	0.006	0.001	0.001	0.001	0.001	0.002	0.000

Table A.9: continue

m/z	Formula	LDV					HDV				
		Average	Std Dev	Med	Max	Min	Average	Std Dev	Med	Max	Min
283.046	C12H10O8H+	0.034	0.014	0.030	0.062	0.020	0.012	0.005	0.012	0.022	0.006
283.256	C18H34O2H+	0.048	0.022	0.043	0.091	0.021	0.171	0.041	0.164	0.271	0.125
284.288	C18H37ONH+	0.041	0.014	0.036	0.069	0.028	0.040	0.009	0.036	0.061	0.026
285.277	C18H36O2H+	--	--	--	--	--	0.463	0.210	0.385	0.816	0.205
286.279	13CC17H36O2H+	--	--	--	--	--	0.097	0.041	0.089	0.177	0.046
287.271	C21H34H+	0.068	0.028	0.058	0.112	0.029	0.199	0.046	0.195	0.308	0.150
289.198	C15H28O5H+	0.037	0.015	0.035	0.061	0.013	0.114	0.027	0.110	0.179	0.088
289.282	C16H36O2N2H+	0.055	0.029	0.043	0.110	0.022	0.152	0.034	0.147	0.229	0.116
291.122	C16H18O5H+	0.035	0.018	0.033	0.076	0.015	0.020	0.009	0.019	0.042	0.009
291.213	C15H30O5H+	0.041	0.015	0.041	0.071	0.016	0.128	0.032	0.123	0.210	0.097
293.174	C17H24O4H+	0.058	0.018	0.059	0.087	0.036	0.058	0.017	0.055	0.100	0.036
293.234	C15H32O5H+	0.043	0.015	0.042	0.076	0.022	0.205	0.055	0.200	0.345	0.147
295.255	C19H34O2H+	0.054	0.019	0.052	0.096	0.030	0.374	0.104	0.358	0.634	0.265
296.254	C18H33O2NH+	0.018	0.008	0.016	0.035	0.007	0.101	0.027	0.097	0.169	0.075
297.077	C10H16O10H+	0.027	0.012	0.025	0.054	0.015	0.018	0.009	0.017	0.034	0.007
297.272	C19H36O2H+	0.086	0.029	0.084	0.149	0.054	0.541	0.147	0.509	0.901	0.379
298.274	C18H35O2NH+	0.022	0.009	0.021	0.042	0.011	0.130	0.034	0.125	0.212	0.090
299.289	C19H38O2H+	0.159	0.051	0.162	0.242	0.085	0.938	0.242	0.884	1.538	0.691
300.293	C18H37O2NH+	0.038	0.013	0.037	0.063	0.023	0.216	0.056	0.209	0.356	0.159
301.100	C12H16O7N2H+	0.038	0.019	0.032	0.085	0.025	--	--	--	--	--
301.284	C22H36H+	0.070	0.020	0.067	0.110	0.038	0.247	0.056	0.238	0.361	0.184
302.286	C21H35NH+	0.020	0.007	0.020	0.032	0.009	0.066	0.015	0.065	0.097	0.046
303.217	C16H30O5H+	0.045	0.015	0.045	0.073	0.021	0.112	0.027	0.107	0.181	0.084
303.299	C22H38H+	0.050	0.017	0.047	0.079	0.024	0.157	0.036	0.153	0.226	0.113
305.132	C12H20O7N2H+	0.045	0.022	0.035	0.094	0.027	0.024	0.009	0.022	0.043	0.010
305.229	C16H32O5H+	0.042	0.016	0.040	0.074	0.018	0.117	0.028	0.111	0.183	0.082
307.143	C13H22O8H+	0.067	0.037	0.057	0.153	0.035	0.018	0.008	0.019	0.031	0.007
307.241	C23H30H+	0.066	0.016	0.070	0.083	0.039	0.146	0.034	0.141	0.228	0.103
309.255	C23H32H+	0.043	0.013	0.042	0.066	0.022	0.180	0.044	0.174	0.284	0.129
311.271	C23H34H+	0.048	0.015	0.047	0.075	0.025	0.203	0.048	0.197	0.311	0.145
313.288	C23H36H+	0.071	0.018	0.069	0.104	0.043	0.221	0.051	0.210	0.332	0.158
314.291	13CC22H36H+	0.025	0.007	0.024	0.038	0.015	0.066	0.015	0.069	0.100	0.047
315.224	C16H30O4N2H+	0.045	0.015	0.045	0.071	0.021	0.095	0.022	0.088	0.142	0.072
315.299	C23H38H+	0.056	0.016	0.055	0.085	0.030	0.239	0.056	0.223	0.343	0.175
316.304	13CC22H38H+	0.018	0.006	0.019	0.029	0.008	0.075	0.017	0.073	0.109	0.053
317.231	C17H32O5H+	0.050	0.021	0.048	0.087	0.021	0.119	0.025	0.116	0.177	0.089
317.314	C23H40H+	0.053	0.015	0.052	0.076	0.027	0.192	0.043	0.184	0.272	0.140
318.318	13CC22H40H+	0.017	0.007	0.016	0.024	0.007	0.061	0.014	0.057	0.087	0.043
319.244	C17H34O5H+	0.047	0.017	0.047	0.079	0.021	0.133	0.030	0.129	0.193	0.089
321.257	C24H32H+	0.049	0.018	0.045	0.081	0.024	0.151	0.036	0.144	0.229	0.098
322.259	C23H31NH+	0.022	0.007	0.021	0.034	0.012	0.045	0.011	0.044	0.069	0.030

Table A.9: continue

m/z	Formula	LDV					HDV				
		Average	Std Dev	Med	Max	Min	Average	Std Dev	Med	Max	Min
323.271	C24H34H+	0.065	0.014	0.063	0.086	0.041	0.187	0.043	0.179	0.282	0.133
324.272	13CC23H34H+	0.023	0.007	0.022	0.037	0.014	0.060	0.014	0.059	0.092	0.042
325.287	C24H36H+	0.075	0.017	0.071	0.104	0.047	0.219	0.051	0.206	0.327	0.155
326.289	13CC23H36H+	0.026	0.007	0.025	0.039	0.015	0.068	0.016	0.065	0.103	0.048
327.301	C24H38H+	0.075	0.024	0.070	0.126	0.044	0.271	0.060	0.256	0.397	0.201
329.315	C24H40H+	0.086	0.022	0.080	0.124	0.054	0.304	0.068	0.294	0.426	0.219
330.319	C23H39NH+	0.027	0.007	0.028	0.037	0.016	0.090	0.020	0.088	0.129	0.064
331.247	C18H34O5H+	0.063	0.016	0.060	0.088	0.037	0.131	0.030	0.125	0.195	0.095
331.332	C24H42H+	0.069	0.016	0.066	0.094	0.043	0.239	0.053	0.235	0.329	0.174
332.335	13CC23H42H+	0.025	0.007	0.025	0.036	0.015	0.077	0.018	0.073	0.112	0.055
333.257	C18H36O5H+	0.053	0.013	0.051	0.074	0.033	0.115	0.027	0.109	0.178	0.080
333.341	C24H44H+	0.041	0.010	0.039	0.058	0.025	0.099	0.023	0.095	0.140	0.069
334.258	C24H31NH+	0.022	0.006	0.021	0.033	0.013	0.043	0.011	0.041	0.069	0.029
335.271	C25H34H+	0.064	0.014	0.062	0.084	0.041	0.152	0.035	0.144	0.229	0.106
336.275	C24H33NH+	0.023	0.007	0.022	0.034	0.013	0.050	0.012	0.048	0.076	0.036
337.286	C25H36H+	0.070	0.015	0.070	0.092	0.045	0.193	0.045	0.189	0.291	0.138
338.290	C24H35NH+	0.019	0.007	0.018	0.033	0.011	0.047	0.012	0.044	0.070	0.031
338.333	C22H43ONH+	--	--	--	--	--	0.028	0.024	0.021	0.106	0.014
339.302	C25H38H+	0.081	0.018	0.078	0.111	0.053	0.221	0.050	0.219	0.322	0.157
340.306	13CC24H38H+	0.030	0.009	0.027	0.047	0.018	0.070	0.016	0.069	0.102	0.049
341.316	C25H40H+	0.080	0.020	0.075	0.116	0.048	0.258	0.056	0.257	0.367	0.190
342.319	C24H39NH+	0.027	0.007	0.027	0.037	0.015	0.080	0.018	0.079	0.117	0.057
343.331	C25H42H+	0.095	0.022	0.091	0.124	0.058	0.330	0.073	0.332	0.460	0.242
344.333	C24H41NH+	0.030	0.007	0.029	0.040	0.017	0.101	0.023	0.100	0.144	0.072
345.259	C19H36O5H+	0.069	0.016	0.067	0.093	0.042	0.137	0.031	0.129	0.201	0.098
345.346	C25H44H+	0.080	0.019	0.077	0.107	0.050	0.270	0.060	0.275	0.368	0.198
346.350	C24H43NH+	0.028	0.007	0.029	0.038	0.016	0.090	0.021	0.090	0.128	0.065
347.272	C26H34H+	0.055	0.014	0.053	0.076	0.034	0.110	0.025	0.106	0.167	0.076
347.357	C25H46H+	0.042	0.010	0.040	0.056	0.025	0.106	0.025	0.104	0.152	0.075
348.276	13CC25H34H+	0.023	0.006	0.022	0.033	0.013	0.043	0.011	0.042	0.069	0.029
349.287	C26H36H+	0.071	0.016	0.070	0.094	0.044	0.157	0.037	0.156	0.243	0.110
350.289	C25H35NH+	0.025	0.006	0.025	0.033	0.014	0.052	0.012	0.051	0.081	0.036
351.301	C26H38H+	0.082	0.018	0.079	0.110	0.051	0.203	0.046	0.201	0.304	0.145
352.305	C25H37NH+	0.028	0.007	0.027	0.038	0.016	0.066	0.015	0.065	0.102	0.048
353.316	C26H40H+	0.094	0.021	0.092	0.127	0.060	0.229	0.054	0.235	0.343	0.162
354.320	13CC25H40H+	0.032	0.009	0.031	0.047	0.019	0.074	0.017	0.073	0.108	0.050
355.333	C26H42H+	0.105	0.024	0.104	0.144	0.064	0.310	0.069	0.312	0.444	0.232
356.336	13CC25H42H+	0.036	0.009	0.036	0.051	0.023	0.099	0.022	0.099	0.142	0.070
357.345	C26H44H+	0.115	0.025	0.112	0.152	0.073	0.354	0.079	0.367	0.495	0.257
358.350	C25H43NH+	0.037	0.008	0.038	0.046	0.023	0.113	0.026	0.114	0.160	0.079
359.275	C20H38O5H+	0.076	0.017	0.073	0.099	0.048	0.139	0.034	0.131	0.214	0.094

m/z	Formula	LDV					HDV				
		Average	Std Dev	Med	Max	Min	Average	Std Dev	Med	Max	Min
359.360	C21H46O2N2H+	0.097	0.021	0.096	0.125	0.061	0.295	0.065	0.305	0.403	0.217
360.279	13CC19H38O5H+	0.026	0.007	0.026	0.038	0.015	0.047	0.012	0.046	0.073	0.032
360.366	13CC20H46O2N2H+	0.030	0.007	0.030	0.040	0.018	0.090	0.021	0.092	0.124	0.064
361.287	C27H36H+	0.059	0.015	0.056	0.084	0.036	0.108	0.026	0.104	0.169	0.073
361.372	C26H48H+	0.043	0.011	0.041	0.057	0.026	0.108	0.024	0.108	0.153	0.078
362.291	13CC26H36H+	0.024	0.007	0.023	0.035	0.014	0.044	0.011	0.043	0.069	0.030
363.301	C27H38H+	0.078	0.017	0.075	0.103	0.050	0.152	0.035	0.154	0.235	0.107
364.303	13CC26H38H+	0.031	0.013	0.027	0.060	0.017	0.058	0.015	0.061	0.085	0.035
365.315	C27H40H+	0.093	0.019	0.092	0.122	0.059	0.202	0.046	0.207	0.300	0.145
366.319	C26H39NH+	0.033	0.008	0.033	0.045	0.019	0.067	0.016	0.067	0.104	0.047
367.332	C27H42H+	0.111	0.024	0.110	0.146	0.068	0.238	0.055	0.238	0.353	0.173
368.334	13CC26H42H+	0.040	0.011	0.039	0.058	0.024	0.078	0.018	0.079	0.116	0.054
369.346	C27H44H+	0.153	0.051	0.138	0.250	0.086	0.343	0.086	0.338	0.501	0.239
370.349	13CC26H44H+	0.054	0.020	0.048	0.093	0.030	0.110	0.028	0.109	0.161	0.073
371.361	C27H46H+	0.176	0.032	0.178	0.213	0.115	0.461	0.100	0.468	0.647	0.335
372.365	C26H45NH+	0.058	0.012	0.058	0.072	0.036	0.149	0.033	0.152	0.214	0.106
373.082	C15H16O11H+	--	--	--	--	--	0.013	0.006	0.012	0.029	0.006
373.292	C21H40O5H+	0.085	0.019	0.083	0.113	0.053	0.132	0.034	0.125	0.207	0.085
373.375	C23H48O3H+	0.122	0.023	0.123	0.152	0.078	0.316	0.071	0.318	0.427	0.228
374.381	C26H47NH+	0.044	0.009	0.046	0.053	0.028	0.110	0.025	0.110	0.154	0.078
375.302	C28H38H+	0.060	0.013	0.058	0.079	0.037	0.101	0.024	0.099	0.158	0.069
375.387	C27H50H+	0.047	0.010	0.047	0.061	0.029	0.105	0.025	0.107	0.151	0.074
376.306	13CC27H38H+	0.025	0.007	0.026	0.037	0.015	0.044	0.012	0.043	0.072	0.029
377.317	C28H40H+	0.082	0.019	0.076	0.113	0.052	0.137	0.033	0.138	0.216	0.095
378.320	C27H39NH+	0.030	0.007	0.031	0.041	0.018	0.049	0.013	0.048	0.081	0.033
379.333	C28H42H+	0.102	0.022	0.099	0.130	0.065	0.184	0.043	0.184	0.284	0.132
380.336	C27H41NH+	0.036	0.008	0.036	0.047	0.022	0.064	0.016	0.064	0.103	0.044
381.346	C28H44H+	0.121	0.024	0.119	0.154	0.079	0.218	0.051	0.216	0.329	0.153
382.350	C27H43NH+	0.043	0.010	0.043	0.058	0.026	0.075	0.018	0.075	0.114	0.053
383.361	C28H46H+	0.173	0.031	0.176	0.212	0.112	0.325	0.075	0.320	0.471	0.232
384.365	C27H45NH+	0.060	0.013	0.060	0.078	0.038	0.109	0.026	0.107	0.165	0.077
385.086	C9H20O16H+	--	--	--	--	--	0.013	0.005	0.012	0.023	0.007
385.375	C24H48O3H+	0.206	0.038	0.210	0.255	0.133	0.429	0.099	0.423	0.608	0.306
386.380	C27H47NH+	0.068	0.014	0.070	0.088	0.043	0.141	0.032	0.140	0.204	0.099
387.306	C22H42O5H+	0.086	0.020	0.084	0.117	0.054	0.114	0.031	0.106	0.179	0.069
387.390	C24H50O3H+	0.143	0.026	0.146	0.176	0.094	0.301	0.069	0.296	0.413	0.216
388.395	C27H49NH+	0.055	0.011	0.056	0.070	0.034	0.110	0.025	0.105	0.156	0.079
389.317	C29H40H+	0.062	0.015	0.060	0.086	0.039	0.090	0.022	0.086	0.143	0.060
390.323	13CC28H40H+	0.028	0.007	0.028	0.038	0.016	0.042	0.011	0.041	0.069	0.028
391.253	C23H34O5H+	0.060	0.020	0.056	0.098	0.037	0.031	0.012	0.030	0.063	0.016
391.327	C25H42O3H+	0.095	0.018	0.091	0.122	0.068	0.120	0.026	0.120	0.188	0.088

Table A.9: continue

m/z	Formula	LDV					HDV				
		Average	Std Dev	Med	Max	Min	Average	Std Dev	Med	Max	Min
392.328	13CC24H42O3H+	0.045	0.011	0.043	0.063	0.029	0.049	0.013	0.046	0.083	0.034
393.346	C29H44H+	0.112	0.024	0.110	0.148	0.071	0.167	0.040	0.163	0.258	0.114
394.348	C28H43NH+	0.041	0.010	0.042	0.057	0.025	0.060	0.015	0.060	0.097	0.041
395.361	C29H46H+	0.145	0.027	0.142	0.180	0.097	0.212	0.051	0.208	0.322	0.146
396.366	13CC28H46H+	0.054	0.012	0.053	0.074	0.033	0.075	0.019	0.074	0.120	0.050
397.377	C29H48H+	0.231	0.038	0.234	0.277	0.154	0.332	0.085	0.320	0.497	0.225
398.380	C28H47NH+	0.082	0.015	0.083	0.100	0.052	0.115	0.029	0.113	0.176	0.079
399.391	C25H50O3H+	0.255	0.043	0.261	0.305	0.170	0.416	0.103	0.399	0.604	0.293
400.395	C28H49NH+	0.089	0.018	0.091	0.112	0.057	0.142	0.035	0.138	0.214	0.100
401.320	C23H44O5H+	0.080	0.019	0.076	0.113	0.050	0.084	0.022	0.080	0.132	0.047
401.406	C25H52O3H+	0.156	0.027	0.159	0.187	0.104	0.264	0.065	0.257	0.371	0.188
402.410	13CC24H52O3H+	0.060	0.012	0.062	0.075	0.038	0.099	0.023	0.093	0.142	0.070
403.332	C30H42H+	0.056	0.014	0.054	0.080	0.035	0.072	0.019	0.068	0.121	0.047
404.335	13CC29H42H+	0.026	0.007	0.026	0.037	0.014	0.036	0.010	0.034	0.061	0.023
405.347	C30H44H+	0.077	0.019	0.074	0.111	0.049	0.100	0.025	0.097	0.161	0.069
406.350	C29H43NH+	0.030	0.008	0.031	0.043	0.018	0.039	0.011	0.038	0.065	0.026
407.361	C30H46H+	0.100	0.022	0.099	0.131	0.064	0.132	0.035	0.126	0.217	0.087
408.364	C29H45NH+	0.041	0.012	0.040	0.062	0.024	0.050	0.014	0.050	0.087	0.033
409.375	C26H48O3H+	0.136	0.026	0.140	0.166	0.090	0.172	0.048	0.160	0.289	0.115
410.380	C29H47NH+	0.056	0.017	0.055	0.086	0.033	0.063	0.019	0.061	0.111	0.041
411.390	C26H50O3H+	0.230	0.054	0.226	0.327	0.143	0.240	0.069	0.222	0.372	0.147
412.395	C29H49NH+	0.089	0.027	0.084	0.143	0.052	0.087	0.024	0.084	0.137	0.053
413.405	C26H52O3H+	0.231	0.040	0.237	0.283	0.155	0.290	0.077	0.272	0.418	0.190
414.409	13CC25H52O3H+	0.089	0.021	0.091	0.124	0.054	0.102	0.027	0.102	0.150	0.066
415.420	C26H54O3H+	0.163	0.028	0.170	0.194	0.109	0.209	0.057	0.190	0.298	0.138
416.425	13CC25H54O3H+	0.061	0.014	0.062	0.083	0.037	0.074	0.019	0.071	0.104	0.047
417.348	C31H44H+	0.049	0.013	0.047	0.071	0.029	0.053	0.015	0.051	0.087	0.032
419.357	C27H46O3H+	0.078	0.021	0.074	0.117	0.049	0.069	0.018	0.066	0.113	0.042
420.363	13CC26H46O3H+	0.033	0.012	0.031	0.058	0.019	0.030	0.009	0.028	0.052	0.018
421.375	C27H48O3H+	0.082	0.021	0.079	0.117	0.053	0.086	0.022	0.084	0.137	0.054
422.379	C30H47NH+	0.035	0.011	0.035	0.054	0.020	0.036	0.011	0.035	0.063	0.023
423.389	C27H50O3H+	0.103	0.025	0.101	0.147	0.068	0.101	0.029	0.092	0.162	0.061
424.393	13CC26H50O3H+	0.046	0.016	0.044	0.080	0.026	0.040	0.011	0.040	0.063	0.024
425.405	C27H52O3H+	0.153	0.027	0.156	0.184	0.103	0.126	0.046	0.102	0.192	0.071
426.408	13CC26H52O3H+	0.070	0.022	0.069	0.112	0.042	0.047	0.015	0.043	0.072	0.025
427.420	C27H54O3H+	0.161	0.029	0.167	0.197	0.109	0.148	0.046	0.130	0.214	0.087
428.423	C30H53NH+	0.070	0.022	0.069	0.114	0.041	0.056	0.016	0.053	0.086	0.034
429.436	C27H56O3H+	0.121	0.024	0.124	0.156	0.079	0.117	0.036	0.101	0.173	0.070
430.440	13CC26H56O3H+	0.051	0.015	0.052	0.077	0.032	0.047	0.014	0.046	0.075	0.027
431.363	C32H46H+	0.056	0.018	0.053	0.092	0.034	0.049	0.013	0.049	0.081	0.028
433.375	C28H48O3H+	0.058	0.019	0.053	0.093	0.035	0.048	0.014	0.048	0.081	0.030

Table A.9: continue

m/z	Formula	LDV					HDV				
		Average	Std Dev	Med	Max	Min	Average	Std Dev	Med	Max	Min
434.378	C31H47NH+	0.025	0.009	0.024	0.043	0.014	0.023	0.007	0.022	0.040	0.014
435.392	C32H50H+	0.069	0.022	0.065	0.106	0.042	0.054	0.014	0.053	0.081	0.031
436.395	C31H49NH+	0.030	0.010	0.030	0.048	0.017	0.026	0.007	0.025	0.043	0.017
437.407	C28H52O3H+	0.080	0.023	0.077	0.121	0.050	0.061	0.019	0.055	0.097	0.036
438.409	13CC27H52O3H+	0.038	0.016	0.036	0.072	0.021	0.028	0.009	0.027	0.049	0.015
439.420	C28H54O3H+	0.104	0.025	0.104	0.138	0.066	0.067	0.025	0.055	0.107	0.032
440.424	13CC27H54O3H+	0.052	0.019	0.047	0.089	0.032	0.030	0.009	0.031	0.045	0.015
441.436	C28H56O3H+	0.108	0.025	0.109	0.141	0.069	0.076	0.026	0.065	0.119	0.043
442.438	13CC27H56O3H+	0.053	0.019	0.047	0.086	0.032	0.032	0.009	0.033	0.048	0.018
443.451	C28H58O3H+	0.091	0.025	0.088	0.135	0.058	0.064	0.021	0.057	0.098	0.039
444.455	C31H57NH+	0.044	0.017	0.040	0.073	0.025	0.030	0.009	0.031	0.046	0.014
445.382	C26H52O5H+	0.049	0.018	0.045	0.081	0.027	0.033	0.010	0.034	0.055	0.018
447.389	C29H50O3H+	0.053	0.021	0.046	0.094	0.031	0.030	0.009	0.030	0.052	0.016
449.405	C29H52O3H+	0.059	0.022	0.052	0.099	0.034	0.034	0.010	0.034	0.056	0.018
450.410	13CC28H52O3H+	0.028	0.011	0.026	0.049	0.016	0.019	0.007	0.018	0.036	0.011
451.421	C29H54O3H+	0.069	0.030	0.057	0.123	0.038	0.033	0.012	0.030	0.056	0.013
452.426	13CC28H54O3H+	0.035	0.016	0.030	0.069	0.020	0.019	0.006	0.019	0.034	0.010
453.435	C29H56O3H+	0.076	0.025	0.068	0.114	0.044	0.039	0.012	0.037	0.057	0.018
454.440	13CC28H56O3H+	0.042	0.020	0.035	0.080	0.024	0.020	0.006	0.021	0.032	0.011
455.451	C29H58O3H+	0.081	0.030	0.070	0.130	0.046	0.040	0.014	0.040	0.061	0.018
456.456	13CC28H58O3H+	0.044	0.020	0.037	0.080	0.025	0.022	0.006	0.023	0.034	0.012
457.466	C29H60O3H+	0.073	0.029	0.064	0.119	0.041	0.036	0.012	0.036	0.059	0.016
458.468	13CC28H60O3H+	0.038	0.018	0.032	0.070	0.021	0.020	0.007	0.021	0.035	0.010
459.389	C30H50O3H+	0.040	0.019	0.034	0.076	0.021	0.022	0.007	0.021	0.036	0.011
461.406	C30H52O3H+	0.043	0.020	0.036	0.078	0.024	0.020	0.007	0.019	0.036	0.010
463.420	C30H54O3H+	0.049	0.023	0.041	0.092	0.028	0.021	0.006	0.022	0.038	0.012
464.427	C33H53NH+	0.024	0.012	0.021	0.044	0.012	0.014	0.007	0.014	0.032	0.006
465.436	C30H56O3H+	0.055	0.025	0.045	0.098	0.030	0.021	0.007	0.021	0.038	0.008
466.438	C33H55NH+	0.027	0.013	0.023	0.053	0.015	0.014	0.006	0.014	0.028	0.007
467.450	C30H58O3H+	0.062	0.029	0.050	0.109	0.033	--	--	--	--	--
468.454	13CC29H58O3H+	0.036	0.018	0.029	0.066	0.018	--	--	--	--	--
469.466	C30H60O3H+	0.066	0.032	0.053	0.121	0.035	--	--	--	--	--
470.468	13CC29H60O3H+	0.037	0.020	0.029	0.072	0.019	0.015	0.006	0.015	0.029	0.007
471.480	C30H62O3H+	0.058	0.029	0.045	0.103	0.033	--	--	--	--	--
475.420	C31H54O3H+	0.029	0.018	0.022	0.062	0.012	--	--	--	--	--
477.436	C31H56O3H+	0.041	0.021	0.034	0.076	0.021	--	--	--	--	--
479.451	C31H58O3H+	0.049	0.029	0.035	0.103	0.025	--	--	--	--	--
481.466	C31H60O3H+	0.054	0.031	0.039	0.108	0.029	--	--	--	--	--
482.465	C34H59NH+	0.029	0.015	0.025	0.056	0.015	--	--	--	--	--
483.480	C31H62O3H+	0.054	0.030	0.041	0.101	0.028	--	--	--	--	--
484.483	13CC30H62O3H+	0.029	0.015	0.025	0.055	0.014	--	--	--	--	--

Table A.9: continue

m/z	Formula	LDV					HDV				
		Average	Std Dev	Med	Max	Min	Average	Std Dev	Med	Max	Min
485.493	C31H64O3H+	0.051	0.030	0.038	0.103	0.025	--	--	--	--	--
489.434	C32H56O3H+	0.020	0.014	0.015	0.045	0.006	--	--	--	--	--
491.445	C32H58O3H+	0.032	0.017	0.026	0.062	0.016	--	--	--	--	--
493.463	C32H60O3H+	0.037	0.021	0.029	0.076	0.018	--	--	--	--	--
495.477	C32H62O3H+	0.043	0.026	0.033	0.085	0.019	--	--	--	--	--
497.493	C32H64O3H+	0.044	0.027	0.032	0.091	0.021	--	--	--	--	--
499.509	C32H66O3H+	0.039	0.021	0.032	0.073	0.019	--	--	--	--	--
507.476	C33H62O3H+	0.029	0.015	0.024	0.053	0.015	--	--	--	--	--
509.491	C33H64O3H+	0.032	0.015	0.027	0.057	0.016	--	--	--	--	--
511.508	C33H66O3H+	0.032	0.017	0.026	0.061	0.016	--	--	--	--	--